Optical Fiber Sensors for Advanced Civil Structures

by:

Marten Johannes Cornelius de Vries

Dissertation submitted to

the Faculty of the

Virginia Polytechnic Institute & State University

in partial fulfillment of the requirements for the degree of

DOCTOR OF PHILOSOPHY

in Electrical Engineering

APPROVED:

Dr. R.O. Claus, Chairman

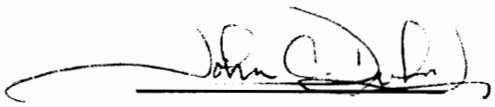

Dr. J. Duke

Dr. T.-C. Poon

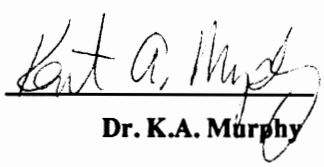

Dr. K.A. Murphy

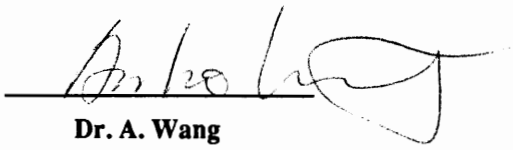

Dr. A. Wang

March, 1995

Blackburg, Virginia

Key words: Optical Fibers, Sensors, Civil Structures, Nondestructive Evaluation

Acknowledgements

I want to first thank Profs. R.O. Claus, J. Duke, K.A. Murphy, T.-C. Poon, and A. Wang for providing me with excellent suggestions and serving on my committee. I would like to thank Dr. Claus for all his encouragement and endless enthusiasm over the last six years. This dissertation is the result of his insightful guidance and invaluable support.

This work was made possible by support from the Turner Fairbanks Federal Highway Administration in McLean, Virginia, Dr. J. Goris at the U.S. Bureau of Mines in Spokane, Washington, Dr. S. Masri at the University of Southern California in Los Angeles, California, Dr. W. Spillman at Simmonds Precision in Vergennes, Vermont, Dr. C. O'Keefe at Martin Marietta, the National Science Foundation, and Fiber & Sensor Technologies Inc..

I am grateful to Vivek Arya for all his help and support during the past year, and to Mary K. Burford, a "true friend," who was always there to help me through all those difficult times. Special thanks go out to Vikram Bhatia, Ashish Vengsarkar, Jonathan Greene, Tuan Tran, Manish Nasta and Angie Plante for their support. A thanks also goes out to the following people for their help with the experiments and presentation: Mohit Bhatnagar, Ravi Kumar, Steve Poland, Asif Malik, Nirmal Vallayadhun, Mallika Sen, Cindy Grinder, Rene Pedrazzani, Paul Schindler, Jason Zeakes, Russ May, Mike Gunther, George Wang, David Scherrer, David Forbis, David Sun, Linda Jones and all other FEORCers.

Finally, I would like to thank my parents, Koop and Gerda de Vries for giving me the strength and support during my stay here at Virginia Tech.

Table of Contents

Table of Figures

Chapter One

Introduction

This dissertation discusses how optical fiber sensors can be used to nondestructively monitor and quantitatively evaluate the condition of existing and advanced civil structures to ensure that the overall quality of the infrastructure is maintained. The advantages of fiber optic sensors over conventional sensors are highlighted and demonstrated in various practical implementations. This chapter discusses the need for monitoring the health of existing and advanced civil structure components, addresses the importance of implementing optical fiber sensors, and provides an outline for this dissertation.

The growth of a civilization as a whole largely depends on the quality of its overall infrastructure. The deterioration of public roads, communication systems, and other critical public infrastructure components can lead, and has led, to the downfall of civilizations. History has shown how the decline of a civilization can be accelerated with the decay of its infrastructure; the Roman and Egyptian civilizations are prime examples of civilizations that flourished with the development of a good infrastructure, and collapsed as their infrastructure deteriorated.[i]

Currently, the United States is seeing a similar trend; the extensive "good" infrastructure that was originally developed and implemented is now rapidly deteriorating with time due to increasing demand, and lack of vital maintenance and repair. For example, according to Federal Highway Administration (FHWA) report estimates, 250,000 of the nation's highway bridges have serious structural problems and are in dire need of repair; it is estimated that it will cost $200 billion to repair bridge deck areas alone.[ii] Over 130,000

Chapter One

Introduction

This dissertation discusses how optical fiber sensors can be used to nondestructively monitor and quantitatively evaluate the condition of existing and advanced civil structures to ensure that the overall quality of the infrastructure is maintained. The advantages of fiber optic sensors over conventional sensors are highlighted and demonstrated in various practical implementations. This chapter discusses the need for monitoring the health of existing and advanced civil structure components, addresses the importance of implementing optical fiber sensors, and provides an outline for this dissertation.

The growth of a civilization as a whole largely depends on the quality of its overall infrastructure. The deterioration of public roads, communication systems, and other critical public infrastructure components can lead, and has led, to the downfall of civilizations. History has shown how the decline of a civilization can be accelerated with the decay of its infrastructure; the Roman and Egyptian civilizations are prime examples of civilizations that flourished with the development of a good infrastructure, and collapsed as their infrastructure deteriorated.[1]

Currently, the United States is seeing a similar trend; the extensive "good" infrastructure that was originally developed and implemented is now rapidly deteriorating with time due to increasing demand, and lack of vital maintenance and repair. For example, according to Federal Highway Administration (FHWA) report estimates, 250,000 of the nation's highway bridges have serious structural problems and are in dire need of repair; it is estimated that it will cost $200 billion to repair bridge deck areas alone.[2] Over 130,000

bridges now have weight restrictions placed on them resulting in inconvenience and lost time to truckers. Approximately two hundred bridges partially or completely collapse annually nation-wide.[3] For bridges, most failures occur due to inclement weather and traffic carrying heavy loads. Water is responsible for scouring bridge foundations, corroding steel and cracking concrete during freezes, and excessive loads cause cracks.[3] In general, both natural and operational causes are responsible for the deterioration and destruction of the civil infrastructure. Natural causes include wind, ice-buildup, earthquakes, floods/washouts, and corrosion, while operational causes include impacts, fatigue due to excessive overuse, fire, overloading, explosions, and improper construction. Some effects build up over time and may not be obvious initially, while others are easily detected. It is therefore extremely important that the U.S. solve the problems related to repairing, maintaining and improving its infrastructure.

Industrial Research and Development spending on structural construction engineering technologies is less than 0.5 percent of gross sales.[1] This figure is much lower than the percentage of R&D expenditures in most other countries. Yet only continued and increased reinvestment, into research for the treatment and repair of the national infrastructure will improve the civilization as a whole. A growing need is therefore being felt for the design and development of advanced construction materials, and the implementation of electrical and mechanical instrumentation that can perform health monitoring of such infrastructure. Fortunately, recent changes in world politics have refocused part of the effort in such sensor-integrated "smart material and structures" from primarily military uses to civilian infrastructure applications.

To assess the damage and to evaluate the condition of the nation's civil structures, novel non-destructive testing and evaluation techniques need to be developed. For this dissertation, optical fiber-based sensors were developed and implemented that can be used to quantitatively monitor the performance of bridges, building structures and advanced building materials that have widespread applications in civil structures. In part this requires sensors to monitor various parameters, such as strain and vibration, over long periods of time on the surface (surface-mounted) as well as internal to the structure (embedded). Sensor data obtained from tests can be used as input to subsequently optimize and improve material and structural design. This data can also suggest possible methods of

implementing long term *in situ* measurement approaches to evaluate the health of constructed structures, and allow the structure to be repaired, restored, or retrofitted. Furthermore, the ability for self-diagnosis will make the "smart" materials of future structures superior to, and more cost-effective than, the materials used today. The design of new materials with improved structural geometries and capabilities for withstanding long term deterioration or short term heavy loading requires extensive laboratory analysis and verification. Information gained from such testing is needed as input to subsequent structural design and optimization, as well as to suggest possible methods to implement long term *in situ* measurement approaches to determine the health of the advanced civil structure components.

Optical fiber sensors, unlike conventional electrically-based sensors, are fabricated with high-strength silica which will not corrode or be affected by electromagnetic interference. Their small size and geometric flexibility allows them to be unobtrusively embedded or surface-attached to the host structure. Fiber optic sensors have been used for the non-destructive evaluation of advanced materials and structures for over ten years.[4,5] For example, in composites, fiber sensors have been demonstrated to be feasible for the measurement of internal material changes during fabrication, the in-service lifetime measurement of strain, temperature, vibration, and other physical perturbations, and the eventual detection of damage or property degradation.[6,7] Recent advances in fiber optics communication technology and the widespread use of fiber communications have made available a large selection of reliable and inexpensive opto-electronic devices and components for use in sensors and sensor instrumentation support systems.

Composite materials have found extensive applications in the high-technology defense industry. Especially in the military aerospace industry where cost was less important than performance, composite materials were implemented because of their light weight, high specific strength, excellent fatigue behavior, low thermal expansion, and good resistance to corrosion and a variety of chemicals.[8,9] Advanced composite materials are also quickly replacing traditional materials in the commercial sporting goods market, where the cost versus performance factor is much more important. So far however due to liability concerns, higher up-front costs, unfamiliar design procedures, and lack of long-term reliability data, few civil structures have been designed with composite materials. Plans to

build those types of structures, however are underway. For example in San Diego, California, a cable-stayed, 60 ft-wide, 450 ft-long all-composite bridge is being designed, and will be built, to connect the two campuses of the University of California at San Diego across route I-5.[10] Composites are ideal for larger structural facilities where weight considerations are an issue. But composite materials are also used to retrofit and augment existing structures and in some cases are making the structures stronger than before.

Since limited information is available on composite materials and few models can accurately predict their durability, it is important to implement monitoring systems that can nondestructively determine the structural integrity of such advanced materials. It has already been shown that optical fiber sensors are ideal candidates for embedding in composite materials to monitor structural health.[11] In the case of advanced civil structures that implement all-composite designs optical fiber sensors would be ideal for monitoring structural integrity since few models can accurately determine the integrity of the structure over time.

A growing number of researchers are now embedding optical fiber sensors into concrete civil structures to monitor various physical perturbations in the structures.[12,13,14] Even though most of this work is qualitative in nature, results show great promise. Relatively low-cost fiber-optic refractive index sensors have been developed by Ansari *et al.* at the New Jersey Institute of Technology in Newark, NJ, for the in situ determination of air-content in fresh concrete.[15] Ansari has also developed a macrobend-type multimode fiber optic sensor to monitor internal displacements in the concrete due to crack tip opening displacements (CTOD).[16] The drawback of this sensor is that the crack path needs to be known *a priori*. Researchers have implemented polarimetric-type optical fiber sensors that can be used to monitor stress concentrations in small concrete specimens. The orientation of the birefringent axis is extremely important and difficult to align, making this type of sensor difficult to implement in large structures outside of the laboratory.[17,18,19]

Sensors embedded in concrete that are not attached to rebar, or some other type of reinforcing material, may not provide accurate, reliable or long term information related to the parameters they are trying to monitor. Mendez and Fuhr have already indicated that it is difficult to obtain good strain transfer between the host material, concrete, and the optical fiber sensors.[20,21,22] In fact, Marjurda reports that in concrete the interfacial bond between

the glass fiber and matrix material is poor since the bond is both discontinuous and irregular.[23] If the interfacial bond between the fiber and the concrete was good, cracks that typically occur in concrete over time, and that are expected, would propagate through the fiber and destroy the sensor.

Despite these problems, however progress in embedding optical fiber sensors in concrete has been made. Fuhr *et al.*, at the University of Vermont, were able to detect vibration signatures from turbine engines used in a dam using modal domain-based optical fiber sensors embedded in the dam wall.[24] Measures *et al.*, using Bragg-type gratings, and Wolf *et al.*, using optical time domain reflectometry techniques, were able to perform strain measurements on composite prestressing strands used to reinforce concrete bridges.[25,26] Even though both techniques can be used to obtain strain information, both systems require complex temperature compensation techniques to obtain truly quantitative strain information.

This dissertation discusses the use of optical fiber sensors for the nondestructive quantitative evaluation of advanced civil structures. It covers a wide range of issues pertaining to sensors embedded in, and attached to these structures. The material presented in this dissertation is organized in the following chapters.

Chapter 2 performs a comparative evaluation of optical fiber sensors that may be used to obtain quantitative information related to physical perturbations in the civil structure. It presents the key characteristics on which the various optical fiber sensors are compared and gives the rationale behind the choice of the specific sensor configurations. The principle of operation of the extrinsic Fabry-Perot interferometric (EFPI) optical fiber sensor is explained using the Kirchhoff diffraction theory approach to help predict the signal-to-noise ratio as a function of gap length. The basic principle of operation of the absolute EFPI (AEFPI) is also presented.

Chapter 3 discusses results obtained from a series of experiments using EFPI-type optical fiber sensors in a wide variety of civil structure applications. The first section describes experiments, performed in cooperation with Dr. Sami Masri *et al.* in the Civil Engineering Department at the University of Southern California, Los Angeles, that concentrate on obtaining strain information from reinforced concrete interior, and exterior,

column-to-beam connections. The second section describes results from strain tests, performed in cooperation with researchers at the United States Bureau of Mines in Spokane, Washington, on roof bolts used in mines. The third section describes the experiments performed in cooperation with researchers at the Turner Fairbanks Federal Highway Administration in McLean, Virginia, that focused on using absolute EFPI (AEFPI) sensors for monitoring strain on composite prestressing strands used for reinforcing concrete. The last section demonstrates that EFPI sensors, when properly attached, can survive in excess of 100,000 loading cycles.

Chapter 4 pertains to the multiplexing of optical fiber sensors. Various multiplexing techniques including time, frequency, and wavelength division multiplexing, (TDM, FDM and WDM respectively) are briefly discussed, whereas the principle of operation of spread spectrum and OTDR techniques are discussed in greater detail. Preliminary results demonstrating that spread spectrum techniques can be used to multiplex EFPIs are given. Results demonstrating that OTDRs can be used for multiplexing EFPI sensors, and to perform quasi-distributed strain measurements are presented as well.

Chapter 5 describes practical considerations that will need to be taken into account with the implementation of optical fiber sensors in the civil infrastructure environment. It presents a possible solution to the problem of fiber breakage at the point where the fiber enters and exits the material. This chapter also shows that the operating range of the EFPI sensor is strongly dependent on fiber endface cleave angle, and thus can put an upper limit on its implementation for structural monitoring purposes.

Chapter 6 provides a brief summary for this dissertation and makes some concluding remarks regarding the future use of fiber optic sensors in civil structure applications.

Chapter Two

Sensor Selection & Analysis

This chapter presents a comparative evaluation of optical fiber sensors that may be used for the nondestructive evaluation of civil structures. Based on this evaluation, the ease of sensor fabrication and installation, and conclusions from a study performed by Sirkis[19], the extrinsic Fabry-Perot interferometric (EFPI) optical fiber sensor was found to be the most promising sensor for nondestructively obtaining reliable quantitative strain information embedded in civil structures. The principle of operation of the EFPI is explained using the Kirchhoff diffraction theory approach.[27] This novel approach, applied to the EFPI sensor, may help to predict the signal-to-noise ratio as a function of the gap length and thus determine the dynamic range of the sensor. The basic principle of operation of the absolute EFPI (AEFPI) sensor is also discussed briefly.

2.1 Optical Fiber Sensor Classification[28]

Optical fiber-based sensors are classified as being extrinsic and intrinsic, referring to the sensing region of the fiber sensor being outside or inside the fiber, respectively. In intrinsic sensors the optical energy in the fiber is affected directly by the incident perturbation (the phenomenon being measured), and changes in the output intensity give an indication of the magnitude of the disturbance. Such fiber sensors include the sapphire fiber-based intrinsic Fabry-Perot interferometric sensor (IFPI),[29,30] which has been successfully implemented for high temperature measurements. Grating-based sensors are also included in this category.[31,32,33,34] In extrinsic sensors the fiber only serves to carry optical power to, and sensing information from, an external region, usually air. Such sensors are often immune to vibration and temperature fluctuations. Extrinsic sensors

based on the extrinsic Fabry-Perot interferometric (EFPI) scheme have been implemented using circular core singlemode[35] and elliptical core two-mode optical fibers for the measurement of strain, temperature[36], and vibrational mode analysis in smart structures.[37]

Fiber sensors are also classified according to the transduction mechanism which brings about a change in some property of optical power passing through the fiber, such as intensity, phase, polarization, modal content and other factors. Hence the corresponding sensors are known as intensity based, phase or interferometric-based, polarimetric type, and modal content based. Intensity based fiber sensors offer the advantages of ease of fabrication, robustness, and simplicity of signal processing. The sensor consist of an optical power source, an optical fiber, and a photodetector or spectrum analyzer. The intensity modulation is effected through the use of periodic microbends,[38,39] dielectric thin films offering differential spectral reflectivity,[40] or Rayleigh scattering used in optical time-domain reflectometry (OTDR).

Phase modulated or interferometric sensors offer extremely high levels of sensitivity as compared to the intensity based sensors. The sensor usually consists of a *reference* fiber which is isolated from the perturbation being measured, and a *sensing* fiber which is made extremely susceptible to the incident perturbation. The output from the two fibers interferes at the photodetector, and the magnitude of the interference is dependent on the incident perturbation. Since the light source and other external fluctuations affect both the sensing and reference fibers equally, the differential interference offers a self referencing mechanism. Interferometric sensors are hence more sensitive and accurate than intensity based sensors. However, they often involve complex output signal processing schemes. Interferometric sensors employ the fiber equivalent of classical interferometer schemes such as the Mach-Zehnder, Michelson, Fabry-Perot, and the Sagnac interferometers.

Fiber-based sensors which depend on the change in fiber property, such as birefringence or modal content, have also been implemented for the measurement of surface currents, liquid storage levels,[41] and vibration modes in advanced avionics.[37]

2.2 Optical Fiber Sensor Selection[42]

This section presents the key characteristics on which the various optical fiber sensor configurations are selected for a given application. The sensor characteristics are compared for most commercially available sensors in Table 1.

- *Sensitivity:* The sensitivity in a fiber sensor refers to the minimum detectable change in measurand (or the phenomena being measured). The higher the rating, the more sensitive the sensor. Phase modulated or interferometric sensors are inherently more sensitive as compared to intensity based or wavelength modulated sensors.
- *Frequency Response:* The supporting electronics used with the optical fiber sensor most often limits the frequency response of the sensor. In Table 1, the frequency response is indicated after taking into account the various devices used with the sensor to improve the frequency response. The sensor sensitivity may vary over a range of perturbation frequencies, or the sensor may be limited in its response at either end of the frequency spectrum. A flat frequency response in the region of interest would give the sensor a higher rating. Another factor that has to be taken into consideration is if the sensor is limited in its response at either end of the frequency spectrum. For example, in some cases like the OTDR sensor, current research status might not allow the measurement of variations on the order of tens of kHz. This may be due to the processing electronics, which may require a minimum amount of processing time for each data point available.
- *Signal Processing Complexity:* The complexity of signal processing needed for the fiber sensor varies with the sensor configuration being employed for the civil structure application. In intensity based sensors, a simple photodetector or spectrum analyzer is capable of providing an output that is proportional to the parameter being measured. In interferometric sensors, however, special electronics such as level detectors and counters, may be needed to process the output signals. A rating of 10 means that the signal processing complexity is minimal.
- *Lead Sensitivity:* A major concern during the implementation of any fiber-based sensing scheme is that the fiber carrying optical power to the sensing

region may itself be affected by the perturbation. Similarly the fiber carrying the sensor information to the signal processing may be prone to environmental fluctuations. The lead sensitivity of the fiber is a measure of the degree to which the lead-in and lead-out fibers are affected by the external perturbations. In the table, the least sensitive are rated highest. It is expected that with the increase in levels of research, sensors will be implemented with lead insensitive input/output fibers.

- *Linearity:* The fiber sensor remains linear only for a fixed range of the sensing signal. If the input/output curve is sinusoidal, as in the case of most interferometric sensors, operation over a limited range of the transfer curve maintains a linear range relation between the input and output signals. A higher rating in the table refers to a greater linear range of sensor operation. It should be noted that nonlinear sensing schemes can be used for various applications by adding post-processing electronics, such as fringe counters in interferometric sensors.
- *Multiplexing Capability:* Multiplexing of sensors allows the health monitoring of a civil structure with a network of sensors without increasing the number of light sources and photodetectors needed. A high rating in the table means that one could implement several multiplexed sensors without raising the cost proportionally. Some multiplexing techniques available today, however, require that specialized components that may raise the cost significantly. Future research in this area may alter these ratings significantly.
- *Range Limitations:* The operating range of fiber sensors is limited by the maximum perturbation that it can measure, and the temperature range within which the sensor must operate. The fewer the restrictions on the sensor, the higher the rating.
- *Cost:* Intensity based sensors are inherently economical due to their optical simplicity and the low source cost. Phase modulated sensors, on the other hand, require stable sources and stabilization techniques for the elimination of drifts. It has been assumed in the table that some intensity based systems use modules and feedback systems for stabilizing the drifts. A high rating means that the sensor is less expensive to implement.

- *Research Status:* Although research in optical fiber sensors is progressing rapidly, application in civil structure monitoring remains to be fully investigated. The comparison shown in the table assigns a higher rank to sensing configurations which have been implemented to a large extent for civil structure monitoring applications.

Most of the optical fiber sensors listed in Table 1, have been implemented in civil structure applications. Results obtained by Sirkis, however, suggest that the extrinsic-type optical fiber sensors are more reliable for embedded applications than intrinsic-type optical fiber sensors.[19] Sirkis theoretically evaluated and experimentally verified the performance of six different types of optical fiber sensors; the Mach-Zehnder, Michelson, and intrinsic and extrinsic Fabry-Perot interferometers, the modal domain based sensor and the polarimetric sensor. These sensors were embedded in a transversely isotropic graphite-epoxy laminated composite and exposed to 5 different types of loading conditions; which introduced axial and transverse strains. From his results we find that the only reliable sensor for embedding is the EFPI sensor. The EFPI sensor was the only sensor that was sensitive to only the axial strain components and unlike the intrinsic sensors, the EFPI sensor was relatively insensitive to temperature variations.[43] For the other sensors, transverse strains introduced large errors in the readings. Based on these results it was decided to implement the EFPI sensor for civil structure applications.

Table 1 Sensor comparisons

Sensor Types	Sensitivity	Frequency Response	Signal Processing	Lead-in Sensitivity	Linearity	MUXing Capability	Range Limitations	Cost	Research Status
Mach-Zehnder	10	8	5	3	4	7	9	7	6
Michelson	10	8	4	3	4	7	9	7	6
Fabry-Perot (Intrinsic)	9	8	6	7	4	6	9	8	8
Fabry-Perot (Extrinsic)	9	8	6	8	4	5	9	8	7
E-core, 2 mode	6	7	6	9	5	7	9	8	7
Twin Core	6	8	5	7	7	4	8	7	6
OTDR (Fresnel)	4	3	4	9	8	8	8	3	10
OTDR (Rayleigh)	3	3	4	4	8	5	6	3	9
Coupler-based	6	8	5	8	7	5	6	7	10
Extrinsic	3	5	8	6	7	5	5	9	10
Polarimetric	8	8	6	8	5	6	8	7	7
Grating-based (Bragg reflector)	9	8	6	9	4	6	5	7	8
Liquid-core fibers	4	4	9	8	7	4	7	5	8

2.3 Extrinsic Fabry-Perot Interferometer: Principle of Operation

Optical fiber-based Fabry-Perot sensors reported in literature have been shown to be highly sensitive to temperature, strain, vibration, acoustic waves and magnetic fields.[44] The fabrication of these Fabry-Perot-type sensors has typically been achieved with the use of air-glass reflectors,[45] in-fiber Bragg gratings,[46] or through the use of semi-reflective splices along the length of the fiber.[47,48] Such fiber sensors include the sapphire fiber-based intrinsic Fabry-Perot interferometric (IFPI) sensor, successfully implemented for high temperature measurements.[35,36] In extrinsic sensors, the fiber only serves to carry optical power to, and sensing information from, an external region, usually air. The main advantages of the extrinsic method over the intrinsic method include the avoidance of polarization problems, and the detection of the axial strain components only. For the extrinsic Fabry-Perot interferometer (EFPI), first described by Murphy *et al.*, the Fabry-Perot cavity is formed between the air-glass interfaces of two fiber endfaces aligned in a hollow-core fiber.[35] Changes in the separation between two fiber endfaces, known as the gap length, cause interferometric fringe variations. In this section we present a theoretical analysis of the optical field reflected off the target fiber using Kirchhoff's diffraction theory. This analysis allows the prediction of the signal-to-noise ratio as a function of the gap length and helps in determining the dynamic range of a given sensor. Experimental results which support the theoretical predictions are also presented.

Murphy *et al.*, have demonstrated the EFPI strain gage on an F-15 at Wright Patterson Air Force Base and in a combustor at the Westinghouse Science and Technology Center.[49,50] The EFPI has been successfully used at temperatures ranging from -200 to 900 °C,[50] and for monitoring of surface acoustic waves.[51] A detailed sensor fabrication method is described by Tran *et al.*,[51] and the interferometric approach to analyzing the signal output is done by Murphy *et al.*.[52]

The EFPI sensor geometry is shown in Figure 1. Here light from a 1300 nm laser light source is coupled into the sensor head which consists of a 126 μm inner diameter hollow core tube into which a 9/125 μm singlemode input fiber and a second fiber, serving solely as a reflector, are positioned. The reflection, approximately 4%, from the first glass-air interface at the end of the input fiber, R_1, and the reflection, R_2, from the air-glass interface

at the input to the second fiber interfere and couple back to a detector via a 2x2 coupler. The resulting interference signal varies sinusoidally in response to microdisplacements in the air-gap cavity. Typical interference fringes observed for displacing the sensor from 0 to 400 μm and from 19.5 to 30 μm are shown in Figure 2 and Figure 3 respectively. In these experiments the target fiber was not epoxied to the hollow core fiber so that it could freely slide inside the hollow core fiber.

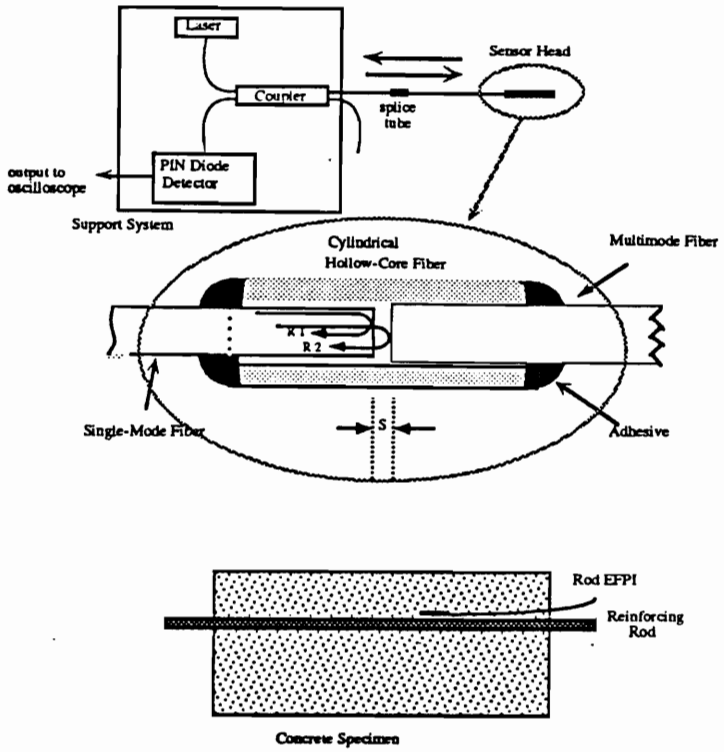

Figure 1. Extrinsic Fabry-Perot interferometric sensor geometry.

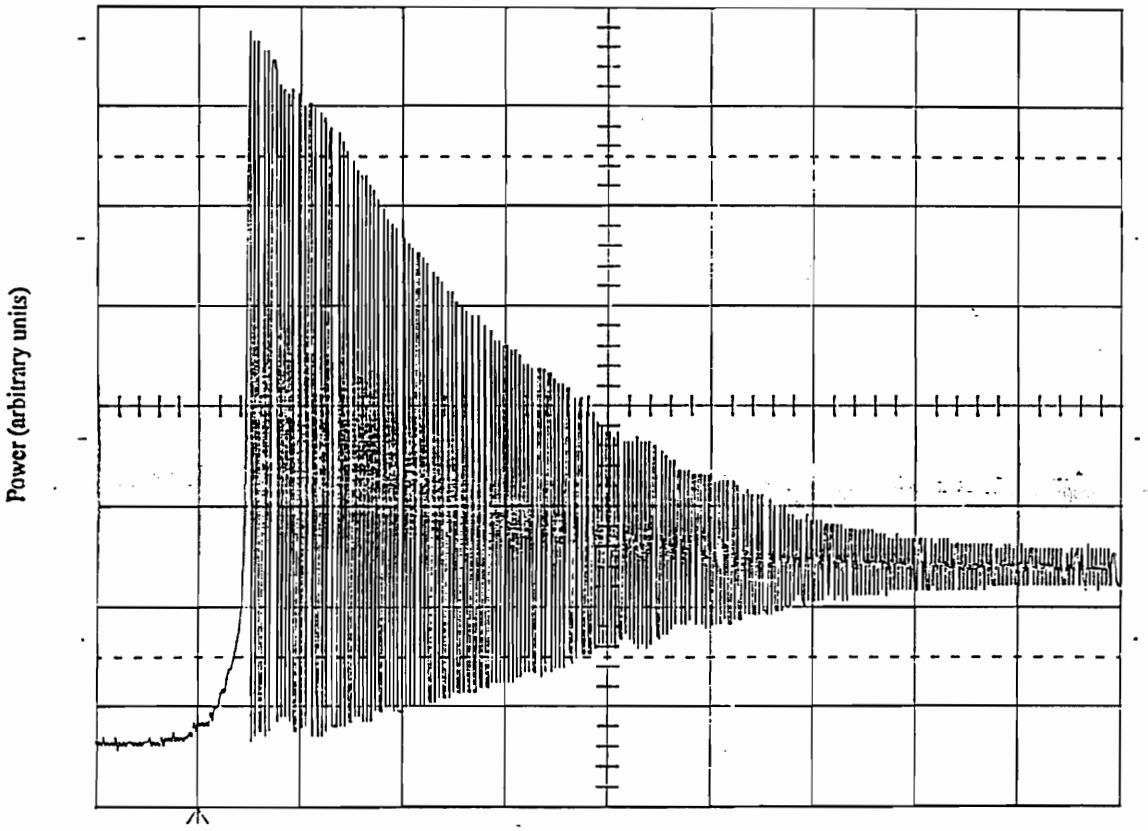

Figure 2. Output response as the EFPI is displaced from 0 to 400 μm.

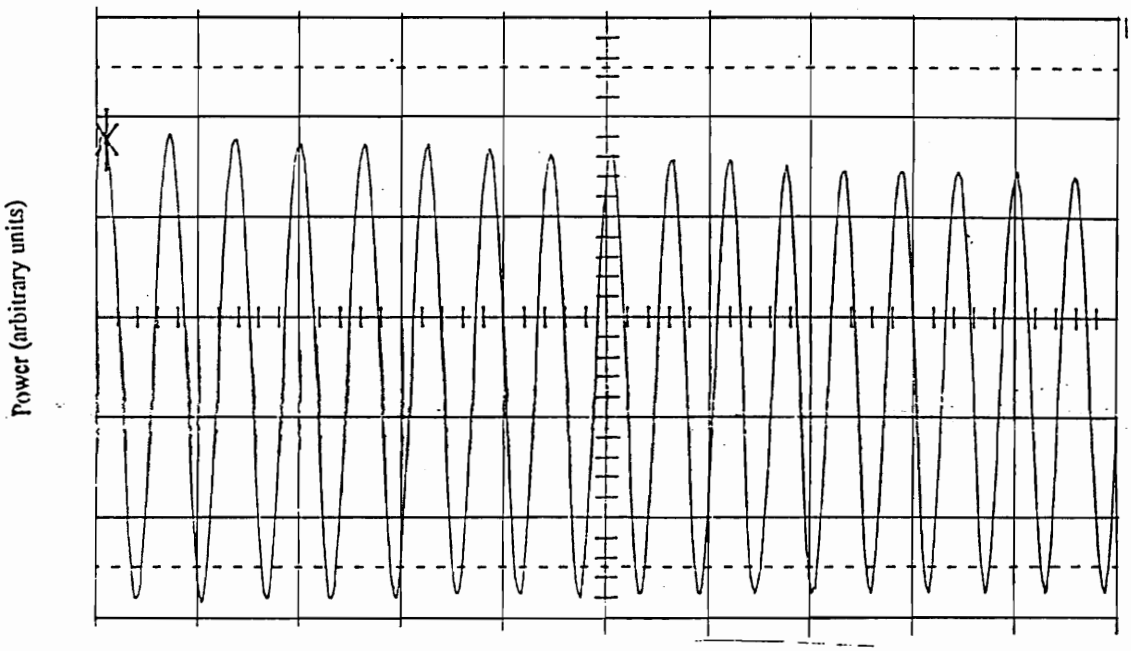

Figure 3. Output response from the EFPI sensor as it is displaced from 19.5 to 30 μm.

2.3.1 Two Beam Interferometer Analysis

The two beam interference approximation can be used to describe the experimental results shown in Figure 3 using

$$I_{det} = \left(1 + \frac{2ta}{a + 2s\tan\left[\sin^{-1}(NA)\right]}\cos\left(\frac{4\pi s}{\lambda}\right) + \left(\frac{ta}{a + 2s\tan\left[\sin^{-1}(NA)\right]}\right)^2\right), \quad (1)$$

where I_{det} is the normalized intensity at the detector, NA, is the numerical aperture of the fiber, t is the transmission coefficient, λ is the wavelength of operation, a is the fiber core radius, and s is the gap separation.[35] These results, shown in Figure 4 look similar to the experimental results in Figure 3. However, a closer look at the fringe contrast (FC), mathematically expressed as,

$$FC = \frac{I_{max} - I_{min}}{I_{max} + I_{min}}, \quad (2)$$

and shown in Figure 5 for both experiment and theory, shows that the two beam interference approximation does not adequately predict the drop in fringe contrast as a function of gap separation. A more rigorous analysis is needed to accurately predict the operating range of the EFPI sensor.

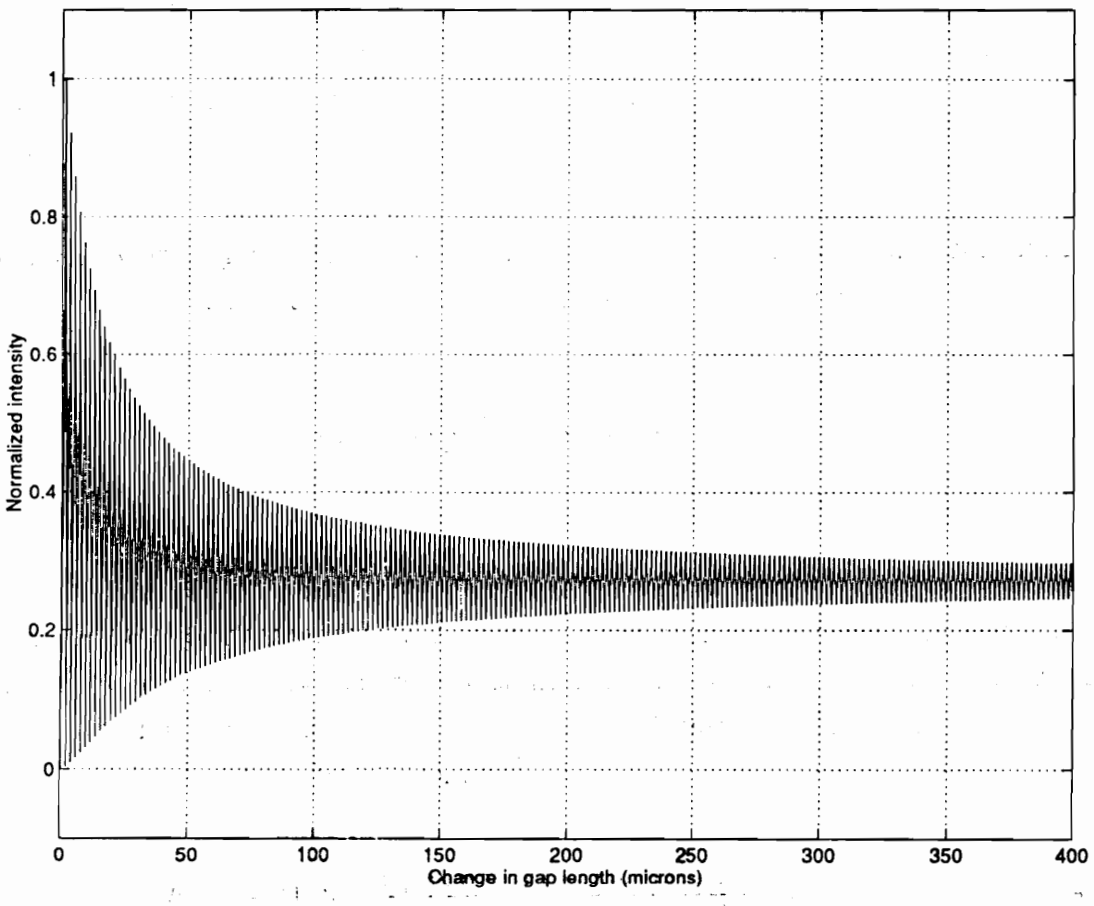

Figure 4. Normalized output power versus gap length using the two-beam interference approach (0 - 400 μm).

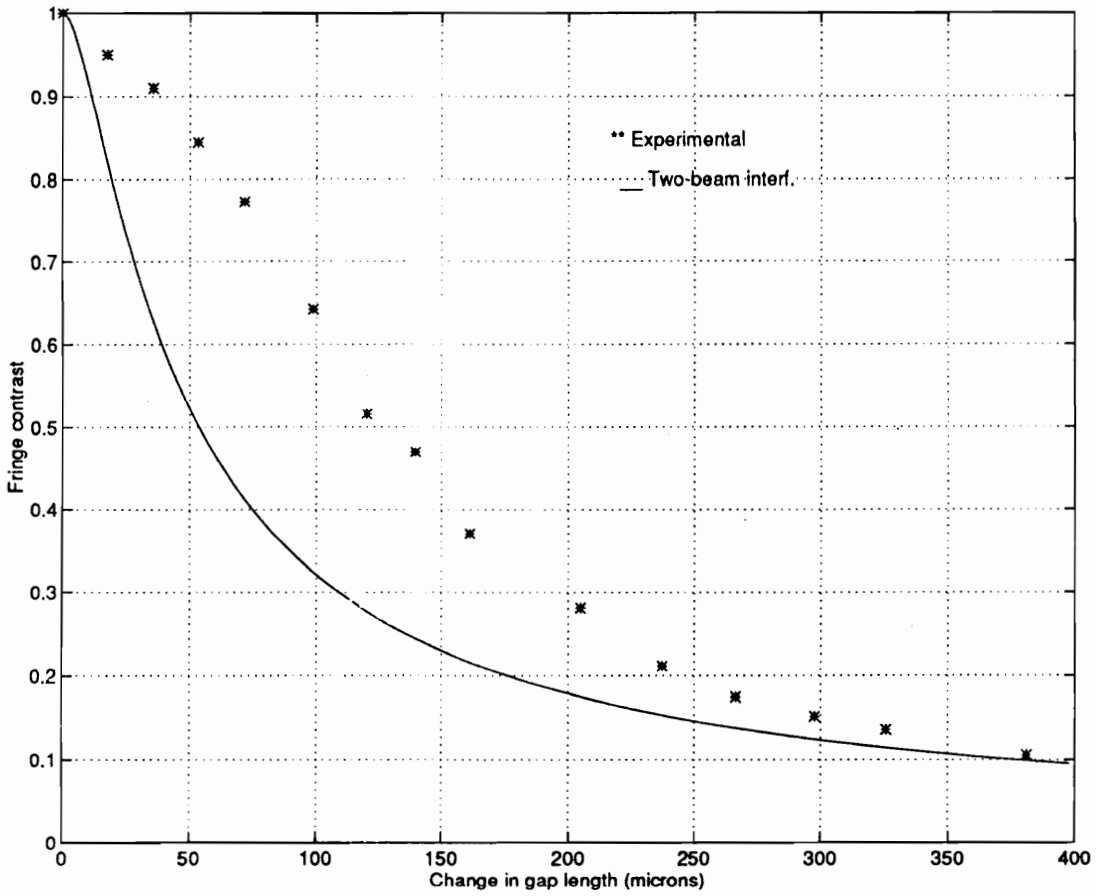

Figure 5. Fringe contrast versus gap length, comparing the two-beam interference approach with experimental results.

2.3.2 Kirchhoff's Diffraction Analysis

The intensity contributed from the target fiber is strongly dependent upon the length of the air-gap and decreases with an increase in gap length. The fringe contrast of the sensor output decays with an increase in the gap length. In order to develop a rigorous analysis of sensor operation, the electric field amplitudes of the reflections from the reference and target fiber must be calculated using an exact approach. This can be accomplished using the following analysis.[27]

For a weakly-guiding, circular-core optical fiber, the scalar field of the fundamental mode, LP_{01}, can be assumed to be approximately Gaussian in shape, given by[53]

$$\Psi_{01} = A\exp\left(\frac{-\rho^2}{\omega^2}\right)\exp(-j\beta z), \tag{3}$$

where ω is the mode field radius, A is the normalized amplitude, β is the modal propagation constant, ρ and z are cylindrical coordinates, and the temporal dependence is implicit. Assuming that the electric field at the endface of the input (lead-in) fiber can be expressed by Equation 3, the electric field at any point P outside the lead-in fiber endface is given by the Kirchhoff's diffraction formula[54]

$$\Psi(P) = \frac{1}{4\Pi}\iint\left[\Psi_{01}\frac{\partial}{\partial z}\left(\frac{\exp(jkS)}{S}\right) - \frac{\exp(jkS)}{S}\frac{\partial\Psi_{01}}{\partial z}\right]ds. \tag{4}$$

In the above equation, $k=2\pi/\lambda$ is the free space propagation constant, and the integral is evaluated over the lead-in fiber endface region. Using Equation 3, Equation 4 may be simplified to be of the form

$$\Psi(P) = \iint\left[\Psi_{01}\left(\frac{\exp(jkS)}{S}\right)\left\{\frac{2L}{S}\left(jk - \frac{1}{S}\right) + jk\right\}\right]ds, \tag{5}$$

where L is the gap length of the Fabry-Perot cavity. The factor S is the vector distance between a point Q at the input/output endface and the point P, as shown in Figure 6. From geometry, S can be written as

$$S = \sqrt{\rho^2 + \rho'^2 - 2\rho\rho'\cos(\phi - \phi') + (z - z')^2}, \tag{6}$$

where ρ, ϕ, and z are the cylindrical coordinates at the lead-in fiber endface, and ρ', ϕ', and z' are the cylindrical coordinates at the point P. Use of the Gaussian approximation for the guided fundamental mode field ensures that light propagating in the cladding is also accounted for while evaluating the integrals.

The target fiber in Figure 1 acts as a partial reflector with a Fresnel reflection of approximately 4%. The normalized electric field amplitude, A', at this reflector may be expressed as

$$A' = \frac{\iint\left[\Psi(P)\exp\left(-\left(\frac{\rho'^2}{\omega^2}\right)\right)\right]ds'}{\iint\left[\exp\left(-\left(\frac{\rho'^2}{\omega^2}\right)\right)\right]^2 ds'}. \tag{7}$$

The total field at the input/output fiber may then be expressed as the summation of E_i, the field due to the first reflection at the glass-air interface, and E_r, the field contributed by the target fiber at this interface. These fields may be written as

$$E_i = C\Psi_{01}, \tag{8}$$

and

$$E_r = C(1 - C^2)|A'|\Psi_{01}\exp(jk_0 L), \tag{9}$$

where $C = (n_f - n_o)/(n_f + n_o)$ is the Fresnel reflection coefficient at the air/glass interface of the fiber. Plots for the normalized electric field at the input/output fiber and the target fiber for different gap lengths are shown in Figure 7. For a typical silica fiber, C is approximately 0.2. Hence using Equations 8 and 9, the total optical power returning through the input/output fiber is given by

$$P_{total} = \iint I ds = \iint \left| E_i + E_r \right|^2 ds, \tag{10}$$

where I represents the intensity contributed by the two reflections at a given point on the endface of the fiber mode field, and the integral is calculated over the endface of this mode field. The gap length, L is half the axial distance used for the Kirchhoff integral (Equation 4). A program was written to perform the numerical calculation of Equation 10. The resulting normalized power versus gap length for displacements from 0 to 400 μm and from 19.5 to 30 μm are shown in Figure 8 and Figure 9, respectively.

The theoretical graph shown in Figure 8 shows oscillations in the near field which indicate the presence of Fresnel zones.[55] The reason for their absence in experiment could be the axial misalignment between the input/output and target fiber due to imperfect fiber endface cleaves and hollow core tube attachment. This observation is important, since for given fiber parameters, the numerical analysis yields the minimum gap length for reliable sensor operation. The experimental fringe contrast versus gap length, along with the theoretical prediction is illustrated in Figure 10. The experimental fringe contrast decreases more rapidly as compared to theory. This could be contributed to the lower sensitivity of the photodetector when the gap length is increased, or backreflections from the couplers. By comparing the Figure 5 with Figure 10, we find that the Kirchhoff approach offers a better correlation with the obtained experimental results.

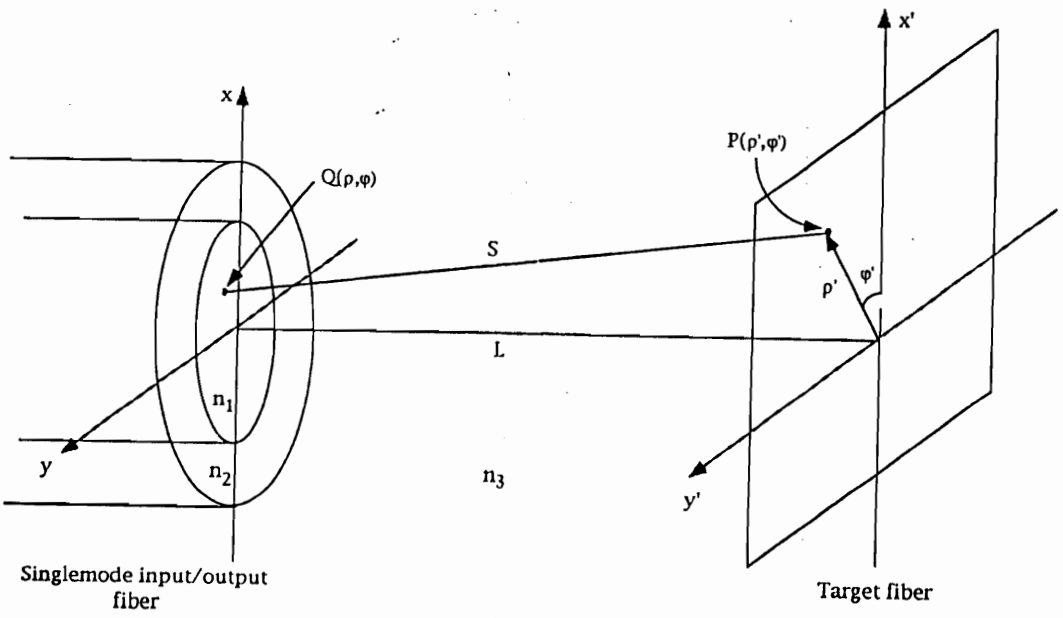

Figure 6. Coordinate system for the Kirchhoff analysis.

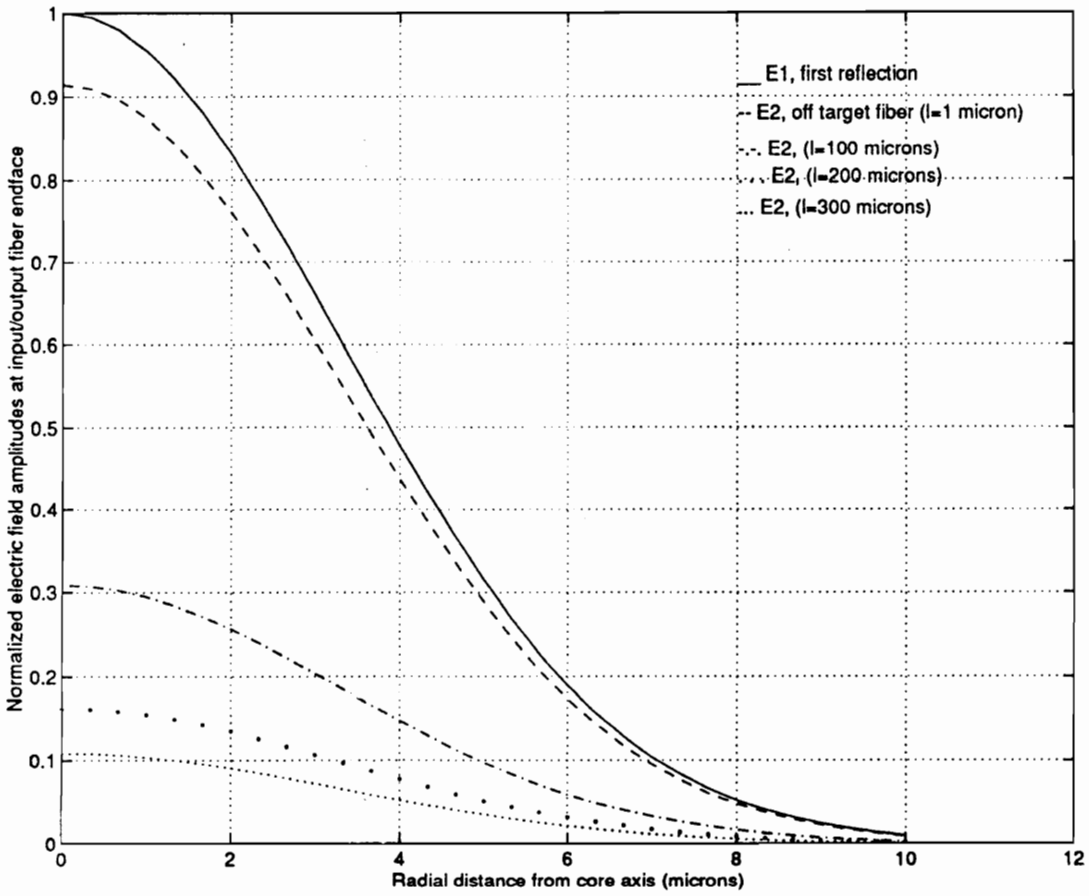

Figure 7. Normalized electric-field amplitude versus radial distance from the core center at the input/output fiber, taken at different gap lengths.

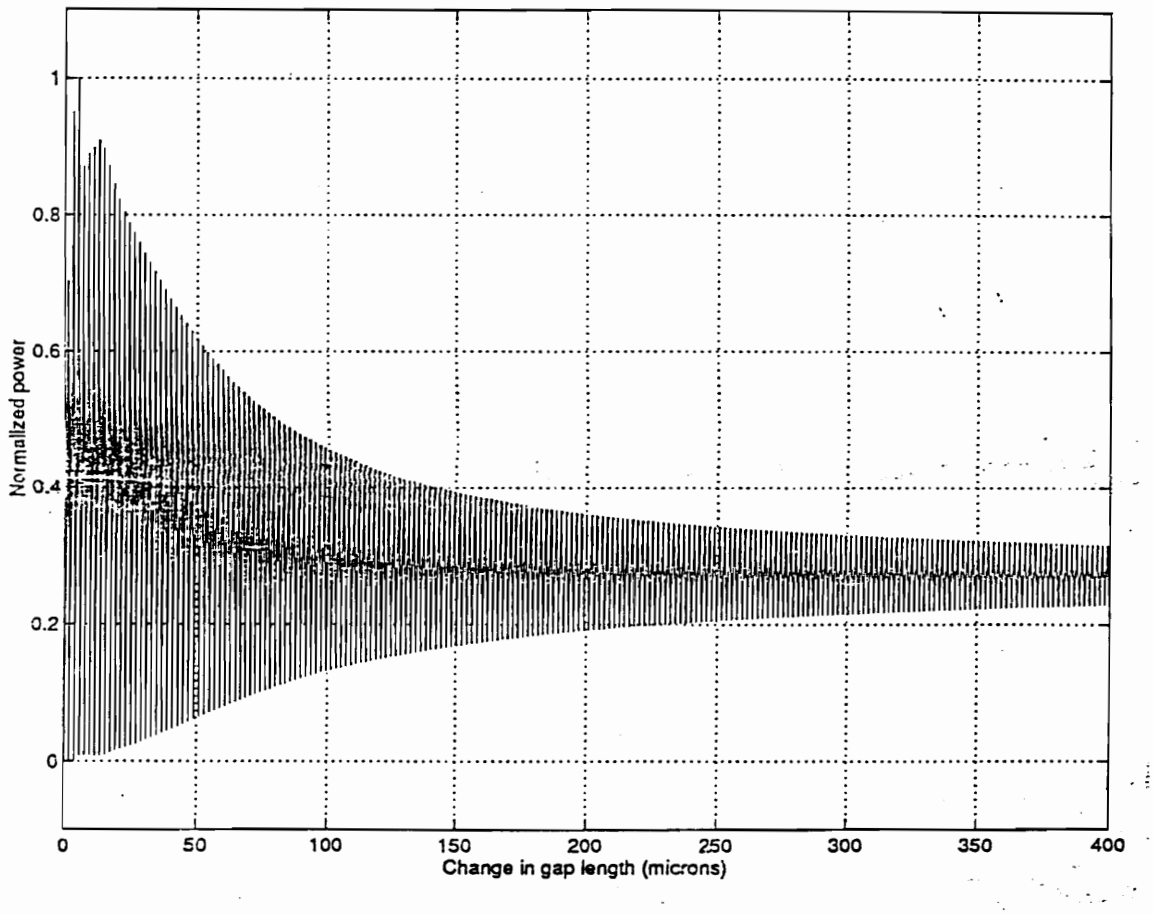

Figure 8. Normalized output power versus gap length (0 - 400 μm).

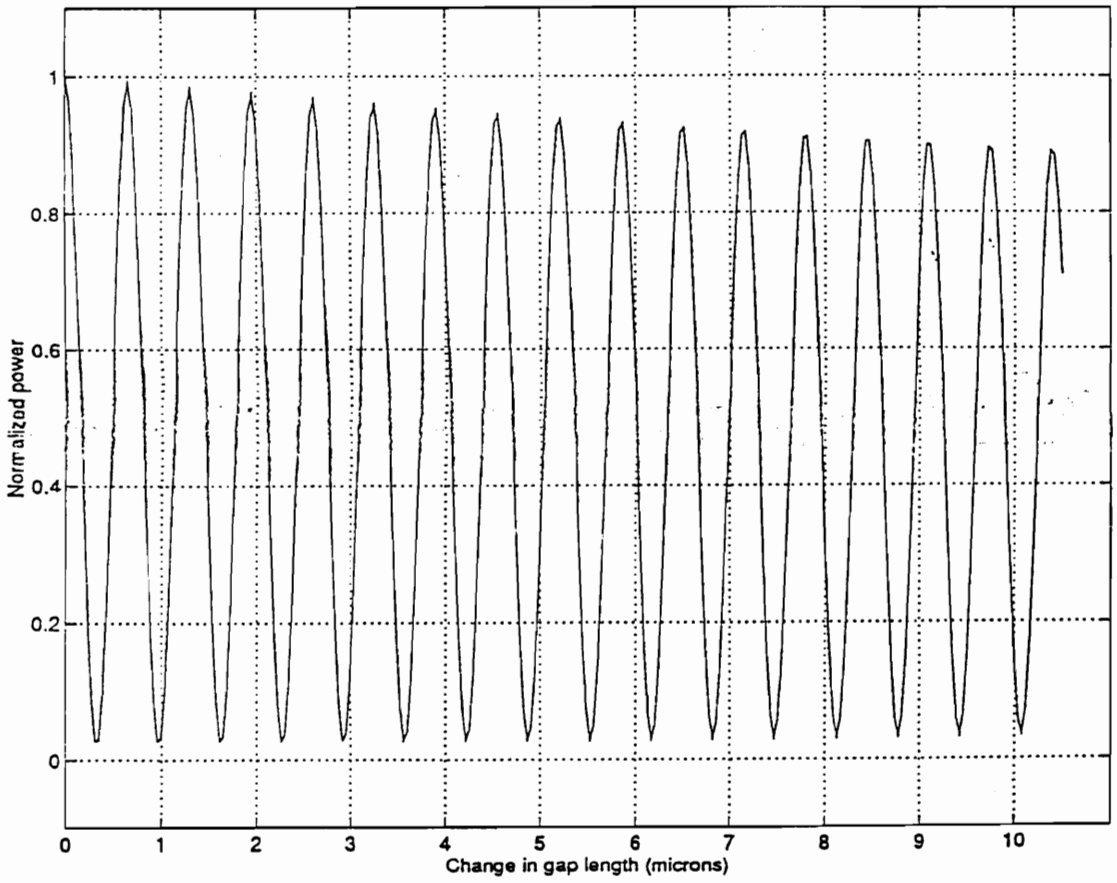

Figure 9. Normalized output power versus gap length (19.5 - 30 μm).

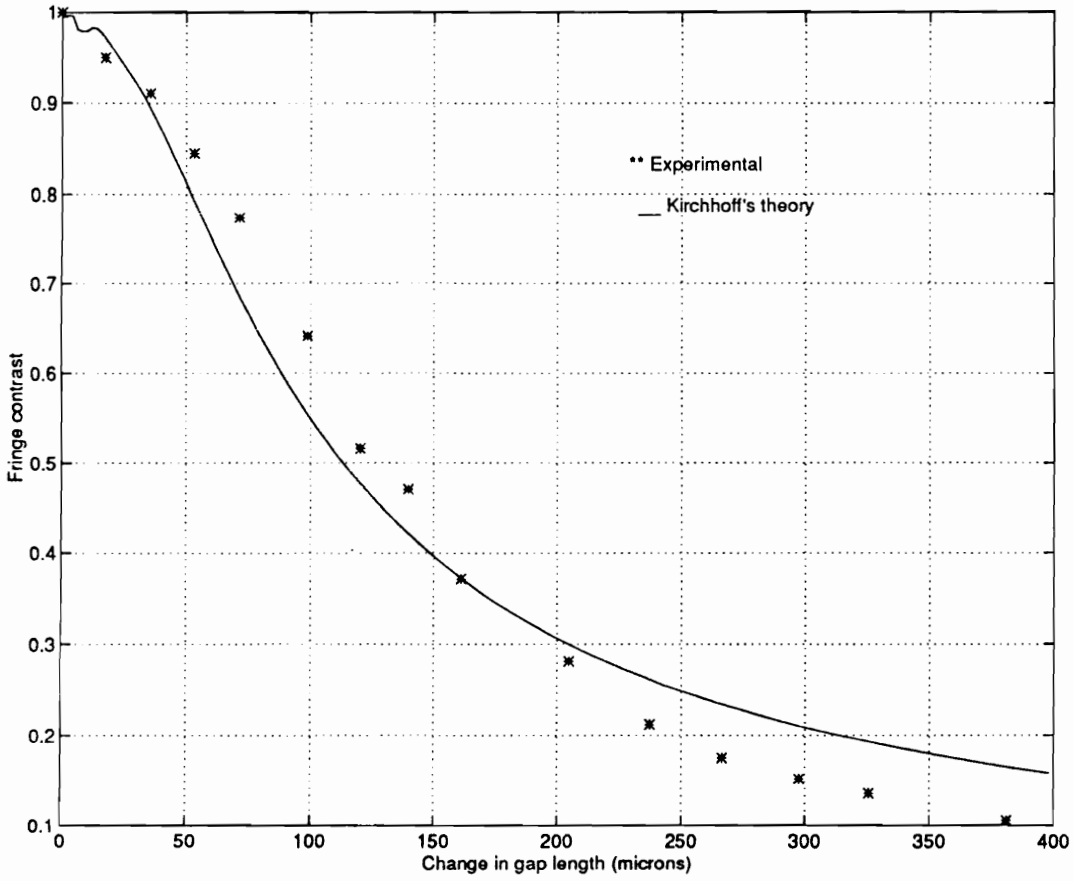

Figure 10. Fringe contrast versus gap length, comparing Kirchhoff's analysis approach with experimental results.

2.4 Absolute EFPI Principle of Operation

The following provides a brief analysis of the absolute EFPI (AEFPI) system used in this dissertation. An in-depth analysis of the AEFPI sensor is given by Bhatia. [56] The intensity, I, at the output of an EFPI is described by

$$I = I_0 \cos\left(\frac{4\Pi}{\lambda} L\right), \tag{11}$$

where I_0 is the maximum value of the output intensity, L is the gap separation, and λ is the laser diode center wavelength. A change in the gap separation, L, caused by an external perturbation such as strain, results in a sinusoidal modulation of the output intensity, I. If a change in direction of the applied strain occurs at a maxima or a minima the system will be unable to detect it, unless quadrature phase shifted EFPIs are used.[35] Still, the EFPI system can only be used to monitor relative strain changes, and cannot be used to monitor absolute strain; once the EFPI system is turned off, strain information is lost.

The AEFPI system uses a superluminscent diode (SLED) instead of a laser diode and is based on the concept of white light interferometry. The signal processing is done using a spectrometer, followed by a personal computer, as shown in Figure 11. Two wavelengths, λ_1 and λ_2, which are 2π out of phase are determined from the spectrometer and the gap separation, L, is calculated using

$$L = \frac{(\lambda_1 \lambda_2)}{2(\lambda_2 - \lambda_1)}. \tag{12}$$

By coating the fiber endfaces inside the hollow-core fiber with a high purity gold, a high-finesse Fabry-Perot cavity is made. The sensitivity of the overall system can be improved by increasing the Finesse, F,

$$F = \frac{\Pi\sqrt{r}}{1-r}, \tag{13}$$

where r is the reflectivity of the endface.[54] Typical output response from an AEFPI sensor is shown in Figure 12.

The AEFPI system can detect temperature changes as small as 2° C and strain changes as small as 100 μm.[57] Since the system is not differential in nature, it does not require a reference measurement to be made prior to the actual sensing procedure, an absolute measurement is made each time the system is turned on. Due to the scanning time needed by the spectrum analyzer, this system is only suitable for quasi-static measurements.

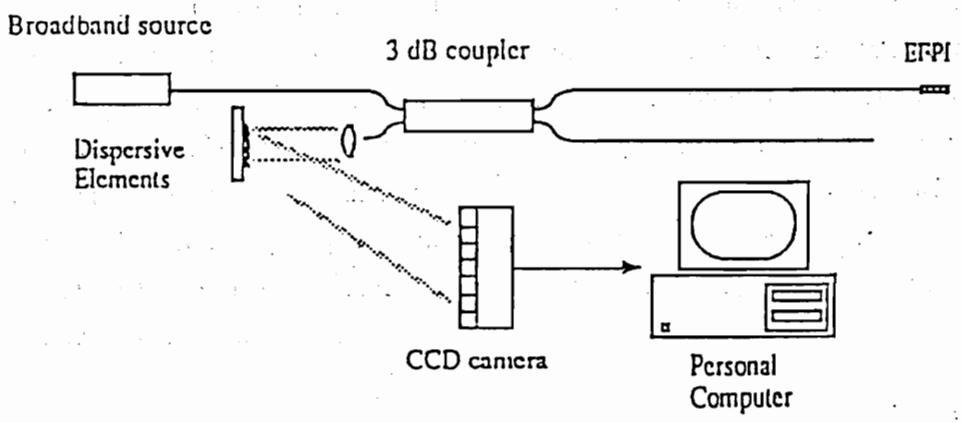

Figure 11. Setup of the Absolute EFPI (AEFPI) system.

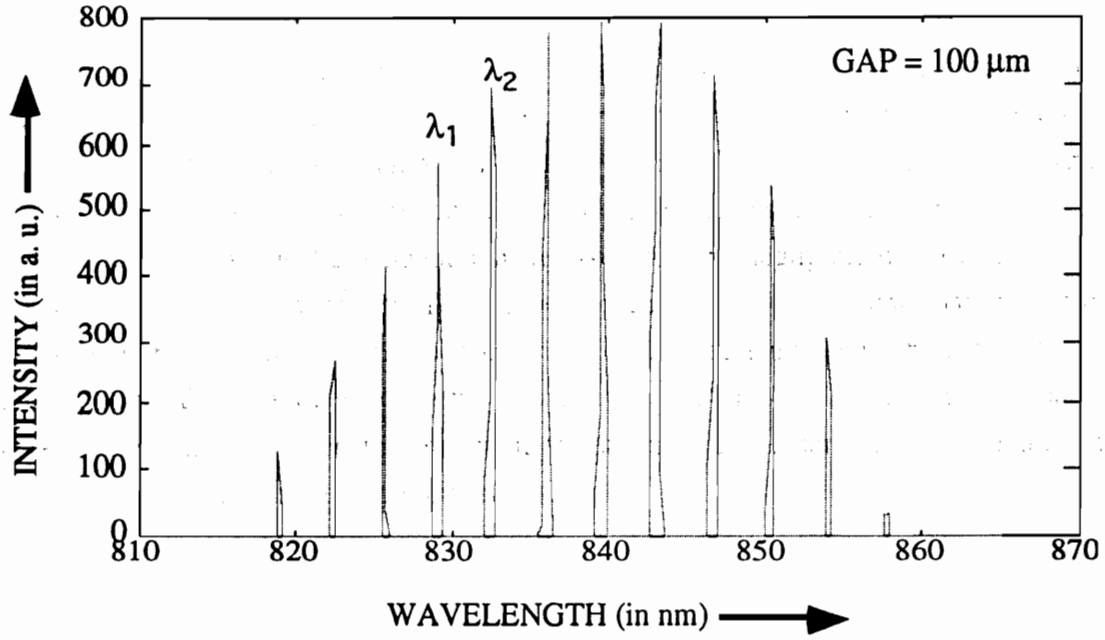

Figure 12. Typical Output of the AEFPI system.

Chapter Three

Experiments

The importance of implementing optical fiber sensors into civil structures for monitoring structural integrity was discussed in Chapter 1. So far, however, only a few field tests implementing optical fiber sensors in concrete have yielded quantitative results. Currently with the rapid deterioration of existing structures and the increasing implementation of composite materials into advanced civil structures, there is a growing need to implement fiber-based gages that can nondestructively, quantitatively, and accurately assess structural integrity. This chapter discusses quantitative experimental results obtained from a series of experiments using EFPI-type optical fiber sensors in a variety of civil structure applications. The first section describes experiments, performed in cooperation with Dr. Sami Masri *et al.* at the Civil Engineering Department at the University of Southern California, Los Angeles, that concentrate on obtaining strain information from reinforced concrete interior and exterior column-to-beam connections. The second section describes results from strain tests, performed in cooperation with researchers at the United States Bureau of Mines in Spokane, Washington, on roof bolts used in mines. The third section describes the experiments, performed in cooperation with researchers at the Turner Fairbanks Federal Highway Administration in McLean, Virginia, that focused on using absolute EFPI (AEFPI) sensors for monitoring strain on composite prestressing strands used for reinforcing concrete. The last section discusses the performance of EFPI sensors as they were cyclically loaded for more than 100,000 cycles.

3.1 Column-to-Beam Connections

The design of reliable civil structures in earthquake prone areas is complicated. Complex designs that make the structure more reliable and resistant to earthquakes may not be economically feasible. Those designs may in fact complicate structure construction and thus make construction cost-prohibitive. For the column-beam interconnects, these economical factors play an especially large role. The beam for such interconnects is usually designed to fail before the column fails because beam failure is considered to be less detrimental to the overall structure than column failure.

In the case of the beam-column assembly, the panel zone (PZ), is the area of most interest.[61] In future designs, as well as in determining the structural integrity of the joint in laboratory experiments for example, it will be very important to monitor the strain concentrations along the different sections of rebars in the panel zone. In most design codes the effects of vertical ground motion are assumed to be negligible or a fraction of the horizontal ground motion.[58,59] But in some earthquakes it has been found that the vertical ground motion was more significant than was originally thought when the structure was designed, with the consequence that the structure did not survive the earthquake. Optical fiber-based gages were used to instrument the structure's interconnections to study the effects of earthquakes on the interconnections.

3.1.1 Internal Connections

The first test specimen was a 1/3 scale model of a multistorey frame joint. The size of this specimen was governed by the size of the loading machine. In order to ensure that failures occurred in the panel zone, the weak-beam strong column approach was not adopted. Details of the specimen are shown in Figure 13 and a photograph of the test specimen is shown in Figure 14.

Ordinary portland cement type II was used with an aggregate size less than 0.375 inch, and a water-to-cement ratio of 0.76, by weight. The mix had a 5 inch slump and after 28 days yielded a 27 MPa average strength. Grade 60 reinforcing steel with a yield stress larger

than 410 MPa and a tensile strength of 520 MPa was used. For the longitudinal reinforcement of the beam and column, number 3 deformed rebars were used. The stirrups used number 2 smooth bars.[60]

A general setup of the apparatus used to perform the dynamic loading on the column-beam joint specimen is shown in Figure 15. Steel angles were bolted to each of the cross-beam specimen ends and covered with 13 mm thick plates. Links and baseplates were used to ensure that proper boundary conditions were maintained. The specimen was tested in the horizontal plane as shown in Figure 15. The USC Dual Seismic Shake table system used for this experiment was designed to impose dynamic loads that lie in the seismic frequency range. It consisted of two shake tables, with hydrostatic bearings, two hydraulic actuators with servo valves, two hydraulic service manifolds and a servo hydraulic power supply. The hydraulic actuators each had a ± 2 inch stroke and a ± 25 kN static capacity. Linear voltage differential transducers (LVDT) were mounted, close to the panel zone, to provide deflection information. [60]

The fiber optic strain gages were placed on the main rebar and on selected beam and column stirrups. The rebar and stirrup surfaces were ground to the required smoothness at the appropriate gage positions prior to attachment. The EFPI sensors were attached to the rebars using an epoxy adhesive and then covered with a silicon layer for waterproofing. Figure 16 shows the locations of the strain gages, and Figure 17 shows a photograph of the overall view of the test article.

Conventional foil strain gages were collocated on the rods with each EFPI sensor to allow direct data comparison. The specimen was poured with concrete and finished without significant fiber sensor or foil strain gage damage. Specimen dimensions measured 13 cm x 15 cm in cross-section, with a short beam length of 0.78 m and a long beam length of 1.59 m. This specimen was designed to allow the interrogation of different internal strain vector components on different rods during fatigue loading, with *a priori* knowledge of the anticipated ratios of strains to be experienced at the different locations. Each EFPI sensor was configured to yield only the strain component parallel to the long axis of the rod on which it was attached. Fatigue loading was performed on a large horizontal load frame capable of independent motions of each of the two ends of the long beam. Cyclic fatigue

loading of the specimen began with displacements of one end of the beam 0.508 cm from the horizontal quiescent position, and increased through steps to a maximum displacement of 5.1 cm. Typical comparative strain data obtained for sensor S3 (shown in Figure 15) for cyclic displacements of 0.76 cm are shown in Figure 18. Note here, both the general agreement between the fiber sensor data (upper trace) and the foil strain gage data (lower trace), and that both measure the periodic dead zones caused by the dynamics of the load frame. Also note that the optical fiber sensor has a much better signal to noise ratio than its collocated foil strain gage. Electromagnetic interference caused by electronic switching transients are clearly visible near the center of the foil gage data record.

Figure 19 shows the increase in the local crack opening displacement, measured by a similar EFPI sensor located at position S7 as the beam was cyclically loaded and the beam tip displacement was increased in steps of 0.1 inch. Here, the sensor was configured as shown in Figure 1 except the epoxy bonds indicated were not applied. The sensor was attached to the surface of the cross-beam at two locations on opposite sides of the anticipated location of a crack. Since the lead-in/lead-out fiber and reflector fiber ends inside the hollow core sensor tube are allowed to move back and forth, no mechanical load is applied directly to the glass parts of the sensor.

Figure 20 shows the onset of additional concrete cracking in a different way. Here raw intensity output data from sensor S7 was obtained as the beam tip displacement reached 1 inch. The slowly varying intensity output fringes to the left of the top trace indicate a gradual increase in local strain until the local crack expands rapidly, resulting in large local relative displacements across the crack, and a strain redistribution within the local region of the concrete. Subsequent compression closes this now large crack, with little change in local relative displacement, and following tension again opens the crack. Additional local cracking is observed as an interruption in the regular fringe envelope seen in the right of this trace.

The EFPI fiber sensors provided calibrated quantitative measurements of strain during the entire fatigue loading test. Figure 21 shows a comparison between raw data obtained from the EFPI sensor (top) and the collocated foil strain gage (bottom) as the displacement amplitude was gradually decreased at the end of the tests. Recall that the number of

periodic fringes in the EFPI output intensity signal is related to the amplitude of the strain signal.

Simple force-deformation results, for the test article are shown in Figure 22. The analysis of the force deformation results is beyond the scope of this dissertation, but is presented by Higazy.[60,61]

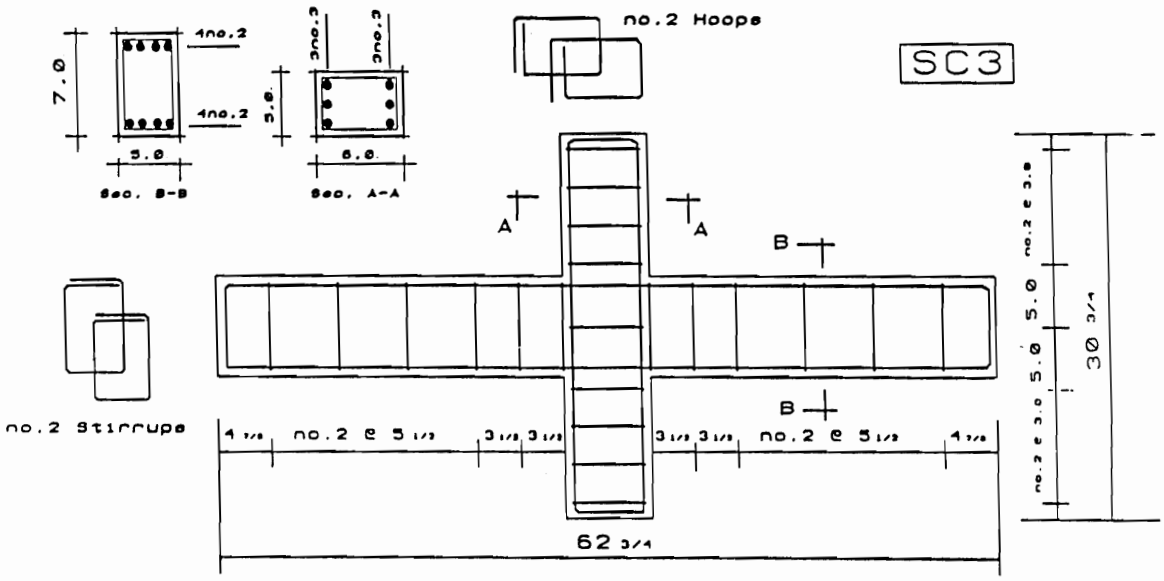

Figure 13. Details of the Reinforced Concrete Test Structure.[60]

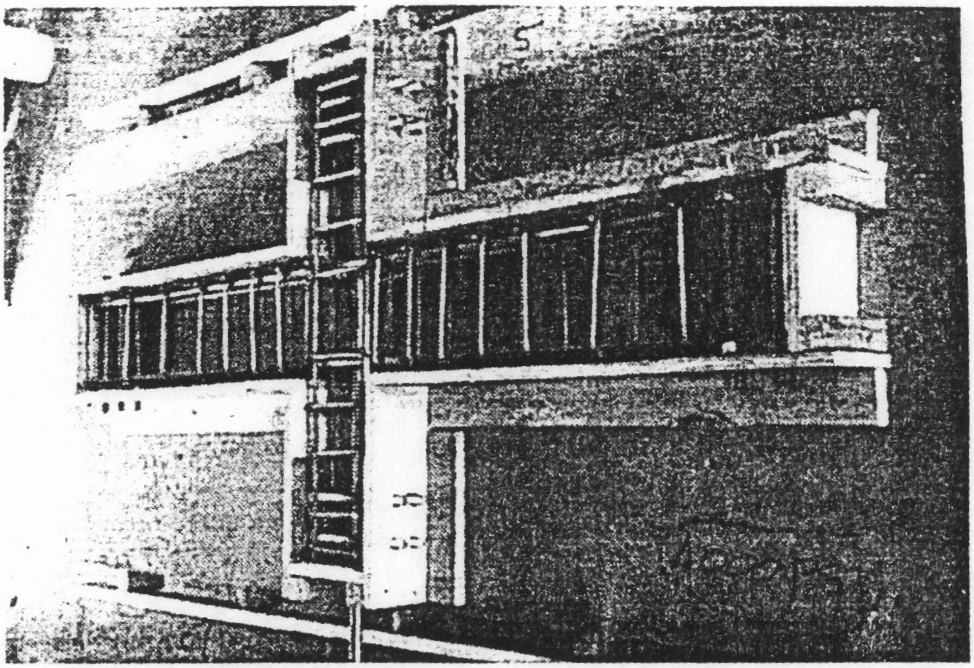

Figure 14. Photograph of the Fabricated Test Specimen.[60]

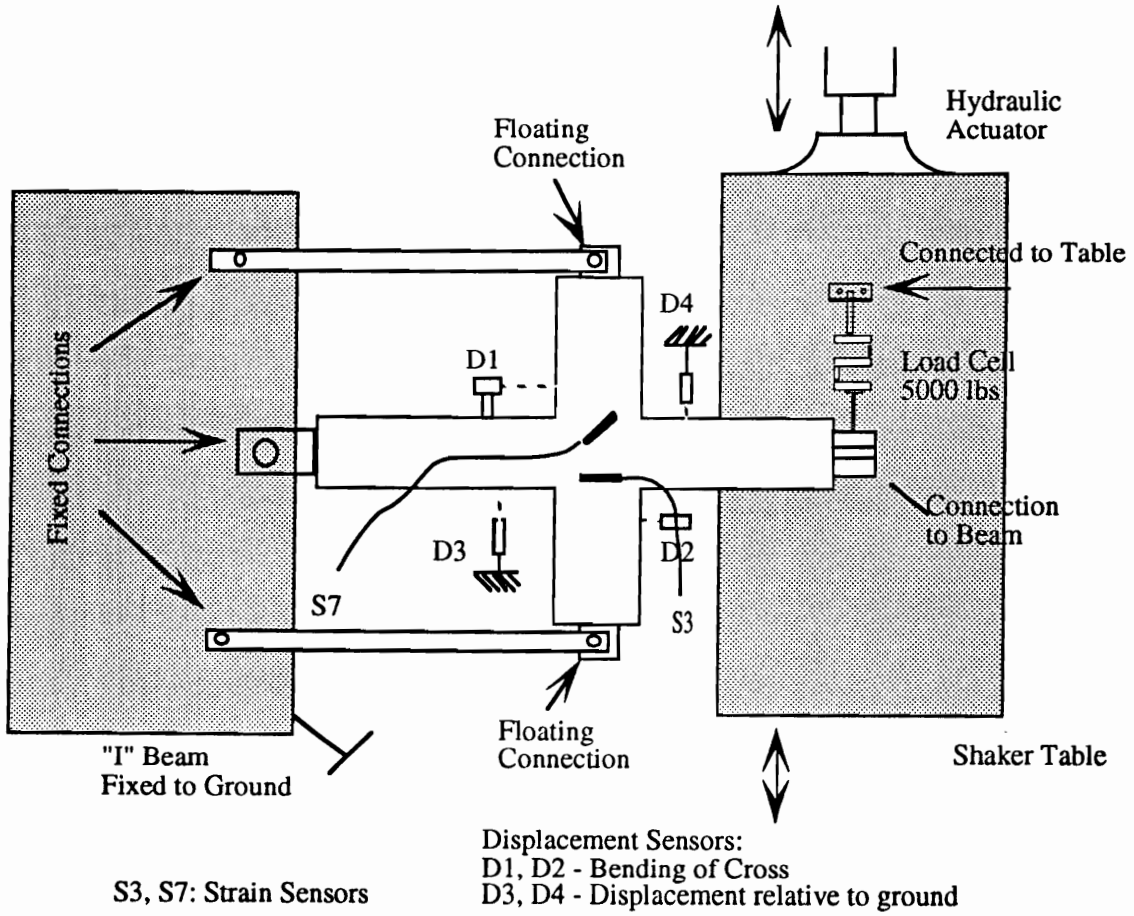

Figure 15. Geometry of reinforced concrete cross-beam and the test apparatus used to impose dynamic loads.

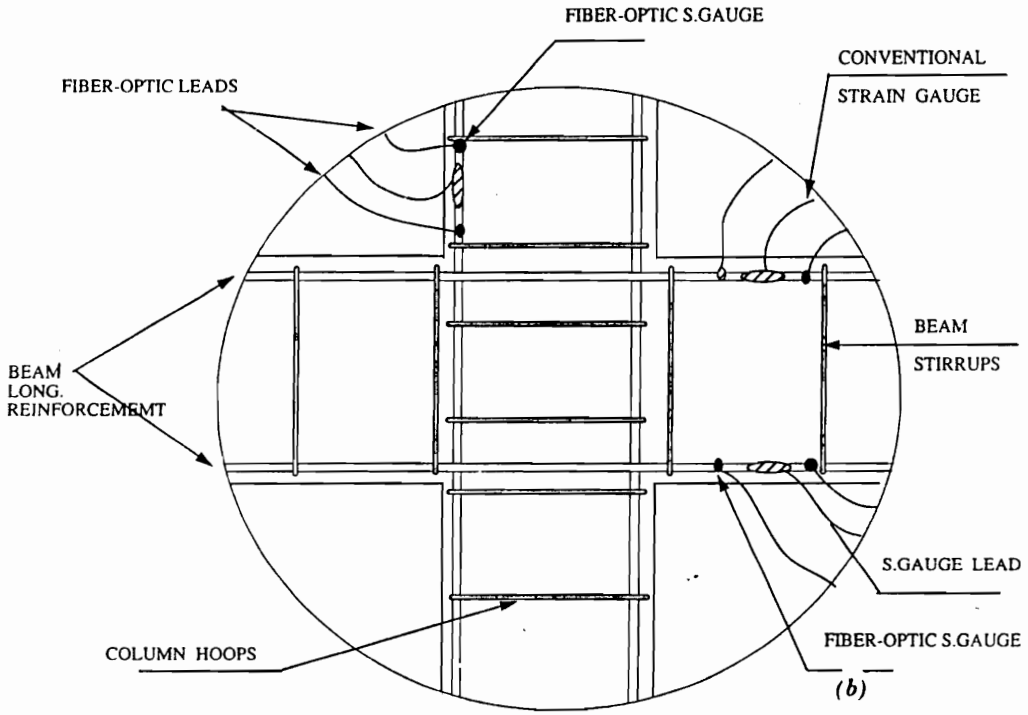

FIG. 7. (*Continued*)

Figure 16. Sensor Locations.[69]

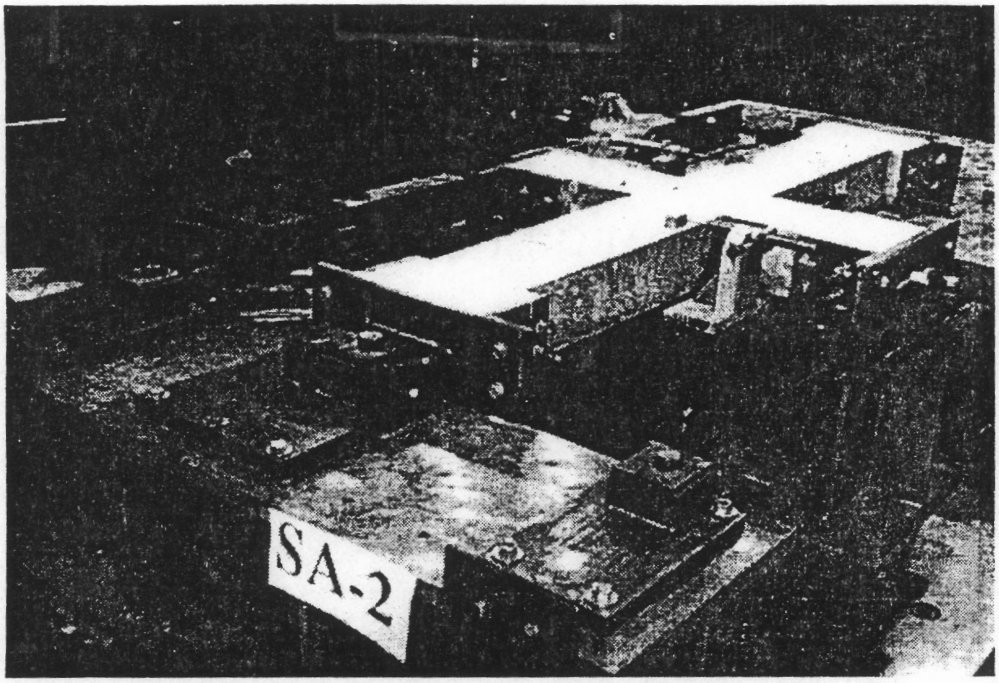

Figure 17. Photograph of the overall view of the test article.[60]

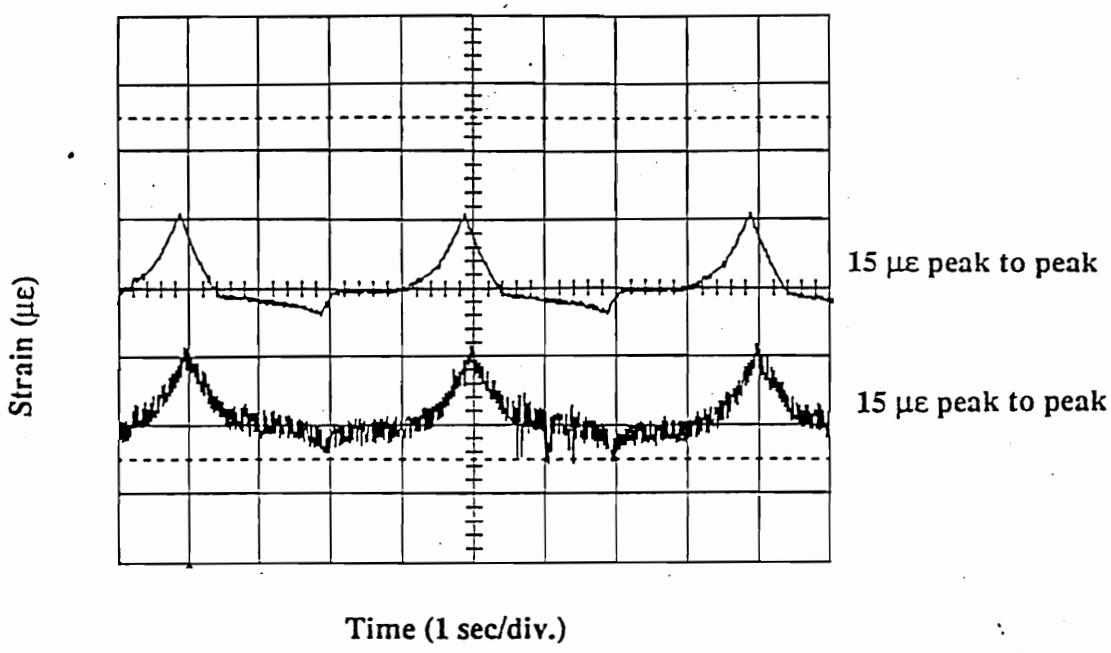

Figure 18. Comparative strain data obtained for EFPI sensor S3 (top) and collocated foil strain gage (bottom) for cyclic displacements of 0.76 cm.

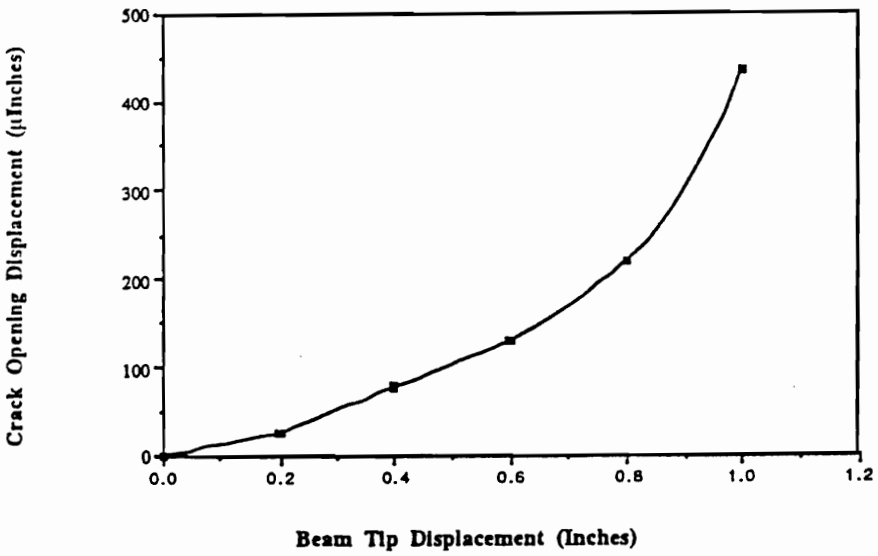

Figure 19. Crack opening displacement versus beam tip displacement, measured by sensor S7.

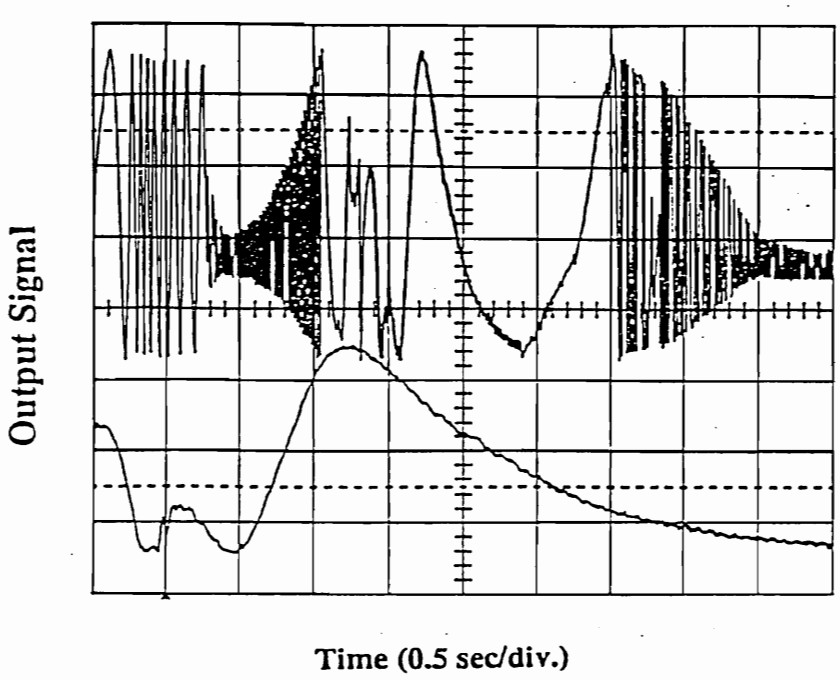

Figure 20. Onset of concrete cracking measured during fatigue loading of sensor S7.

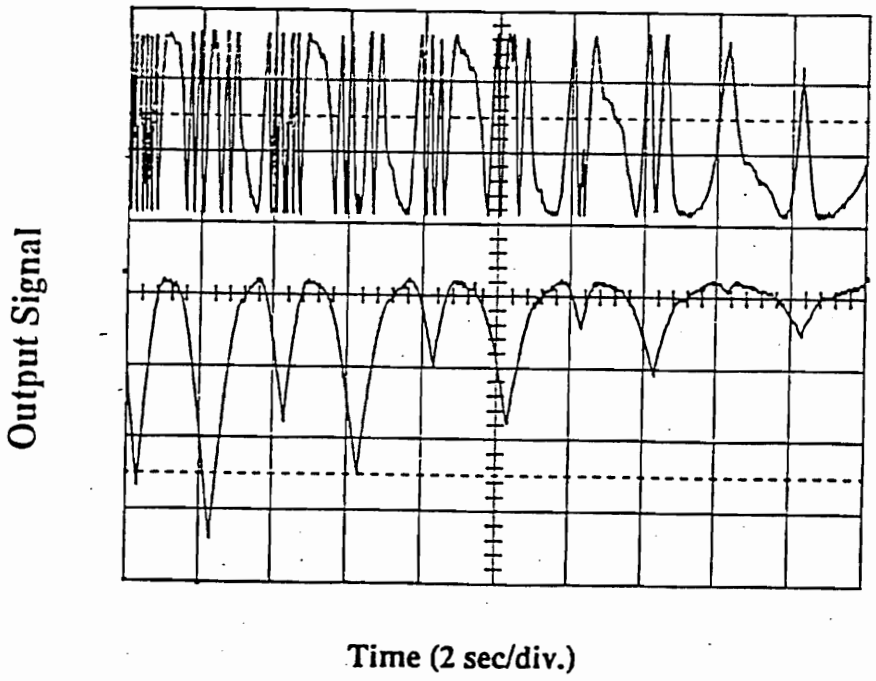

Figure 21. Comparison of embedded EFPI (top trace) and foil strain gage data (bottom trace) as loading amplitude is decreased at the end of the test.

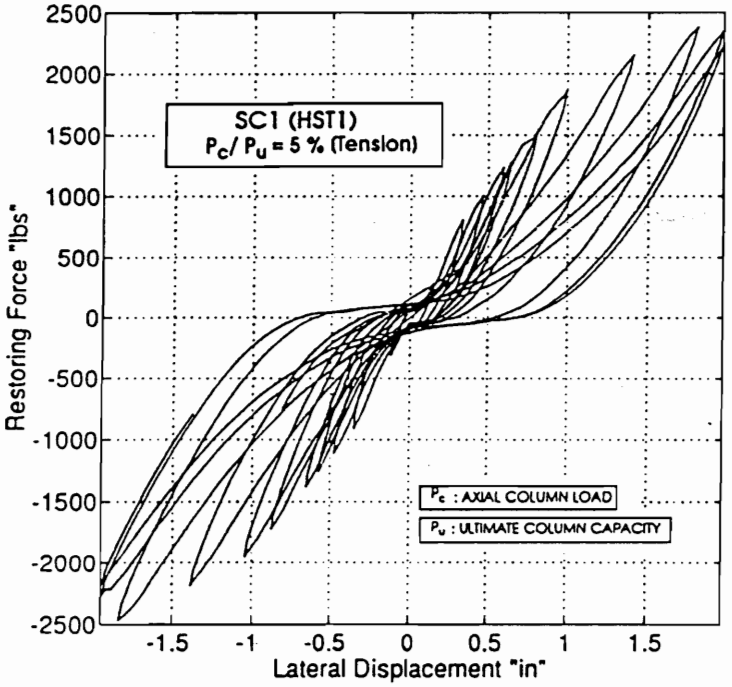

Figure 22. Sample Force-Deformation Results for the Test Structure.[6]

3.1.2 External Connections

Due to the success of the 1/3 scale interior column-beam interconnect specimen, a full scale external column-beam interconnect specimen, shown in Figure 23, was designed and constructed at the USC Civil Engineering Department in Los Angeles. Again a rebar cage was constructed and EFPI strain gages, with collocated foil strain gages, were placed on main rebar, and selected beam and column stirrups. The rebar and stirrup surfaces were ground to the required smoothness at the appropriate gage positions, prior to attachment, and a silicon layer was used for waterproofing the sensors. Figure 24 shows the locations of the fiber optic strain gages and Table 2 lists the sensor number, fiber gage length, and the appropriate locations for each fiber optic sensor. Due to unforeseen delays, the specimen was not poured with concrete for 6 months after the sensors had been attached, and the actual tests were not performed until 3 months after the concrete had set. These delays did not affect the performance of the gages. Figure 25 gives the locations of the LVDTs used to monitor relative beam and column displacements.

The EFPI strain gages were configured to yield only the strain component parallel to the long axis of the rod on which it was attached. To determine which sensors had survived the embedding process, small cyclic loads were applied to the specimen. All sensors showed a response. With the setup that was used only two sensors could be monitored, and it was therefore decided to dedicate one channel to monitoring one sensor throughout the entire test and to use the other channel to periodically switch over to the other sensors.

Specimen dimensions, as given in Figure 24, were 8 x 16 x 63 inches for the beam, and 12 x 12 x 108 inches for the column. The column-beam interconnection was tested in the vertical plane as can be seen in the photograph in Figure 26. The beam tip was displaced at a constant rate and the periodic loading cycle shown in Figure 27 was used for the beam tip displacements shown in Table 3.

Typical comparative strain data obtained from sensors at BL2 and BL5 for beam tip displacement from 0 to 0.5 inches are shown in Figure 28. Here, note the general agreement between the sensor located at BL2, upper graph, and the sensor located at BL5, lower graph. The upper traces on both graphs are expansions of the lower traces. Figure

29 shows typical EFPI fringes as the beam tip is displaced from 1 to -1 inch, placed at rest, and displaced from -1 to 1 inch. The top trace of each graph shows an expansion of the actual signal that was obtained. The oscillations, apparent in the bottom graph (sensor BL5), indicate that the lead-out fiber was squeezed somewhere inside the concrete. This random-bending of the fiber caused light output signal fluctuations at the detector. The lead-out fiber for BL5 was destroyed during the -2 to 2 inch loading cycle series.

Figure 30 summarizes all the data that was obtained from fiber optic sensor BL2. The horizontal axis indicates the maximum displacement of the beam, as it was displaced from its minimum position, through zero, to its maximum position. The vertical axis accounts for the total change in strain as the beam moves from its minimum to its maximum position and consists of both compressive and tensile strain. At first glance, the data in Figure 30, looks promising and reliable. A closer look at the strain data obtained for sensor BL2, however, will show that the data is not valid for strains greater than 10,750 μstrain. Sensor BL2, with a gage length of 1.395 cm and an initial gap separation of 75 μm, cannot measure compressive strains greater than 5,375 μstrain. Therefore, for the loading cycle, the total change in strain cannot be greater than 10,750 μstrain. For compressive strains greater than 5,375 μstrain, either the fiber endfaces in the air-cavity will touch and damage each other, or the epoxy-bond between one of the hollow core fiber ends and the solid core fibers will be broken. In this particular case we can assume that the epoxy bond broke, and that the gage length is no longer reliable once the compressive strain exceeded 5,375 μstrain. The total strain data up to 10,750 μstrain however should be reliable and this data is shown in Figure 31.

Towards the end of the test, after the beam was already severely damaged, other sensors in locations not damaged were monitored. For example, the response from sensor BT1 is shown in Figure 32. Since this sensor was not monitored since the beginning of the experiment, and because the beam was already severely damaged, this result does not provide any useful information other than that the sensor survived.

Unfortunately, for this experiment, data from the foil strain gages was not available for comparison. The foil strain gage did survive the specimen fabrication process, but,

possibly due to improper installation procedures, none of the gages were able to provide reliable data.

Table 2. Sensor Locations.

SENSOR SPECIFICATIONS		
Sensor #	Gage Length (mm)	Location
1	15.24	CL1
2	11.60	CL2
3	13.76	BL1
4	15.54	BL5
5	13.78	
6	13.95	BL2
7	15.84	
8	15.24	CT4
9	13.56	
10	13.90	CT2
11	15.73	
12	11.25	
13	13.78	BL6
14	12.75	BT1
15	16.61	BL3

Table 3. Beam-tip Displacements.

Test	Deflection (inches) Max	Min	Number of Periods
1	0.1	-0.1	3
2	0.2	-0.2	3
3	0.3	-0.3	3
4	0.4	-0.4	3
5	0.5	-0.5	3
6	0.75	-0.75	3
7	1.0	-1.0	3
8	1.5	-1.5	3
9	2.0	-2.0	3
10	2.5	-2.5	3
11	3.0	-3.0	2
12	4.0	-4.0	2

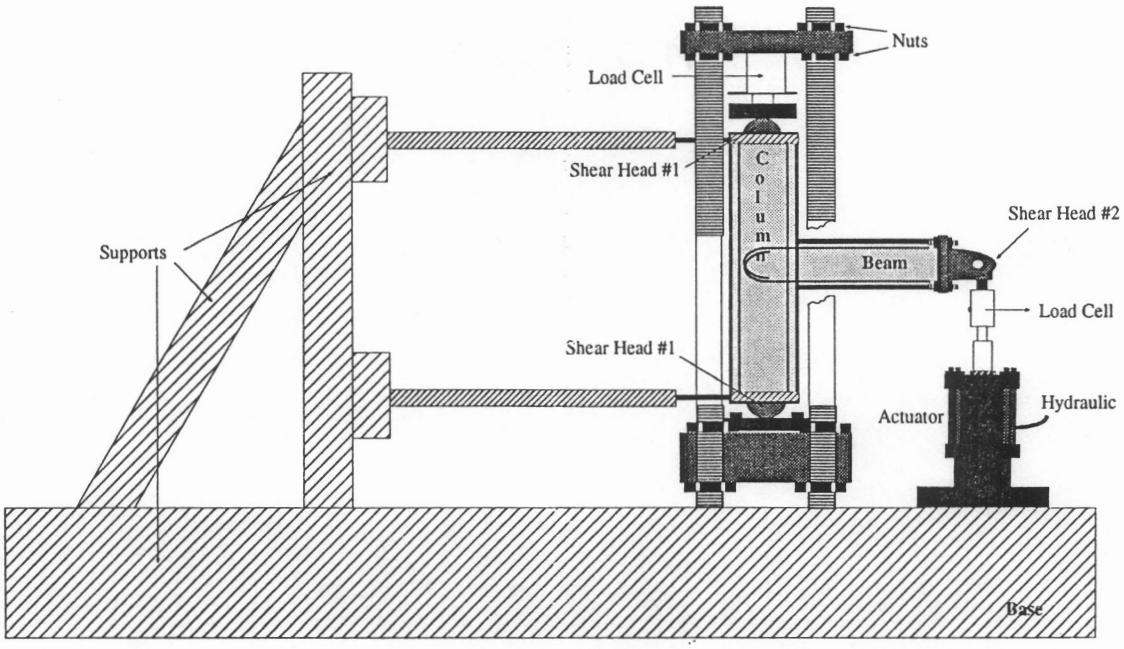

Figure 23. Overview of the external column-to-beam setup used to impose dynamic loads.

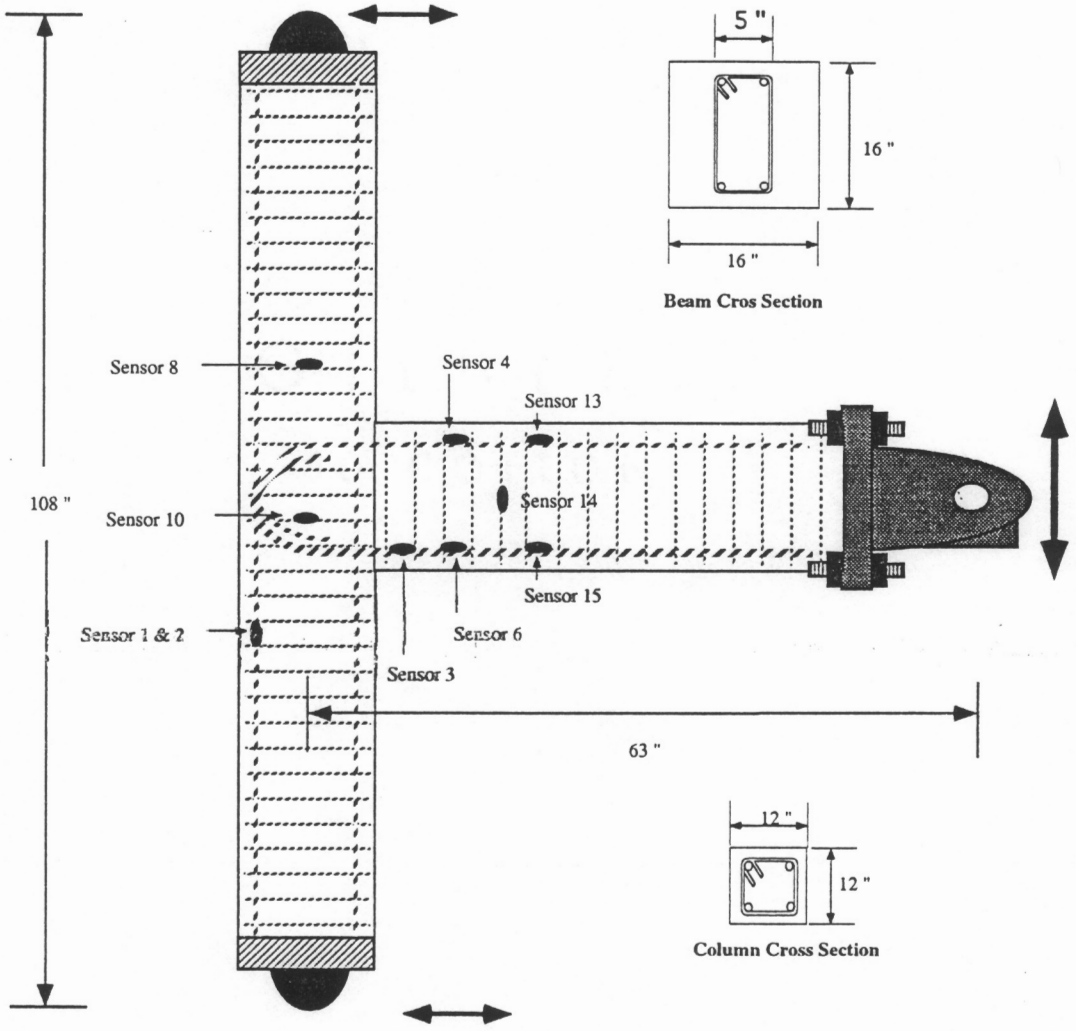

Figure 24. Dimensions of the specimen and location of the fiber optic and collocated foil strain gage sensors.

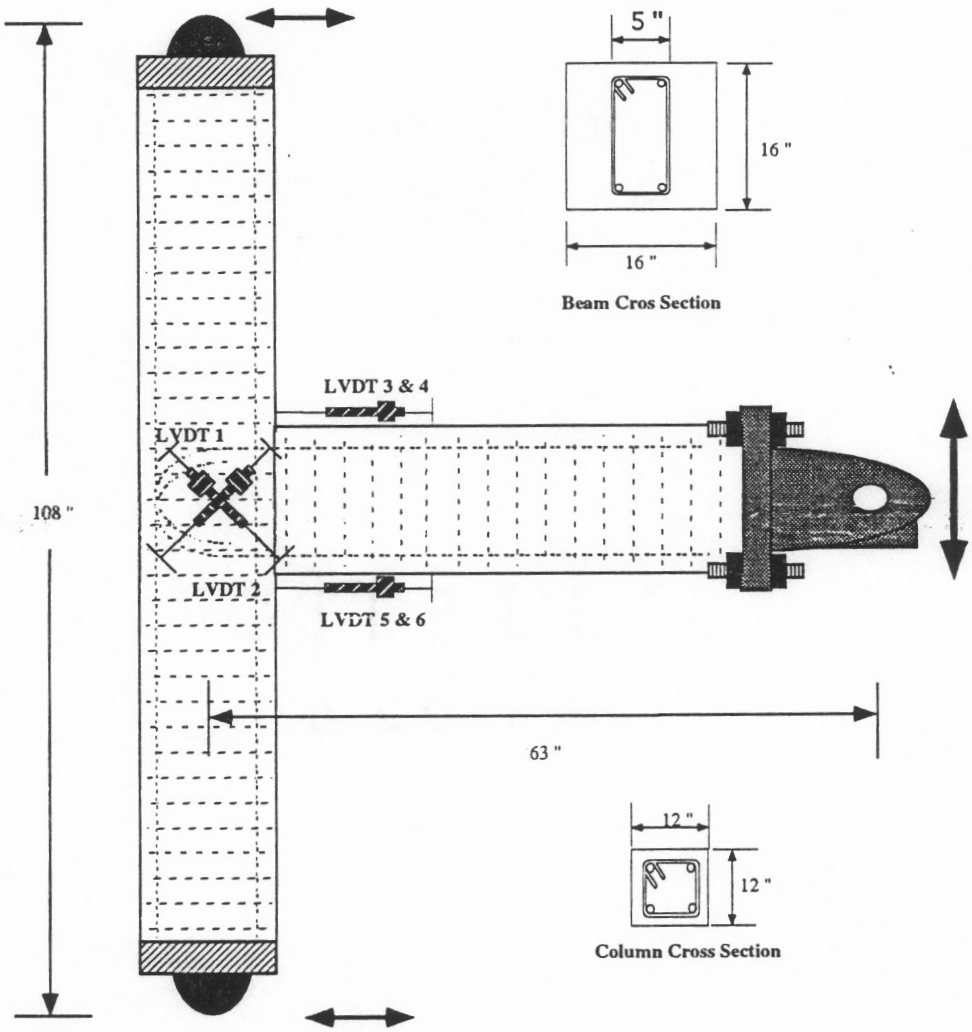

Figure 25. Location of the linear voltage differential transducers (LVDTs).

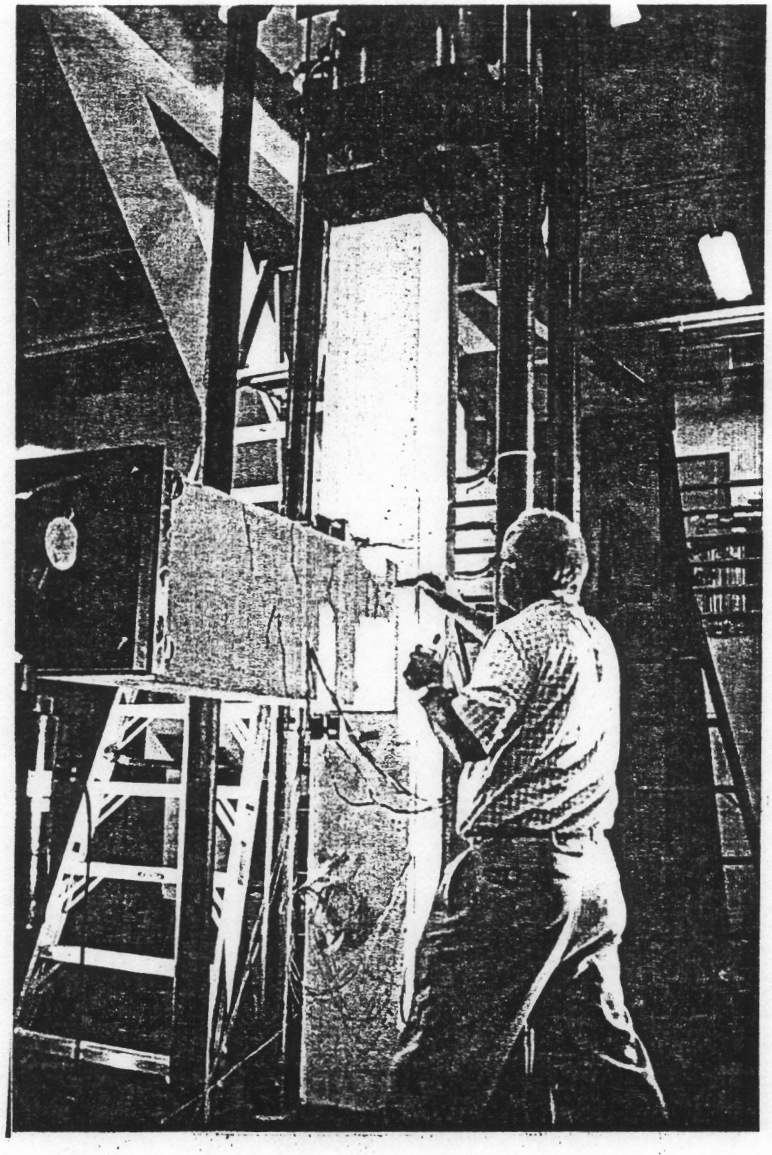

Figure 26. Overall photograph of the column-to-beam interconnection.

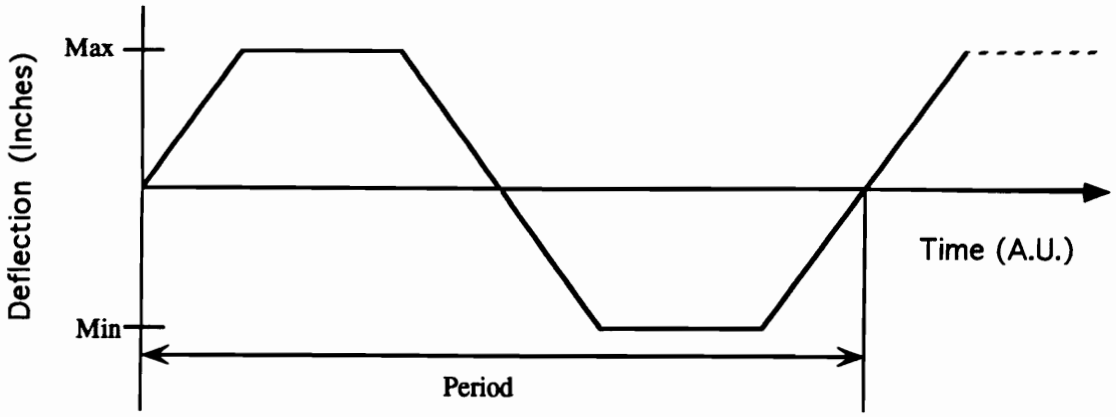

Figure 27. Periodic loading cycle used for displacing the beam-tip.

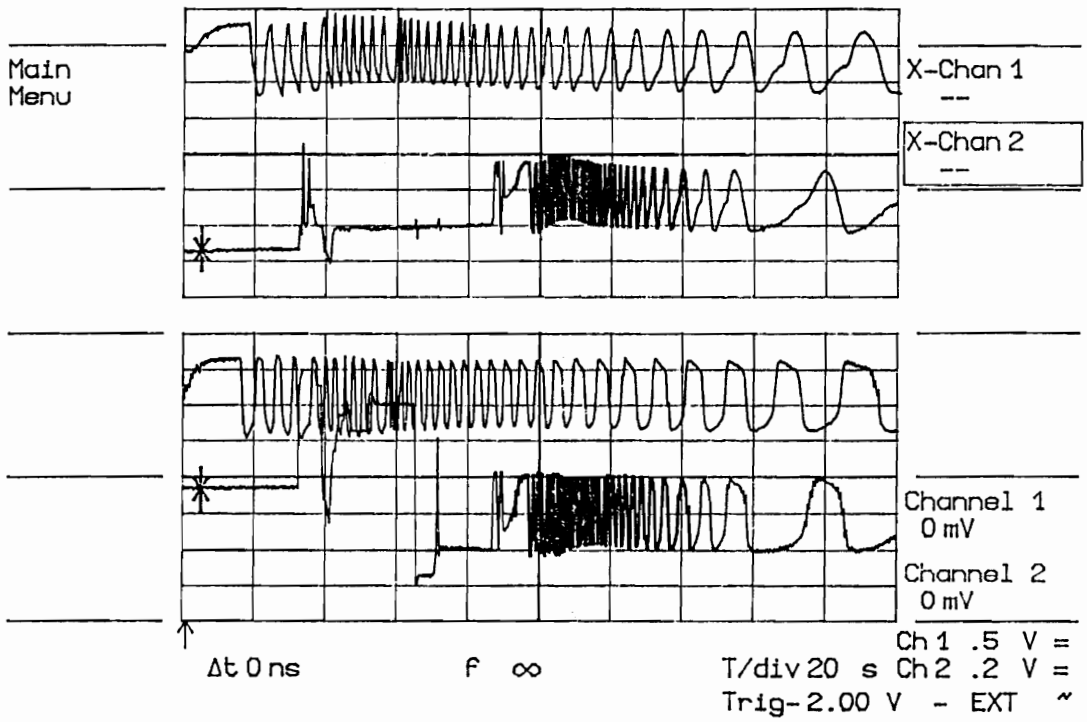

Figure 28. Comparative strain data obtained from sensors located at BL2 (top graph) and BL5 (bottom graph), for the beam-tip displacement from 0 to 0.5 inches.

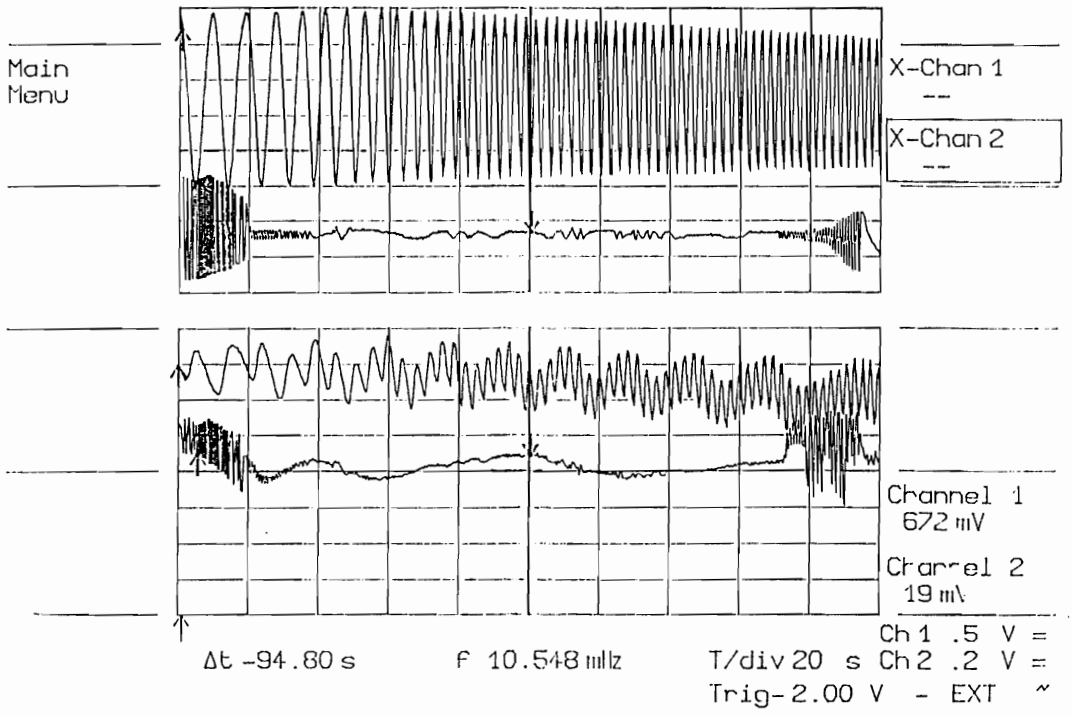

Figure 29. Typical EFPI fringes as the beam is displaced from 1 to -1 inch, placed at rest, and displaced from -1 to 1 inch.

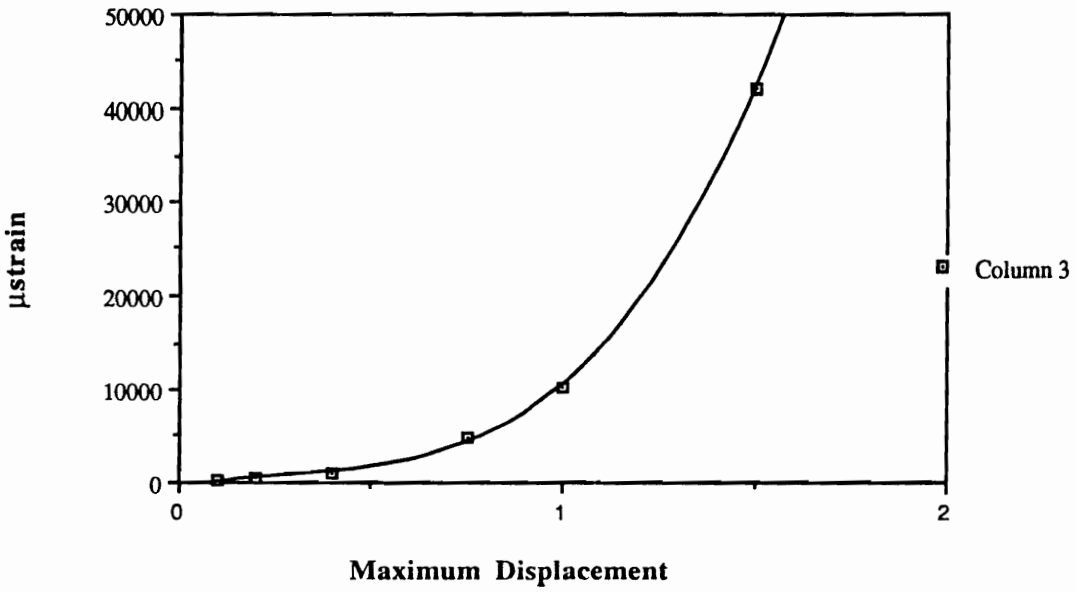

Figure 30. Strain data obtained from sensor BL2.

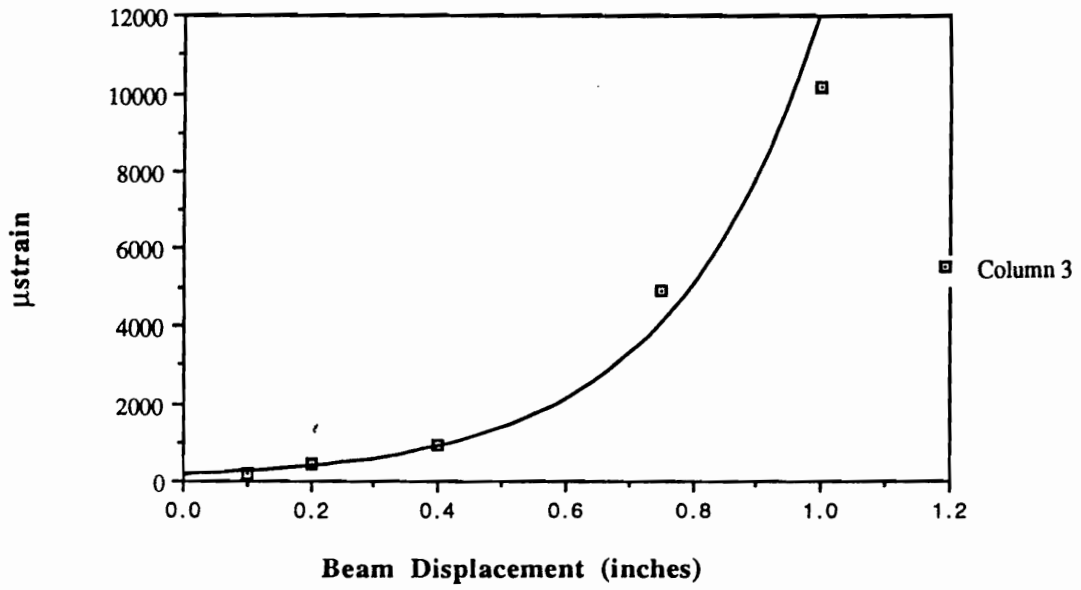

Figure 31. Corrected strain data from sensor BL2.

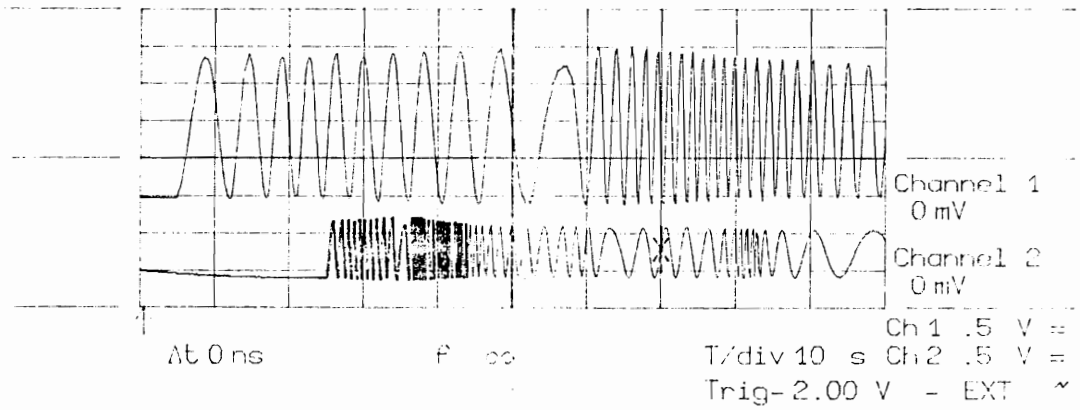

Figure 32. Typical EFPI fringes obtained from sensor BT1.

3.2 Mining Bolt Instrumentation

Falling rocks, and the collapse of mining openings, are responsible for 35% of all underground metal mining accidents.[62] Ground control and roof supports in underground mines are therefore very important, and various methods, among which, timber props, steel arches and roof bolts, are currently being used to support mining roofs. Among those methods, the cable-type and rebar-type bolts appear to be the most effective in stabilizing the rock-mass. For rebar-type bolts, steel rods are anchored into the rock, as shown in Figure 33. A disadvantage of the rebar-type bolt is that it is difficult to install large lengths of steel rods. Cable-type bolts are similar to the rebar-type bolt, but they are, due to their inherent flexibility, easier to transport and install. For example, cable lengths of over 50 ft can easily be installed in openings with clearings less than 8 ft, by bending the cable.[62]

Typically bolts are installed into the roof, and sometimes into the wall, by drilling a hole 6 cm in diameter, with the required length. A breather tube and a grout tube are installed along with the bolt. The cement slurry is pumped into the hole through the grout tube, and the air in the hole is displaced through the breather tube. The effectiveness of the bolt is controlled by bolt strength, strain transfer between the rock-mass and the grout, and the strain transfer between the grout and the bolt. When the interface between the grout and the bolt, or between the grout and the rock is broken, the bolt's effectiveness is greatly reduced. A large load on the bolt would also result in the break of interface-bonds, and very high loads can eventually result in bolt failure. When bolts are not pretensioned, they can function as passive supports. But for current uses, bolts are usually pretensioned. Buttons are features that are added to the mining bolt to increase their load carrying capability. For research purposes, and to develop numerical models for analyzing rockmass behavior, bolts are instrumented with gages. Traditional monitoring techniques have proven to be inefficient, unreliable, or difficult to install, and new methods need to be developed.

Ultrasound techniques show a great promise for monitoring rebar-type bolts. Problems arise, however, when corrosion sets in, or bends occur along the length of the bolt. For cable-type bolts, especially when the cable is bent or has a long length, the ultrasound technique is not yet reliable.[63] Goodyear pressure pads can also be used to monitor the

amount of load placed on the bolts, and are easy to install.[64] Finally, foil strain gages and extensometers have been used for monitoring strain along the side of the bolt. While all these methods work relatively well for rebar-type bolts, they are still difficult to implement on cable-type bolts. Also, with most of these methods, monitoring distributed strain along the entire bolt length is impractical, or just not feasible. An optical fiber-based sensor may offer a novel and attractive approach, with advantages over the traditional methods, to instrumenting bolts.

3.2.1 Rebar-type Bolts

A two-inch section, in the middle of a five foot rebar-type bolt, with a 0.42 inch^2 cross-sectional area, was ground to the required smoothness prior to attaching the EFPI sensor with an epoxy adhesive. The tensile test on the bolt was performed on the Tinius Olsen machine shown in Figure 34. The rebar-type bolt was loaded in three cycles of 0 to 17,000 lbs, in 2,000 lbs increments.

The strain versus time and load versus time results from these tests are shown in Figure 35 and Figure 36. The load versus strain graph, shown in Figure 37, was obtained by combining the strain versus time and load versus time results in Figure 35 and Figure 36. The theoretical strain values, shown in Figure 38, were calculated using,

$$\sigma = \frac{F}{A} \qquad (1)$$

$$\varepsilon = \frac{\sigma}{E} \qquad (2)$$

where σ is the stress, F is the force, A is the cross-sectional area, and E is the modulus of elasticity for the rebar bolt.[63]

The results in Figure 37 and Figure 38 immediately show that the theoretical strain values are twice as large as the experimental strain values. The rebar-to-fiber bond quality, or the fiber gage length measurement technique may provide two possible explanations that can help clarify these discrepancies. First, the rebar may not have been cleaned thoroughly enough, and second, the fiber gage length was estimated to be the length of the hollow core fiber and had not been checked under a microscope. It is not unlikely that the fiber gage length was much smaller than 1 cm. When manufacturing an EFPI, epoxy often wicks into the hollow core fiber and effectively reduces the fiber gage length.

Even though the experimental results did not match the theoretical prediction, the bolt was loaded to failure. Figure 39 shows machine exentsometer-reading versus load, and strain versus load results. Since the fiber gage length was not known, and this sensor's data was not considered to be reliable, a theoretical comparison was not performed. The data is qualitative in nature, but the strain results correlated well with the machine's extensometer results.

Since the goal of this series of experiments was to instrument a cable-type bolt, the experiment was not repeated with another rebar-type bolt. For the cable-type bolt, however, care was taken to precisely determine the EFPI gage lengths.

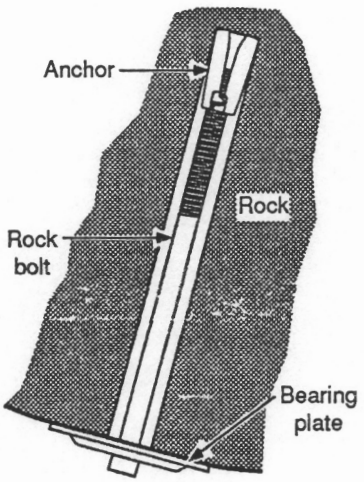

Figure 33. Rebar-type bolt anchoring.[64]

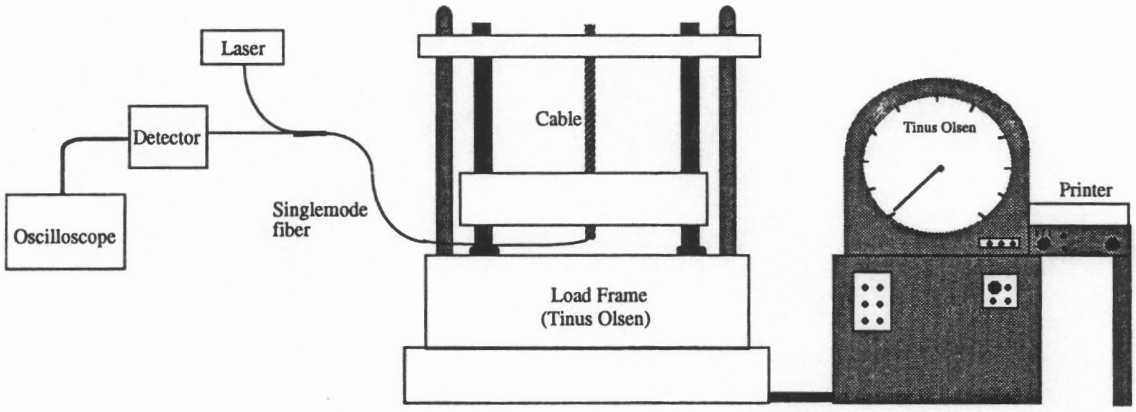

Figure 34. Experimental setup used for loading the rebar- and cable-type bolts.

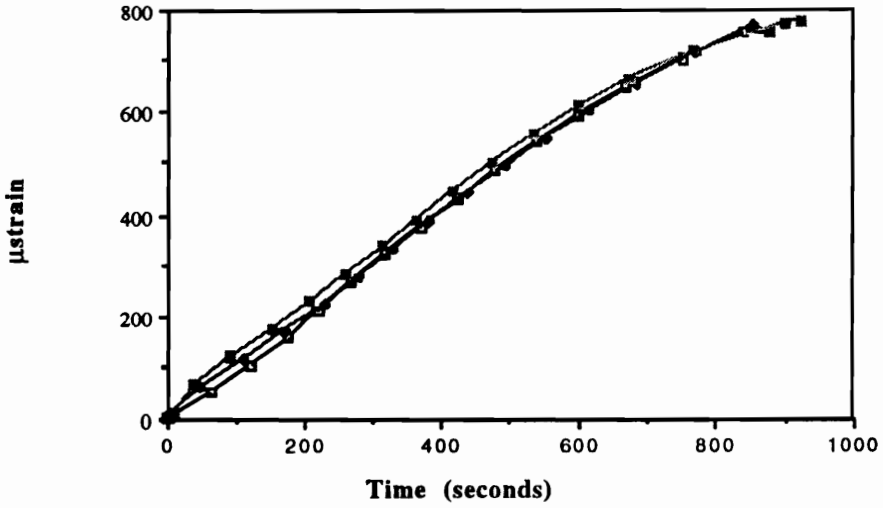

Figure 35. Strain versus time data for the rebar bolt.

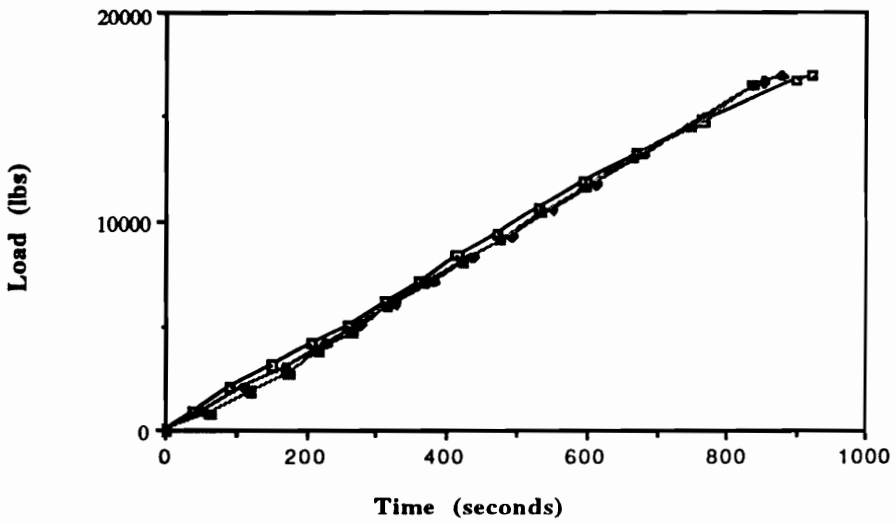

Figure 36. Load versus time data for the rebar bolt.

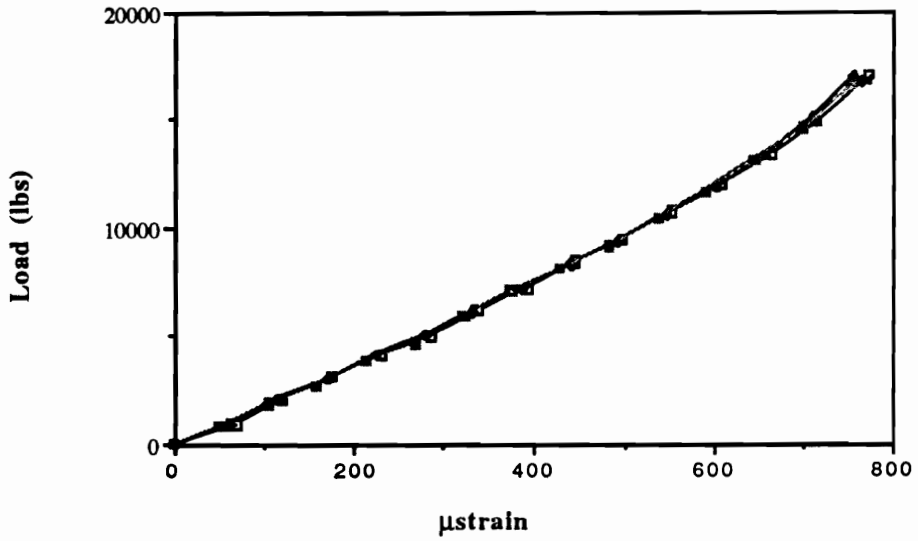

Figure 37. Load versus strain for the rebar bolt (experimental).

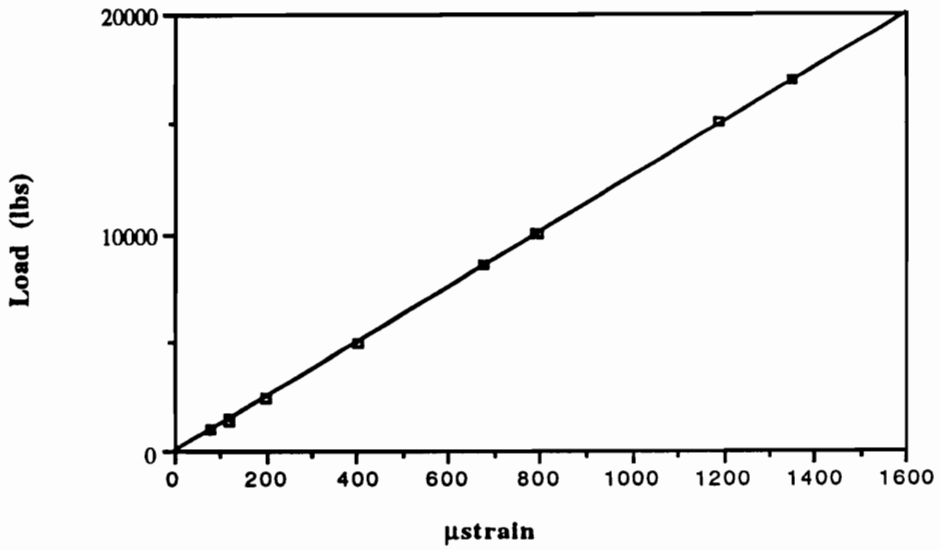

Figure 38. Load versus strain for the rebar bolt (theoretical).

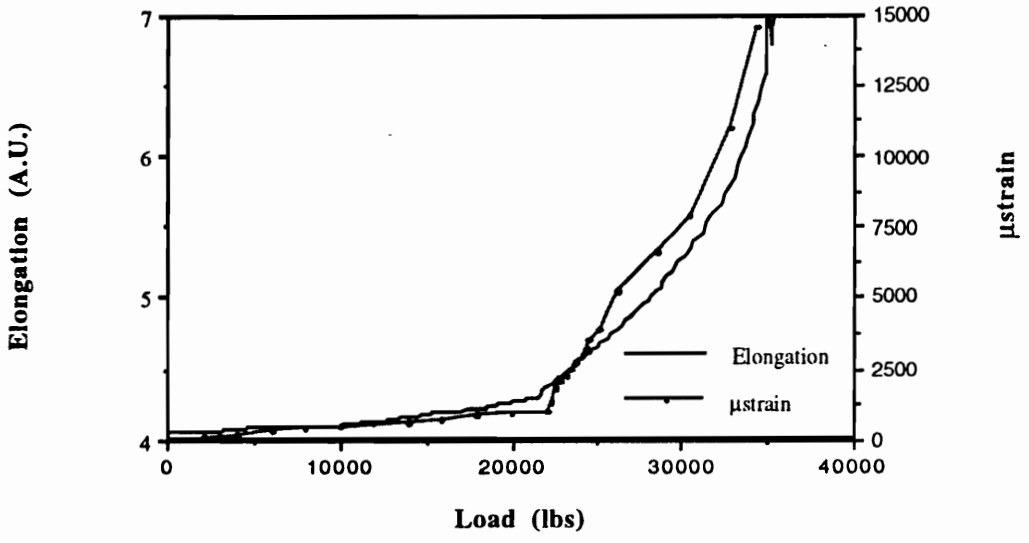

Figure 39. Machine extensometer elongation readings versus load, and fiber sensor strain readings versus load.

3.2.2 Cable-type Bolts

Most cable-type bolts have an ultimate strength of approximately 58,000 lbf, a diameter of 5/8" and consist of 7 wires as shown in Figure 40. Typically, nickel chromium wire extensometers, protected by plastic tubing, are wound along an outer strand of the cable, and terminated at both ends with rubber anchors. The extensometer lead-out wires are placed inside fiberglass tubes for protection, and are routed, through those tubes, to the instrumentation setup at the cable-end. Readout from such gages is in volts, and can be converted to elongation or strain.[65,66,67] May *et al.* have attached optical fiber sensors on the outside of a wire rope to demonstrate that it is feasible to use optical fiber gages to monitor strain.[68] It is not difficult to imagine how fragile or vulnerable these gages, exterior to the cable, are in the harsh mining environment.

Three EFPI sensors were mounted on the king-wire (center-wire) of the 7 strand cable. A sixteenth-inch-wide groove was machined along the entire length of the king-wire. The groove was cleaned and prepared according to recommended foil strain gage installation procedures and the EFPI sensors were attached using an epoxy adhesive. The gage-length for each sensor was carefully determined under a microscope. The leads to the fiber sensors were placed in the groove, the outer wires were wrapped around the king-wire to form the cable, the anchors were placed around the cable-ends, and the fibers were allowed to hang out of the end of the cable, as shown in Figure 40.

The cable-type bolt was clamped and then loaded using the Tinius Olsen load frame, shown in Figure 34. The cable-bolt was loaded from 0 to 40,000 lbs. Load versus strain results obtained for this test are shown in Figure 41. The theoretical strain values, shown in Figure 42, were again calculated using Equations (1) and (2). The cable was assumed to have a cross-sectional area of 0.23 $inch^2$ and a modulus of elasticity of 29.5 x 10^6 psi. Comparing Figure 41 and Figure 42, we can see that the theoretical and experimental data compares very well. Discrepancies in the results can be attributed to machining the groove into the king-wire, and to unwrapping and rewrapping the cable.

Also, as the cable loading approached failure, modulations were observed, similar to the modulations seen for the external column-beam test. These modulations were probably

caused by the outer cable strands, microbending the lead-out fibers in the king-wire groove that was being pinched, resulting in optical power fluctuations. The optical fibers were severed during the final loading cycle when the cable was loaded to failure (48,000 lbs). The king wire was examined, after the cable was unwrapped. The king wire had twisted and the groove had collapsed and crushed the optical fiber at the location of the anchors. The fiber optic gages were reconnected to the sensor support electronics and tested. Two out of the three of the installed sensors were still functioning.

The results obtained in this section demonstrate that EFPI-type optical fiber sensors are useful laboratory tools for quantitatively and nondestructively monitoring strain at locations along bolts. It is also important to note that with optical fiber sensors, unlike with conventional gages, the lead-in fibers, and the sensor itself, can be placed inside the cable, protected from the grout and rockmass. For actual field tests sensor packaging, as well as lead-out fiber protection issues, need to be studied. The inherent advantages of multiplexing these optical fiber sensors also need to be exploited in future experiments. For actual long-term monitoring of these bolts, the absolute EFPI (AEFPI) sensor, described in the next section, or the optical time domain reflectometer (OTDR) technique, described in the next chapter, may be better suited.

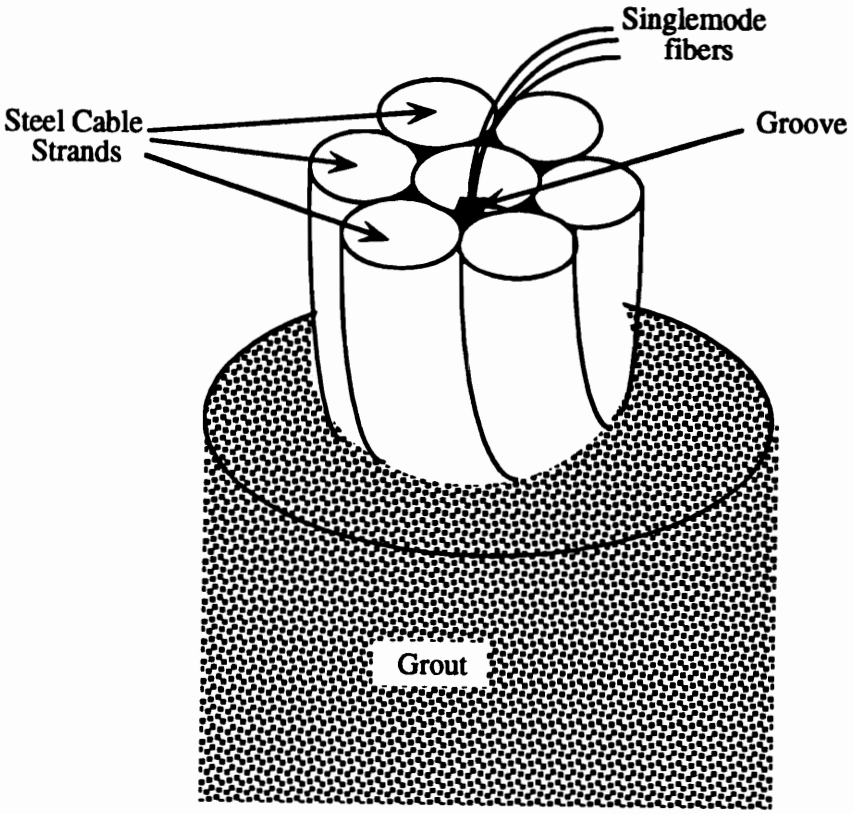

Figure 40. Cable type bolt diagram.

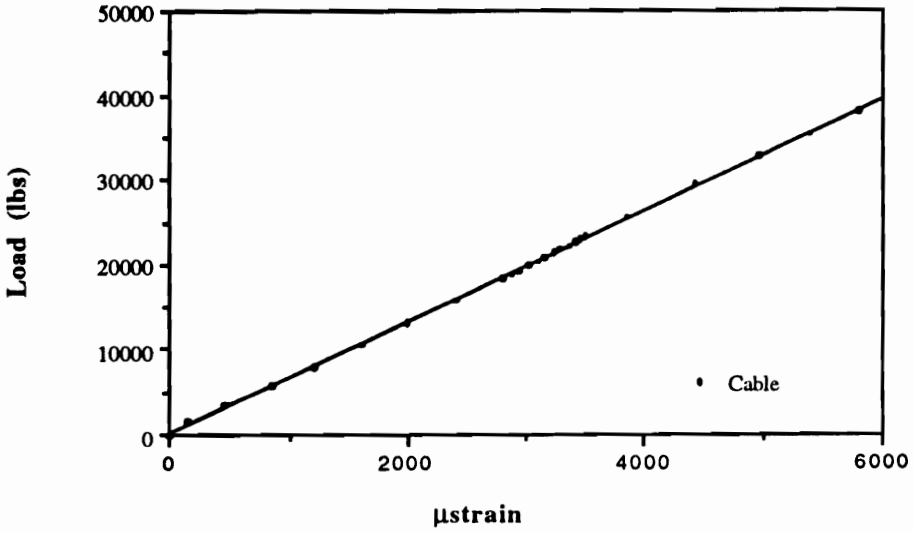

Figure 41. Strain versus load as the cable was loaded to 40,000 lbs (experimental).

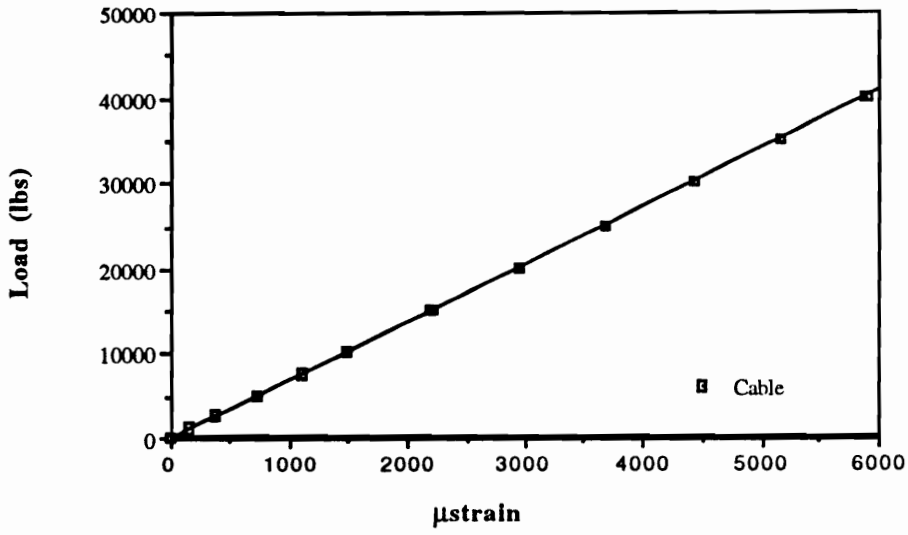

Figure 42. Strain versus load for the cable bolt (theoretical).

3.3 Absolute Fiber Sensor Applications.

The standard EFPI implemented in the previous experiments is unable to provide absolute measurements and may be susceptible to directional ambiguity. Moreover, when the system is turned off, all the phase information is lost and hence it is impossible to obtain absolute strain data for long-term field test measurements. These drawbacks have focused current research in optical fiber sensors on "absolute" optical fiber sensors which yield non-relative strain information. In the experiments described in the following sections the absolute EFPI (AEFPI), briefly described in Chapter 2, was implemented.

3.3.1 Feasibility Study

To demonstrate feasibility, an AEFPI sensor was attached to a 15 inch section of steel rebar which was subsequently embedded in a small concrete block (9 x 4 x 1.5 inches) to form a small reinforced concrete specimen. The cured concrete specimen was subjected to a three point bend test. This was done to obtain a qualitative assessment of the strain field induced in the concrete specimen due to three point loading. Figure 43 shows the increase in gap separation of the Fabry-Perot cavity as the load on the concrete was increased with the specimen in the three point bend configuration. The loading function is given in arbitrary units and the gap separation is in micrometers. Given the gage length of the AEFPI sensor, strain information can be derived from the change in gap separation. As seen from Figure 43, the gap separation and hence the strain induced in the concrete specimen increases as a linear function of the increasing load in a three point bend test.

To obtain quantitative strain measurements, a load frame experiment was conducted. The concrete specimen with embedded AEFPI sensors was loaded in an Instron Model 1331 load frame. The specimen was subjected to a series of incremental static compressive loads. The load was applied in steps of 100 lbs up to a maximum of 1000 lbs. The wavelength domain information was recorded using an ANDO 6310 optical spectrum analyzer and the change in gap separation was calculated mathematically using the wavelength data. Two loading tests were conducted for incrementally increasing and decreasing the load. The data obtained from the two tests is shown in Figure 44. As seen

the strain versus load plot exhibits a certain amount of hysteresis between the strain experienced by the concrete specimen for increasing and decreasing loads. This may be due to the fact that the concrete had not cured completely and the applied load induced residual strain (creep) in the specimen.

3.3.2 Pretensioning of Tendons used in Prestressed Concrete

Concrete, though strong in compression, is quite weak in tension, and compressive stress on it can be used to counterbalance any tensile force due to loading, which might lead to either cracks or deflection. Although prestressed concrete is more expensive to manufacture than reinforced concrete, the long-term savings due to reduced maintenance and extended lifetime are making it a popular choice for use in long-span structures, such as segmented bridges.[69] In pre-tensioning prestressed concrete, a tendon is tensioned before concrete is placed and the prestress is transferred to the concrete after it has cured, usually for 8 to 10 days, by releasing the tendon. If this prestressing force is applied along the axis of the structure, the procedure is termed linear prestressing. In linear prestressing it is often required to determine the axial strain on the tendon during the initial procedure of pre-tensioning, so that the required longitudinal force to achieve maximum concrete strength, can be accurately determined.

The experiment was performed at the Turner Fairbanks Federal Highway Administration research facility located in McLean, Virginia.[70] The reinforcing of concrete was implemented using a pretensioned graphite composite strand. In order to enable survivability of the sensors in high strain environments, the input fiber was epoxied to the hollow core fiber while the output/reflective fiber was allowed to move freely inside the hollow core fiber by epoxing it to the prestressing strand. The gage length, L, was determined by measuring the distance between the point where the input fiber was epoxied to the hollow core fiber and the point where the output fiber was epoxied to the prestressing strand. Since the strain was not directly transferred to the glass fiber, strains in excess of 10,000 μstrain could be monitored. The fiber sensors were attached so that the axis of the strand and that of the hollow core fiber were parallel to each other. Five foil strain gages were also attached at different locations on the graphite prestressing tendon.

One end of the prestressing tendon was kept anchored while the other end was loaded, so that the strand was axially strained with increasing load. The load was increased in steps of approximately 2,000 lbs. Figure 45 shows the processed output on the AEFPI screen when no load was applied. Figure 46 shows the output for a load of 12,279 lbs. The frequency of the output fringes increases with increase in load, due to the increase in the gap length, d, and a consequent reduction in $\lambda_2 - \lambda_1$ (Chapter 2). The measured strain is plotted versus the applied load in Figure 47. The final value of strain measured by the AEFPI system was 12,255 μstrain, which was within 2% of the value measured by a collocated foil strain gage. The strain from the AEFPI sensor were obtained in real-time. It is interesting to note that two of the foil strain gages failed at higher loads.

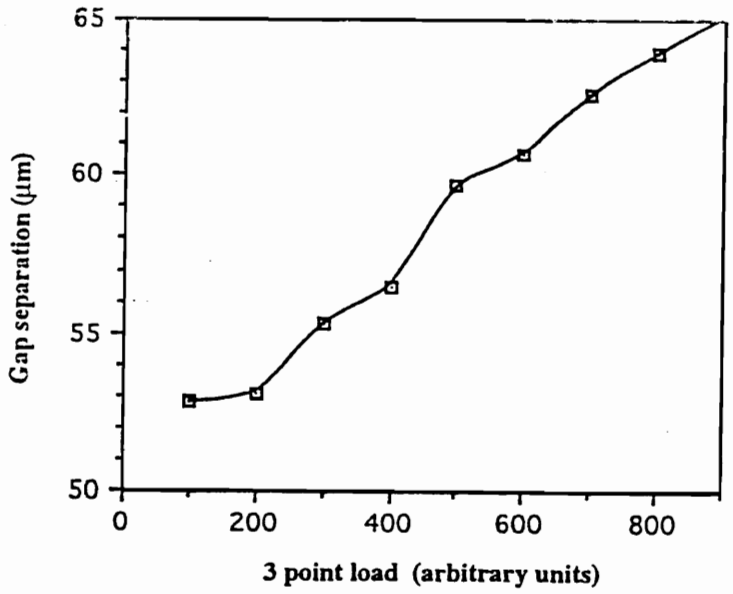

Figure 43. Gap separation in AEFPI sensor plotted as a function of increased three point bending.

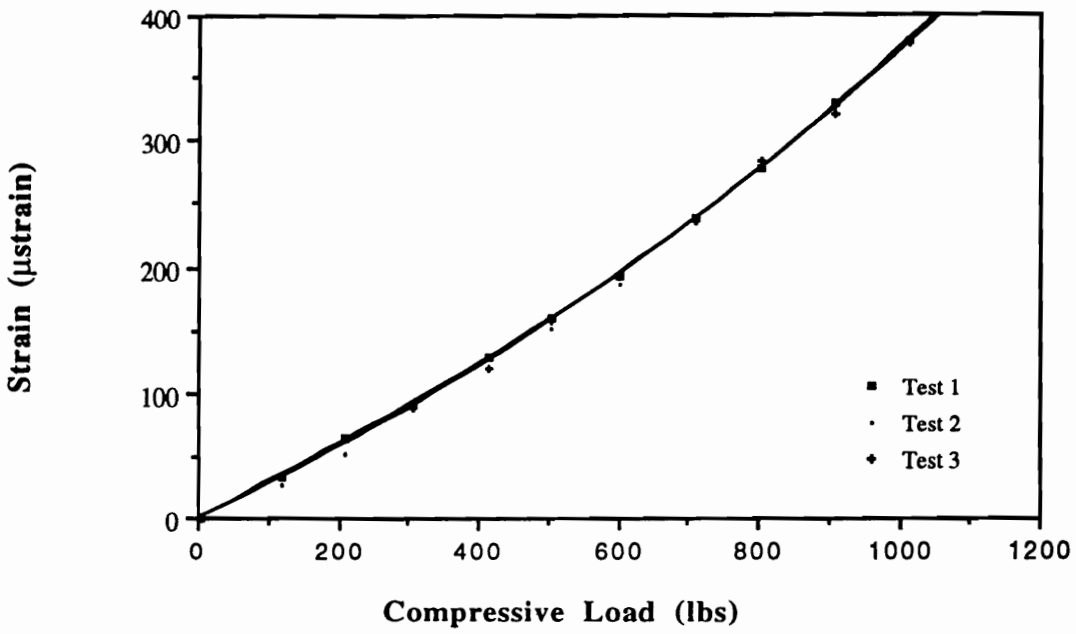

Figure 44. Strain measured by the AEFPI sensor as a function of increasing load on the reinforced concrete sample.

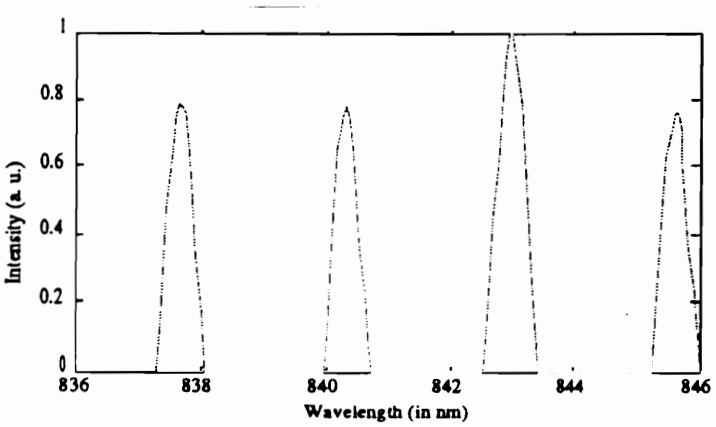

Figure 45. Output of the AEFPI system at no load. The corresponding gap length, L, is 132 μm.

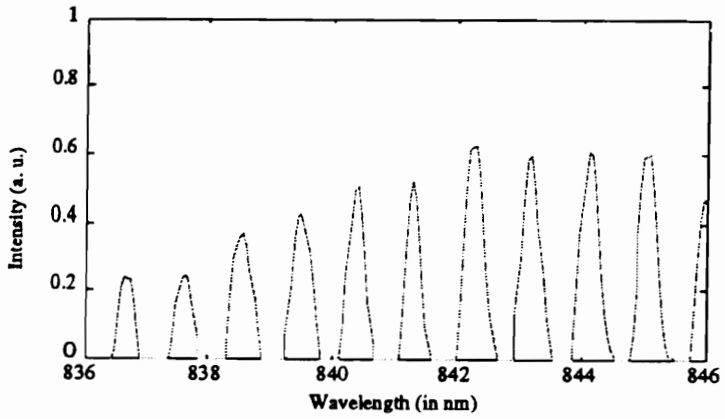

Figure 46. Output of the AEFPI system at a load of 12,279 lbs. The corresponding gap length, L, is 346 μm.

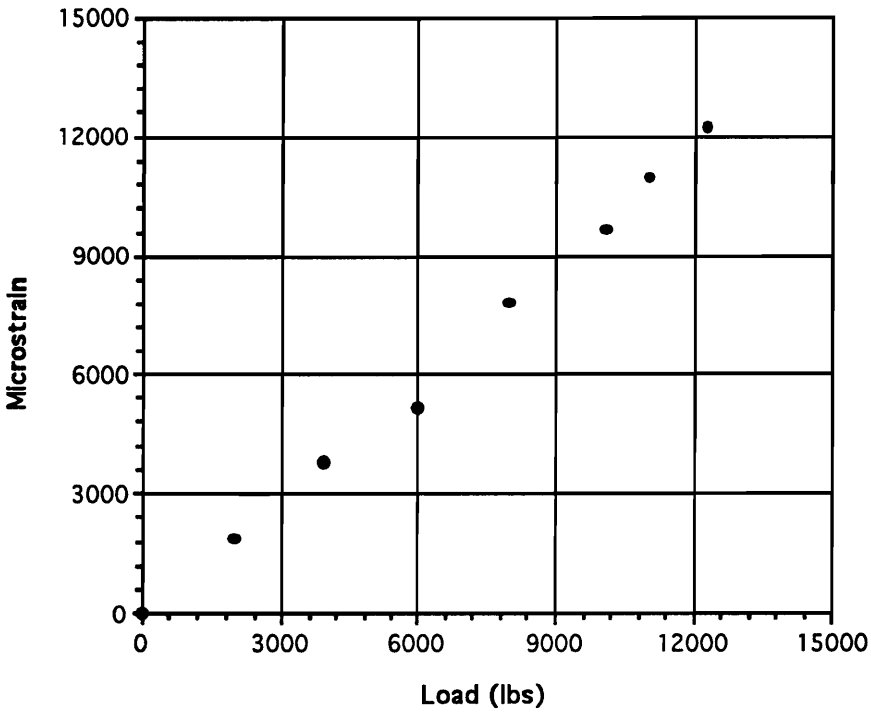

Figure 47. Measured strain versus applied load.

3.4 Fatigue Loading

Sensors used in civil structure applications must be able to provide accurate and reliable information regarding the building's structural integrity for extended periods of time. This section reports on the performance of EFPI sensors as they were cyclically loaded for more than 100,000 cycles.

Two EFPI sensors were embedded in rebar reinforced concrete block. One sensor was attached onto the flattened portion of a rebar placed axially in the concrete block. This sensor was collocated with a metal foil strain gage. Another sensor was attached to a very small piece of rebar placed near the center of the concrete block. An Instron Model 1331 hydraulic load frame was used to apply the cyclic loading stimulus to the concrete specimen. Custom-built adapters were used to affix the concrete specimen to the Instron load frame. A half sinusoidal compressive loading function with a peak load value of 760 lbs at 8.4 Hz was applied to the specimen for 100,000 cycles. The output signals of the two EFPI sensors were recorded and compared with the loading function as seen from the load cell output terminals. Figure 48 shows the output signal of an EFPI sensor attached to the rear and the load cell output. It was observed that the EFPI sensor signal follows the load cell output exactly. The EFPI sensor operated in the linear region of its transfer function or at its quadrature point, thus producing a response which is a linear function of the stimulus signal instead of an interferometric fringe output.

During another 100,000 cycle fatigue loading test of a similar concrete specimen, the output signals of two embedded EFPI sensors were recorded and compared. Figure 49 shows the two EFPI signals and their expansions. The two traces in the top portion of the oscillograph show the response of the EFPI embedded in the concrete and the two traces in the bottom part of the oscillograph show the response of the EFPI attached to the rebar embedded in the concrete specimen. The load cell stimulus was a half sinusoidal function with a frequency of 8.4 Hz. As observed before, the EFPI attached to the rear operated in quadrature and linearly followed the load cell stimulus. This linear EFPI output signal showed small peaks interspersed between the half sinusoidal signal. These small peaks occur due to a spring-like recoil of the rebar during the 'resting phase' of the half sinusoidal stimulus signal. The EFPI sensor embedded in the concrete showed an interferometric fringe output.

In Figure 49, each set of fringes corresponds to either the increasing or the decreasing part of the half sinusoid thus providing an indication of dynamically varying strain within the concrete specimen. From Figure 49, the sensor output shows five interference fringes as the sinusoidal loading function increases or decreases. Since the sensor had a gage length of 10 mm and the operating wavelength was 1300 nm, these fringes correspond to a dynamic strain of 325 μstrain induced in the concrete block as the load increases or decreases sinusoidally to a peak value of 760 lbs. The change in direction of the stimulus can be seen in the EFPI response, indicating a good dynamic response. The output of the EFPI embedded in the concrete specimen was recorded at different times during the 100,000 cycle fatigue load test. Figure 50 shows the output of this EFPI toward the end of the test. Again it is noted that the output shows five fringes as the loading function increased or decreased. Thus the fiber sensors provided reliable, stable and consistent strain information throughout the 100,000 cycle fatigue load test.

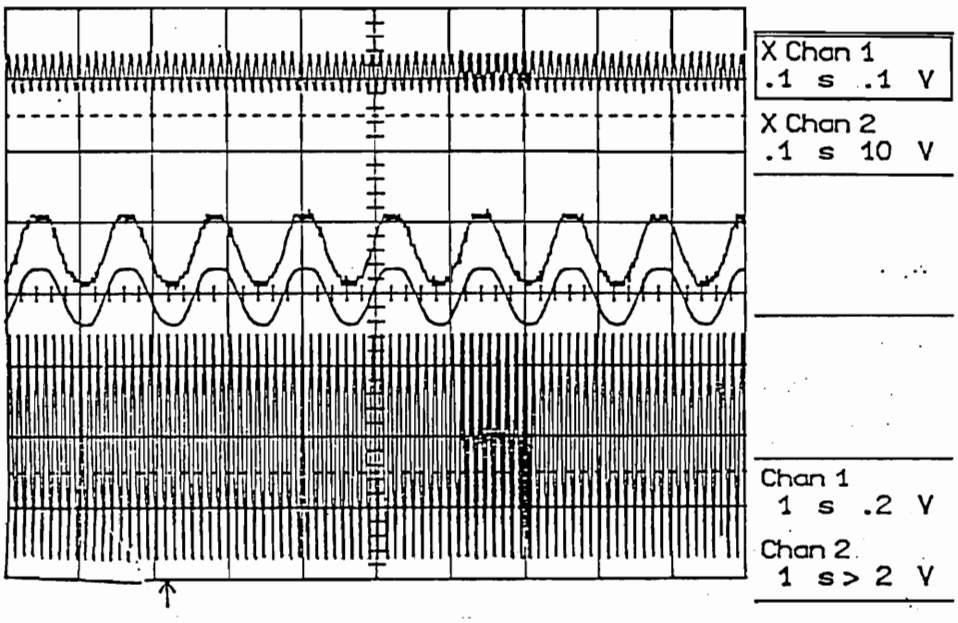

Figure 48. Comparison of embedded EFPI response to output load of the load cell (stimulus signal) for a half sinusoidal compressive loading function.

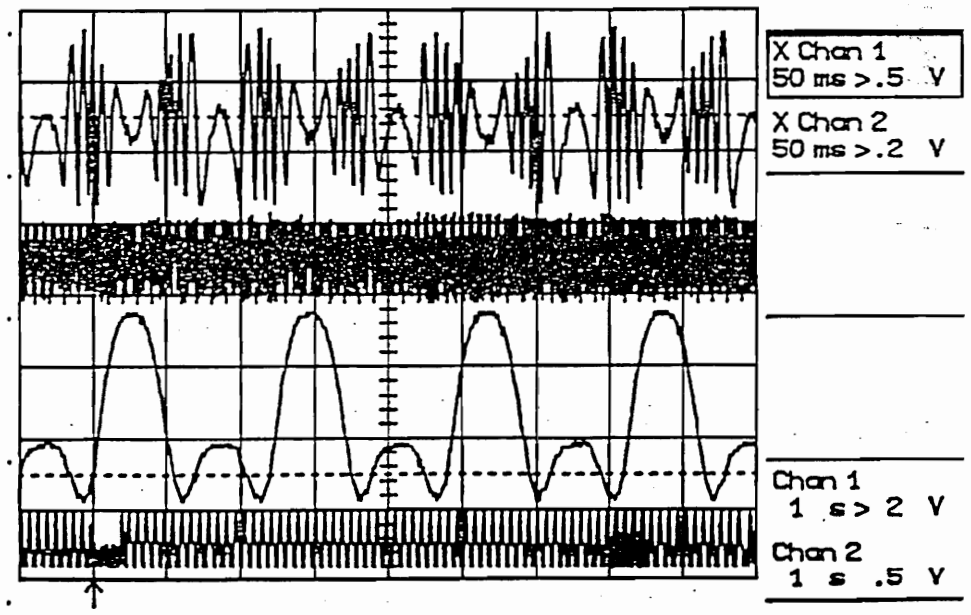

Figure 49. Response of EFPIs embedded in concrete to a half sinusoidal compressive load. Top trace = EFPI in concrete, Bottom trace = EFPI on rebar

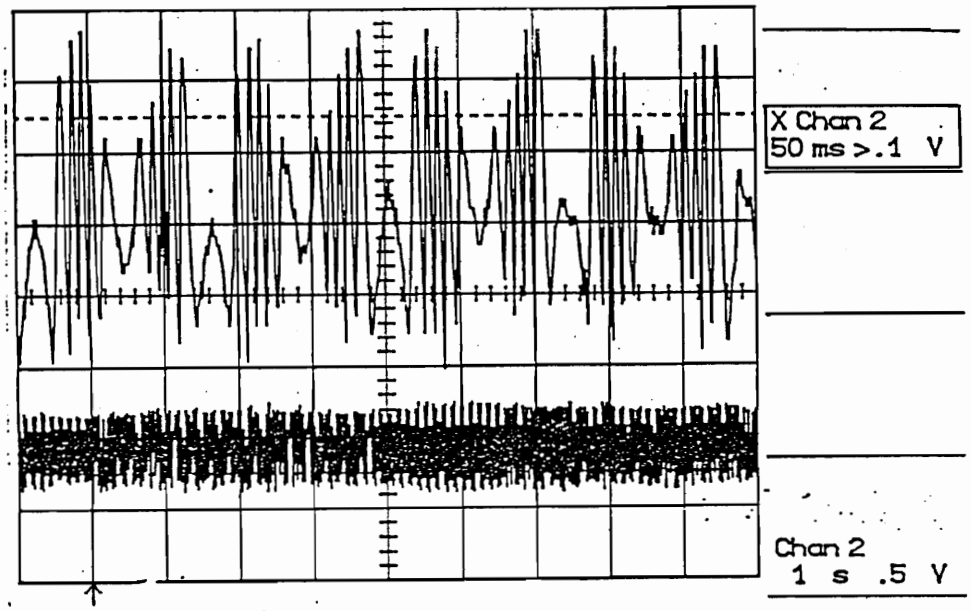

Figure 50. Response of EFPI embedded in concrete to a half sinusoidal compressive load towards the end of the 100,000 cycle fatigue load test.

Chapter Four

Fiber Sensor Multiplexing

Multiplexing a great number of optical fiber sensors onto a single optical fiber is one of the inherent advantages of using fiber-based sensor instrumentation. For example, 10,000 sensors, each with a 10,000 Hz bandwidth requirement could be multiplexed onto a single fiber having a transmission bandwidth of 100 MHz. Other multiplexing advantages include an overall savings in weight, a reduction in cost, and the potential for monitoring several different parameters simultaneously. Various multiplexing techniques and methods for performing distributed measurements have been proposed and implemented over the past 10 years.[71,72,73,74,75,76,77,78] For time, frequency, and wavelength division multiplexing schemes, the sensor information is respectively encoded in a particular time slot, a specific frequency range or on a separate wavelength. In this chapter, optical time domain reflectometry (OTDR) and spread spectrum techniques are discussed in detail, whereas time division multiplexing (TDM), frequency division multiplexing (FDM) and wavelength division multiplexing (WDM) techniques are also briefly discussed.

4.1 Multiplexing Overview

4.1.1 Time Domain Multiplexing

The basic TDM approach uses a pulsed laser source to interrogate the different sensors that are separated in time using fiber delay coils. For TDM systems it is very important for the pulse width to be smaller than the fiber coil delay-time. The output pulse train at the detector corresponds to the sampled sensor signal, and each pulse corresponds to a specific

sensor. The number of sensors that can be multiplexed depends on the power budget, sensor-to-sensor crosstalk, sampling rate, and pulse width. Both serial and parallel network topologies are being implemented to multiplex transmissive- and reflective-type interferometric sensors.[79,80,81,82]

4.1.2 Wavelength Division Multiplexing

For WDM systems each sensor operates within a window of pre-defined spectral width, dictated by the characteristics of the optical source being used. In theory this technique seems very elegant, but in practice this concept has encountered a great number of difficulties. While WDM was primarily considered for fiber communication applications, the design of wavelength selective devices, as well as the development of appropriate sources has not been fully developed. Most WDM systems use WDM-type couplers to combine light from multiple sources with distinct wavelengths onto a single fiber that distributes the light to the sensor network. WDM couplers are again used to demultiplex the optical wavelengths. A full review of WDM systems, and their applications is presented by Ishio *et al.*.[83] The complexity of the devices required and the poor sensor-to-sensor isolation are the major drawbacks for implementing the WDM approach. Hybrid multiplexing systems that use both TDM and WDM techniques may offer a solution to some of the drawbacks mentioned before and are discussed by Kersey *et al.*[84]

4.1.3 Frequency Division Multiplexing

An array of unbalanced optical fiber sensors, usually of the Mach Zehnder-type, can be frequency division multiplexed (FDM) by addressing them with a frequency-chirped source. By assigning different optical path differences to each of the sensors, beat frequencies corresponding to each sensor can be distinguished from each other. The fiber sensors can be arranged in series, or in a matrix array configuration.[85] Another FDM technique that is used to address interferometric sensors uses a sinusoidally frequency

modulated laser diode to give phase-generated carrier outputs and is presented by Dandridge *et al.*[86,87]

4.1.4 Coherence Multiplexing

Coherence multiplexing of interferometric sensors utilizes a sensing and reference interferometer pair. Coherence multiplexing is mostly implemented in those applications where only a limited number of sensors are needed and phase sensitivities are not required.[88] A more detailed description of the coherence multiplexing approach, based on path matched differential interferometery (PMDI), is given by Brooks *et al.*[89]

4.2 Optical Time Domain Reflectometry Techniques

An optical time-domain reflectometer (OTDR), sometimes, also referred to as optical radar, is mostly used to monitor the amount of light that is scattered back to the source due to Rayleigh scattering (of course other uses for OTDRs exist as well).[90,91,92,93,94] If the signal at the source is pulsed and the intensity of the backscattered light is monitored as a function of time, variations along the entire fiber length can be monitored. Normally for an unperturbed fiber the backscatter intensity decays exponentially due to inherent losses in the fiber as a function of length. Any localized perturbation along the fiber, strong enough to induce small refractive index changes in the fiber core, shows up as an increase in loss at the detector. For communications applications this type of an OTDR is used to locate the imperfections along an optical fiber. For practical sensor applications, however, the detected signal needs to be averaged many times, in order to obtain a good signal-to-noise ratio. This averaging of the optical pulse is an inherent disadvantage of the OTDR technique and limits the use of this sensor to quasi-static measurements only.

By using semi-reflective splices between different sensor elements multiple sensors can be multiplexed in series. If the entire length of fiber serves as the sensing fiber, this type of a sensors is considered to be a quasi-distributed sensor. The EFPI-type sensors described in Chapter 2 also function similar to semi-reflective splices; when multiplexed in this configuration they themselves would be the sensors.

4.2.1 Distributed Sensing using OTDR

As was previously mentioned, OTDRs are commonly used in the telecommunications industry to locate breaks and imperfections in optical fiber cables. The OTDR measures the time-of-flight of a short optical pulse in an optical fiber launched by a pulsed laser diode source and detected by a photodetector. Knowing the speed of the light pulse in the fiber, it is possible to calculate the location of a break (which reflects some of the pulse) by measuring the round trip time-of-flight of the light pulse to and from the break. The OTDR may be used for measuring the strain in an optical fiber, since the strain induces a length change in the fiber and increases the time-of-flight of a pulse propagating through the fiber.

In our case, in order to eliminate pulse drifts, we monitor the pulse location with respect to a reference pulse that does not fluctuate in time. The reference pulse is generated by a reflection from the air-gap in the connector joining the lead-in fiber to the pulsed laser pigtail fiber. This is done to reduce the effects of jitter in the pulsed laser repetition rate. The time resolution of the OTDR is approximately ± 2 ps, primarily due to laser jitter.

When an axial strain is applied to an optical fiber the length of the optical fiber is changed. This change in fiber elongation can be determined using optical time domain methods where a change in the time-of-flight of an optical pulse that has traveled through the fiber can be measured. The time, t, required for an optical pulse to travel through an optical fiber of length, l, and refractive index, n, can be determined by,

$$t = \frac{nl}{c}, \tag{1}$$

or by,

$$t = \frac{l}{v_g}, \tag{2}$$

where c is the speed of light in free space and v_g is the group velocity of the optical pulse. By differentiating both sides of Equation (1) we obtain[95]

$$dl = \frac{cdt}{n} - \frac{tcdn}{n^2}. \tag{3}$$

Substituting Equation (1) into Equation (3) we now obtain

$$dl = \frac{cdt}{n} - \frac{ldn}{n}. \tag{4}$$

the axial strain, ε, on an optical fiber is expressed as elongation divided by the total length of the optical fiber. By examining Equation (4), one observes that a change in the length of optical fiber results in a change in the arrival time of the optical pulse as well as a change in the refractive index of the fiber. The change in index of refraction of the fiber is dependent on the axial strain applied to the fiber and can be determined from Equation (5) below,

$$\frac{dn}{n} = \alpha\varepsilon, \tag{5}$$

where the photo-elastic coefficient, α, of the optical fiber can be determined for each optical fiber by applying a strain to the fiber in a load frame. Once the photo-elastic coefficient has been determined Equation (4) can be expressed as

$$\Delta l = \frac{c\Delta t}{n}\left(\frac{1}{1+a}\right). \tag{6}$$

Figure 51 gives a plot of the theoretical shift of an optical pulse caused by elongation of hollow core, solid core and liquid core optical fibers, with indices of 1.0, 1.45, and 1.492, respectively.

In order to verify Equation (5), and the results shown in Figure 51, the change in time-of-fight of an optical pulse in a hollow core fiber, where n=1, a solid core fiber, with n=1.45 and a liquid core fiber, with n=1.492, as a function of elongation, were determined using an optical time domain reflectometer. The setup shown in Figure 52 was used. It consists of a high resolution OTDR, manufactured by Opto-Electronics Inc., (which houses a pulsed laser diode that is repetitively triggered by a clock circuit, a detector, a delay generator, a sampler, and a signal processor), a display oscilloscope and the optical fiber sensors. [95,96,97] In the cases of the hollow core fiber and the liquid core fiber, the photo-elastic coefficient is absent. The hollow core, solid core and liquid core fibers were strained by attaching the fibers to posts and translating one post, as shown in Figure 53, with a micropositioner. This experiment demonstrates the feasibility of measuring strain

with the optical fibers. Figure 54 shows the reflected pulse averaged 512 times on an oscilloscope at 100 ps/division.

The plotted results of this experiment, in Figure 55, show that an increase in elongation results in an increase in pulse shift. The results in Figure 55 also show that the fiber with the higher refractive index (the liquid core fiber) is more sensitive to strain.

4.2.2 Quasi-Distributed Strain Measurement

In order to show that such a strain sensor could also be used to perform quasi-distributed strain measurements, four such sensors were placed in series and attached to a steel cable rope. The distributed 100/140 μm optical fiber sensor was attached to the steel cable at the air-gap splice locations using an epoxy (see Figure 56). Great care was taken to ensure that there was no slack in the optical fiber. The steel cable was loaded in increments and readings, averaged 512 times, were taken for the five backreflected pulses. Results in Figure 57, show the pulse shifts for each pulse reflected from the air gaps. Pulse #1 measures the elongation for the first fiber segment, while Pulse #2 shows the elongation for both the first and the second segment. By using

$$\varepsilon_j = \frac{(\Delta t_j - \Delta t_{j-1})c}{2nl_j}\left[\frac{1}{1+\alpha}\right], \tag{7}$$

where Δt_j and Δt_{j-1} are the pulse delays of the far- and near-end reflections from the j^{th} segment, l is the length of the j^{th} segment of, we can determine the elongation in each fiber segment.[96]

4.2.3 OTDR for Localized Strain Measurement

In order to demonstrate that the OTDR can also be used for localized strain measurements, four EFPI sensors were embedded in a graphite composite beam 50 cm long. The EFPIs were positioned such that the sensors were located at 49 cm, 25 cm, 13 cm and 1 cm respectively from the clamped end, as illustrated in Figure 58. When the graphite composite beam was removed form the hot-press the sensor located at 13 cm broke. (This difficulty of fiber breaking off at the location where the fiber enters and exits the material is discussed in the following chapter.

We are not quite sure why the sensor located at 48 cm did not respond when the beam was statically loaded. The strain at the tip of the beam may have been negligible. Tapping the sensor however did provide an output response with a standard 1300 nm support system. The intensity of both pulses, (one fiber broke and the other fiber did not respond because it was too close to the beam-tip end) was monitored as a function of beam-tip displacement and was later normalized. As expected, sensor 2, which was located closest to the clamp experienced more strain than sensor 1. Both EFPI sensors had a 1 cm gage length. Figure 59 shows the intensity fluctuations, typical of the EFPIs, for the two embedded sensors. Each sensor reading had to be averaged and thus in practice only quasi-static measurements are possible. Sensors could be placed in series but the small core diameter of the single mode fibers could make it difficult to couple light from one fiber to the next.

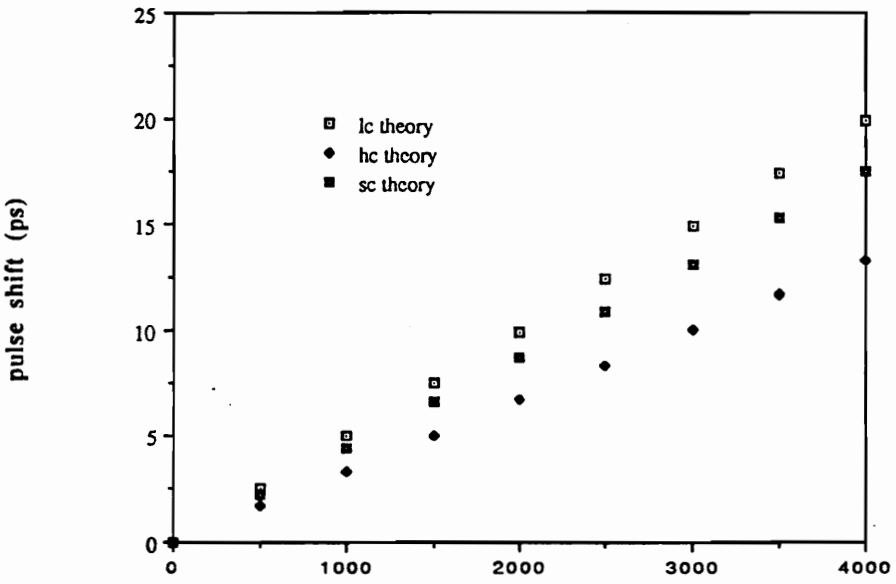

Figure 51. Theoretical pulse shift as a function of elongation for hollow core, solid core and liquid core optical fibers.

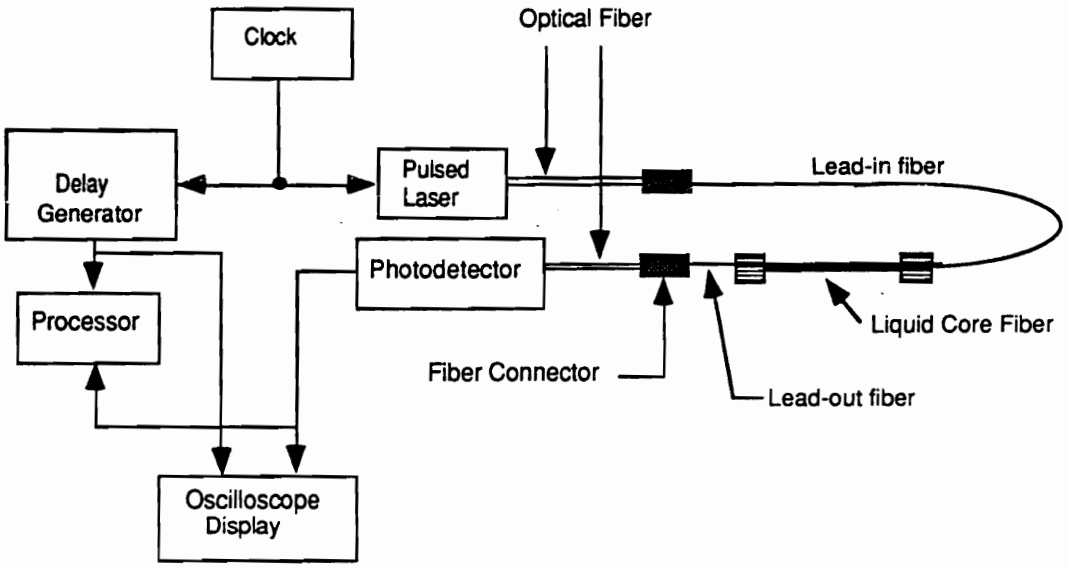

Figure 52. OTDR components.

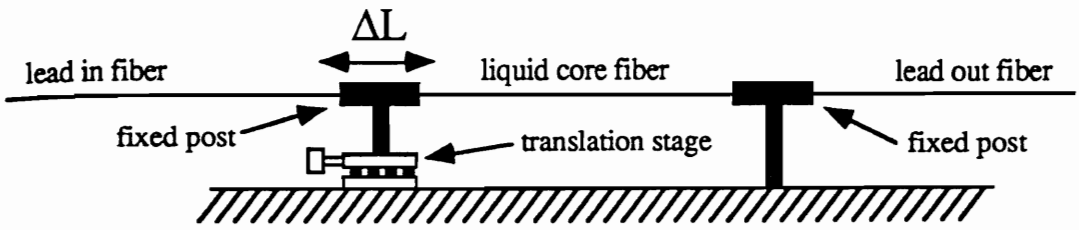

Figure 53. Setup used for monitoring the elongation of the hollow core, solid core and liquid core fibers.

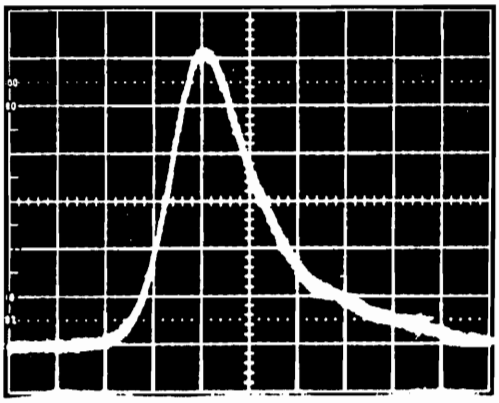

Figure 54. Reflected optical pulse averaged 512 times shown on an oscilloscope at 100 ps/division.

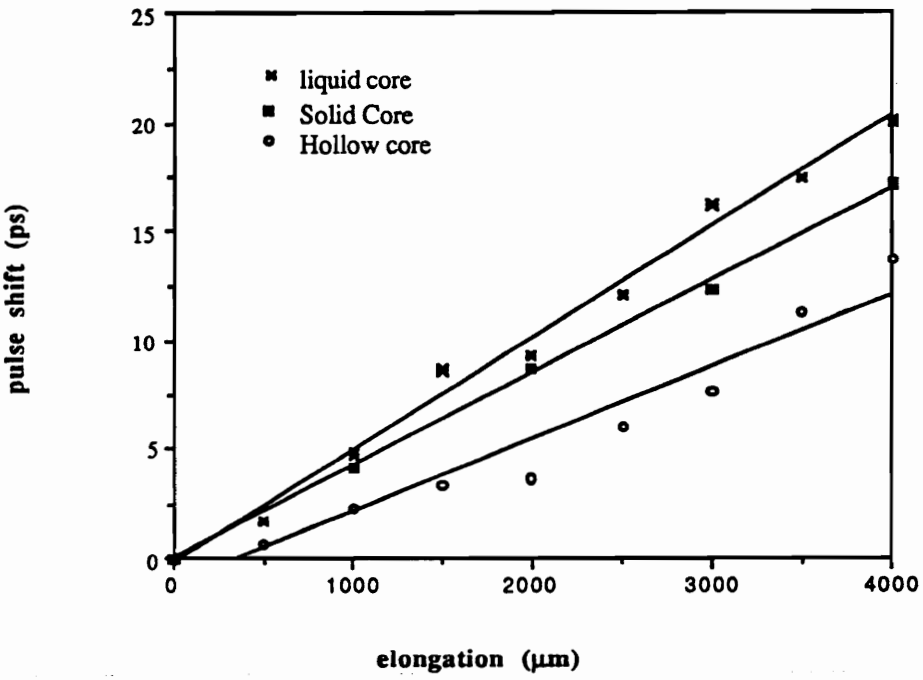

Figure 55. Elongation versus pulse shift for hollow core, solid core and liquid core optical fibers.

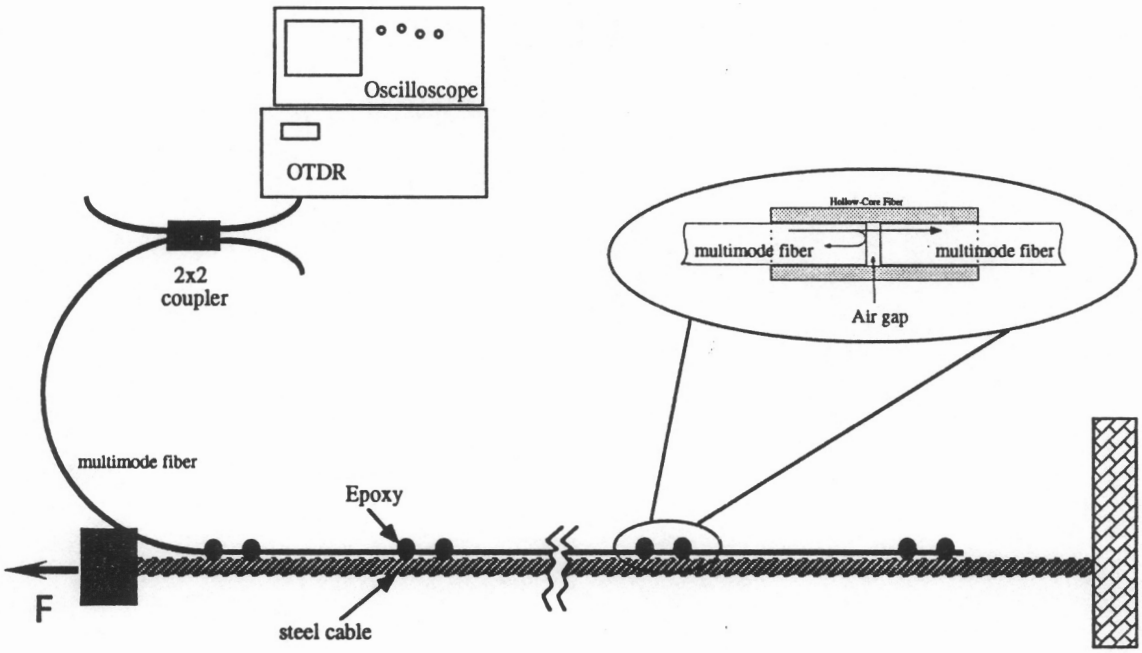

Figure 56. Attachment of the optical fiber to the steel cable

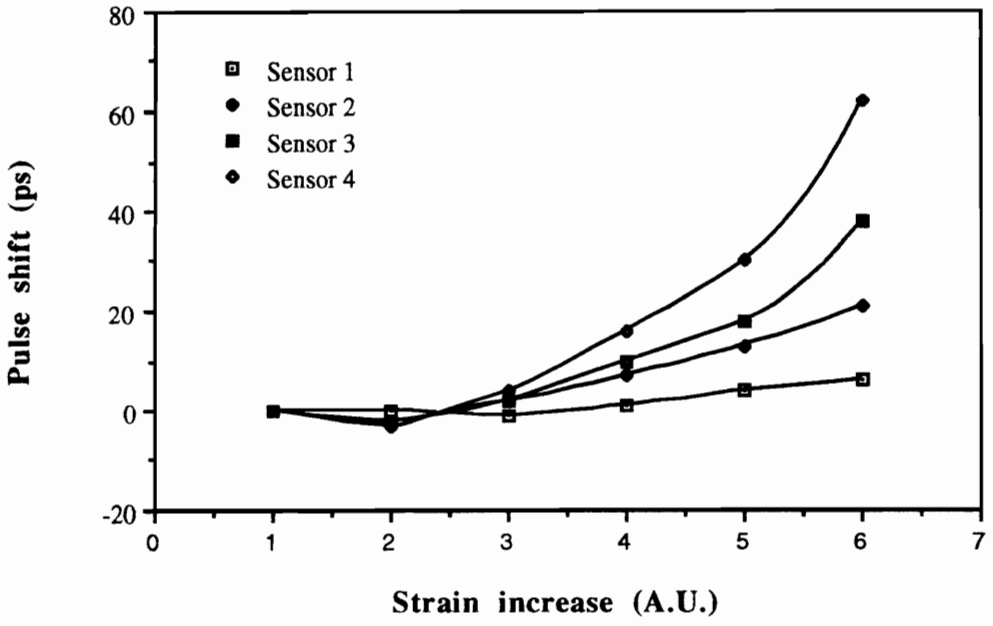

Figure 57. Relative pulse shift versus load for each of the air-gap splices

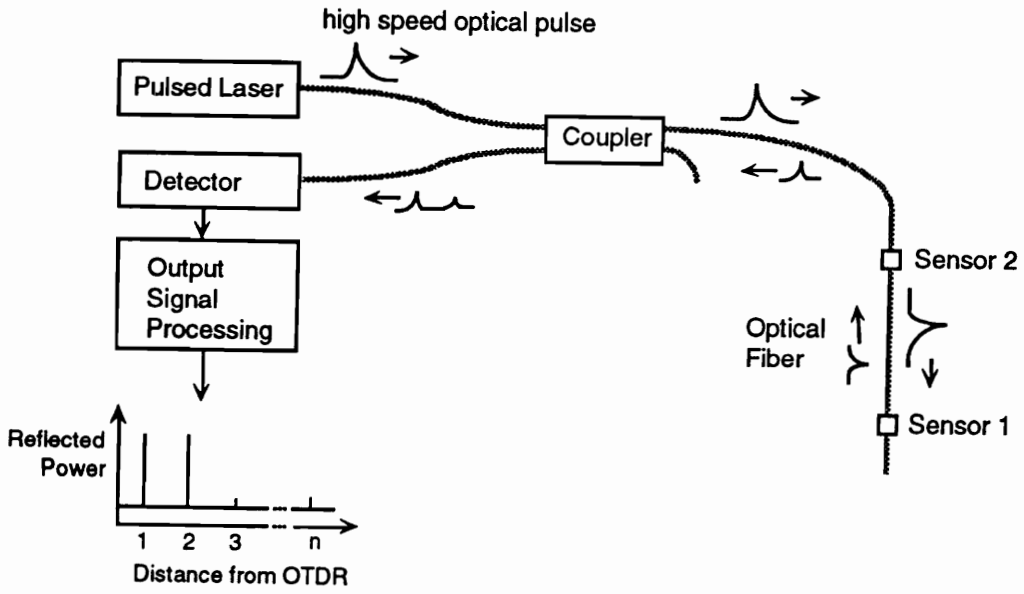

Figure 58. OTDR setup for the measurement of localized strain.

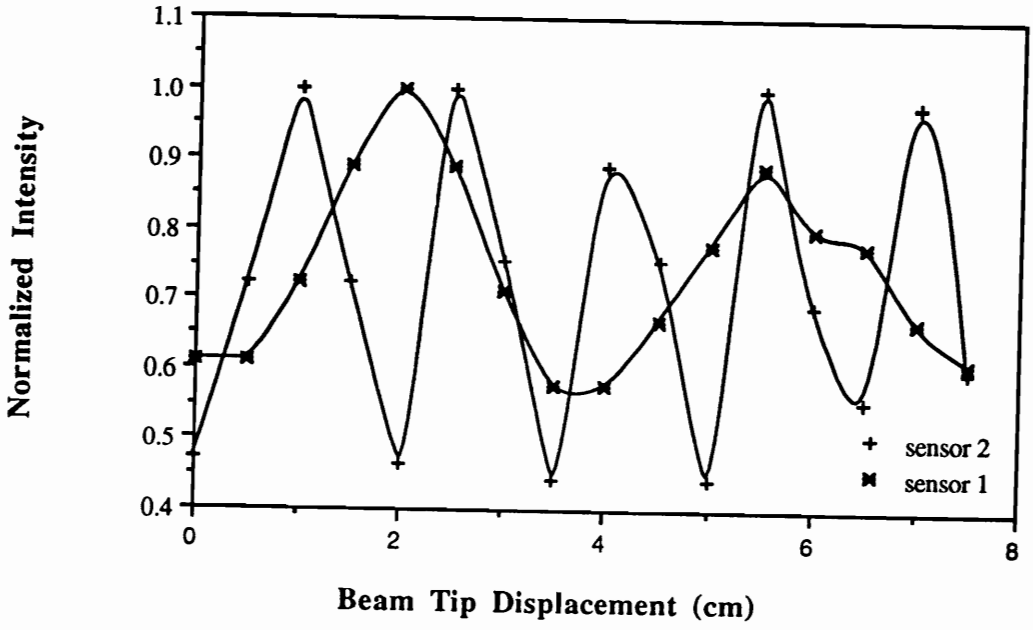

Figure 59. Normalized Intensity for two EFPI sensors embedded in a graphite composite beam, sensors 1 and 2, are respectively located at 25 cm and 1 cm from the clamped end.

4.3 Code Division Multiplexing

Spread Spectrum techniques, originally developed for applications in communications, are also finding application in the multiplexing of optical fiber sensors.[98,99,100,101,102,103,104] In a spread spectrum system the information signal is spread over a wide range of frequencies, using a code sequence, with a bit rate much higher than the signal. This type of a system is also known as a direct sequence modulated system. The transmitted bandwidth is made greater than the original information bandwidth. Using this system a group of receivers can be addressed by assigning a unique reference code to each of them. Despreading the signal is accomplished by correlating the spread spectrum signal with a similar reference signal. If the two signals match, the original signal is left and a filter can be used to recover all but the desired bandwidth.

The CDM approach can be used to address different sensors due to the unique correlation behavior of specific mathematical codes (maximal length sequences), which are used to code sensor outputs. These codes are pseudo random in nature and are generated using shift registers. For these maximal length codes the following properties need to be satisfied:

1. the number of ones should be one greater than the number of zeros,
2. the statistical distribution of ones and zeroes should be the same in every sequence period,
3. the modulo-2 addition of any maximal length sequence added to a phase shifted maximal length sequence will produce a phase shifted maximal length sequence different from the other two codes,
4. and the autocorrelation of the optical signal and the electrical signal yields a correlation value of zero whenever the two bit sequences are shifted by more than one bit .[105]

A pseudo random bit sequence (PRBS) is a continuous repetition of this maximal length code. In our case the two bit sequences consist of an electrical reference PRBS, c_i, and an optical PRBS, c'_i, that is detected at the detector. The two sequences can be defined as

$$c'_i \in \{0,1\} \forall i \quad \text{such that } 1 \le i \le K \tag{8a}$$

$$c_i \in \{0,1\} \forall i \quad \text{such that } 1 \le i \le K, \tag{8b}$$

where K is the bit-sequence length. The autocorrelation function R(m) is then written as

$$R(m) = \frac{1}{K} \sum c'_i c_{i+m} = \begin{cases} 1, & m = 0 \\ 0, & 0 < |m| < K \end{cases}, \tag{9}$$

or for the continuous signals the autocorrelation function $R(\tau)$ can be represented as

$$R(\tau) = \frac{1}{K_T} \int c'(t) c(t+\tau) dt = \begin{cases} 1, & \tau = 0 \\ 0, & |\tau| > 0 \end{cases}, \tag{10}$$

where K_T represents the normalization factor.[106] A more detailed explanation on spread spectrum systems is provided by Holmes and Dixon.[105,107]

Figure 60 shows a plot of a typical continuous correlation function.[106] When the optical signal PRBS and the electrical PRBS are shifted by more than one bit the output of the autocorrelation function is zero. Autocorrelation is really a measure of the similarity between the signal and its phase shifted replica.

For communication applications, the communication signal is encoded onto the PRBS, transmitted, and reconstructed by the receiver with the right reference PRBS. If the receiver did not have the right reference PRBS it would end up with a signal resembling white noise. The individual EFPI sensors described in this section are addressed using this spread spectrum technique. The optical path length difference between the different sensors corresponds to an integer number of bits in the PRBS. The laser used in the experimental section is modulated with a PRBS sequence. The light detected at the end of the fiber sensor network is a delayed version of the PRBS used to modulate the laser. The

actual signal is then recovered by correlating the detected PRBS signal with the appropriately delayed (by the appropriate number of optical path lengths), PRBS reference signal. A more in-depth analysis of the CDM of extrinsic Fabry-Perot interferometric optical fiber sensors is given by Ravikumar and Bhatnagar.[108,109]

In the experimental setup, illustrated in Figure 61, a laser diode is intensity modulated by a PRBS of maximal length "m." The optical signal is transmitted to the sensor array where the individual sensors are separated by a delay equal to an integer multiple of the PRBS bit period. The sensor information is superimposed on the PRBS carrier signal and the signal is reflected back to the detector through a coupler. Received signals from the different sensors in the network are thus encoded by delayed versions of the PRBS code. The individual sensor information is retrieved by correlating the detector signal to the delayed version of the original PRBS. If this delay is matched by the optical delay corresponding to Sensor I, then the contribution from Sensor I is extracted and the other sensor signals are averaged out. The output of the correlator is integrated with a low pass filter and the final output consists ideally only of the signal from the sensor that was matched to the reference PRBS. The maximum sensor frequency must be less than half of the word repetition rate of the PRBS since the PRBS carrier must be separated from the baseband sensor signal by the low pass filter. For a 7 bit shift register and a bit rate of 100 kbit/sec the sensor frequency must be less than 100 Hz and the optical fiber delay coils between the fiber sensors needs to be 1 km. In fact, the optical delay, L, must provide a delay that matches an integer multiple of bit-length in the modulating sequence. If this delay is not properly implemented degradation of the correlation operation will occur.[108,109]

4.3.1 Multiplexing 2 EFPI Sensors

The following experiments are used to demonstrate the feasibility of multiplexing two EFPI sensors using the setup shown in Figure 61. The experiments were directed towards observing the amount of crosstalk between the two sensors. In the experiments, arbitrary modulation of one of the sensors was applied while the system parameters were varied. The varied parameters were the length of the PRBS code (15 or 127 bit) and the bit rates of the codes. The optical delay that was used in this experiment was 2.2 km and bit rates of

45.3 and 136 kbits/sec were used. Hence, the optical delay, was used to delay the PRBS modulated signal relative to the second sensor by 1 and 3 bits. Due to the electronics in the supporting hardware, an initial delay is imposed to the entire sensor system. This initial delay introduces an inherent error in the correlation operation which was not removed.

In the first experiment a 15 bit PRBS code was used with a bit rate of 45.3 kbits/sec. In Test 1, Sensor 2 was disturbed (Figure 62a) while Sensor 1 was isolated (Figure 62b) from external perturbations. In Test 2, Sensor 1 was disturbed (Figure 62c) while Sensor 2 was isolated (Figure 62d). To analyze the data, Sensor 1 experienced a 0.3481 V_{pp} swing when it was disturbed, whereas it only experienced a 0.0877 V_{pp} swing when it was isolated. Thus, Sensor 1's undisturbed output was 25% of its disturbed output. In comparison, Sensor 2 experienced a 0.2588 V_{pp} swing when it was disturbed versus a 0.0375 V_{pp} difference when it was isolated. Thus Sensor 2's undisturbed output was only 14% of its disturbed output. We can therefore infer that Sensor 1 is suffering from more crosstalk error than Sensor 2 at this bit generation rate.

Figure 63 shows typical data from the 136 kbits/sec generation rate tests with 15 bit PRBS. In Test 3, Sensor 2 was disturbed (Figure 63a) while Sensor 1 was isolated (Figure 63b) from external perturbations. In Test 4, Sensor 1 was disturbed (Figure 63c) while Sensor 2 was isolated (Figure 63d). In these two tests we observed that Sensor 1's undisturbed output was 25% of its disturbed output. In comparison, Sensor 2's undisturbed output was only 6% of it disturbed output. We can therefore infer that Sensor 1 is suffering from more crosstalk error than Sensor 2 at this bit generation rate. In addition, we see that although there has been no change in the crosstalk level relevant to Sensor 1 (between Tests 1, and 2 and Tests 3 and 4), the increase in bit generation rate does seem to have improved the crosstalk associated with Sensor 2. However, since the physical length of the optical delay is fixed for all theses tests, Tests 3 and 4 involved a 3 bit delay for Sensor 2 whereas Tests 1 and 2 involved a unity bit delay for Sensor 2. Thus, the observed improvement in the crosstalk associated with Sensor 2 could be attributed to moving the PRBS harmonics further away from the passband of the low-pass filter (from increasing the bit generation rate) or to the changes in the correlation process (a change in the reference PRBS associated with Sensor 2).

In the second set of experiments a 127 bit PRBS was used. In theory, a 127 bit PRBS sequence will provide lower crosstalk levels than a 15 bit PRBS for the same bit generation rate. Figure 64 displays data from Tests 5 and 6, in which a 127 bit PRBS was generated at 45.9 kbits/sec. In Test 5, Sensor 2 was disturbed (Figure 64a) while Sensor 1 was isolated (Figure 64b). In Test 6, Sensor 1 was disturbed (Figure 64c) while Sensor 2 was isolated (Figure 64d). Using the same criteria as before, Sensor 1 reported 10% of its disturbed amplitude when it was isolated, and Sensor 2 reported 14 % of its disturbed amplitude when it was isolated.

In Tests 7 and 8, the 127 bit PRBS was generated at 135.6 kbits/sec. For Test 7, Sensor 2 was disturbed (Figure 65a) while Sensor 1 was isolated (Figure 65b). And finally in Test 8, Sensor 1 was disturbed (Figure 65c) while Sensor 2 was isolated (Figure 65d). In these tests, Sensor 1 had a 10% fluctuation in the isolated test and Sensor 2 had a 9% fluctuation in the isolated test. Hence, with the increase in bit rate, a decrease in crosstalk of Sensor 2 can be inferred. In addition, the effect of the bit rate increase had a minimal effect on the crosstalk parameter for Sensor 1. Note the same trend is observed in the data from Tests 1-4.

From the test data discussed above we can make some general observations that are helpful in the refinement of the multiplexing system. The crosstalk observed in Sensor 1's signal is fairly consistent for a given PRBS chip length, regardless of the rate at which the code is generated (Sensor 1's crosstalk did drop with an increase in chip length). In contrast, the crosstalk observed in Sensor 2's signal was somewhat consistent for a given bit rate but a reduction of crosstalk was observed for an increase in the chip length. Some of the crosstalk can be attributed to the initial delay that was introduced by the electronic circuit.

4.3.2 Multiplexing 4 EFPI Sensors

In a later implementation the four EFPI sensor CDM system shown in Figure 66 was used. This system uses a bit generation rate of 1 Mbit/sec and can provide a 15 or a 127 bit maximal length code. 100 m optical delay coils are used to ensure that sensor 1 is exactly

one bit, two bits and three bits out of phase with sensors 2, 3 and 4. This system does use a tunable delay and detailed explanation on the operation and calibration of this delay is provided by Poland.[106]

Figure 67 shows a sample output from the experiment when all the sensors were arbitrarily modulated. Crosstalk, the interference from other sensors in the network, is a measure of overall performance of the system. Bhatnagar uses EFPI sensors attached to tuning forks to quantify the amount of crosstalk between sensors. He also describes how either an increase in the code length, or a two bit delay instead of a one bit delay between the sensors drastically can minimize the interference between individual sensors.[109] A more detailed analysis of the amount of crosstalk is given by Poland *et al.* and Kersey *et al.*[106,110]

This chapter demonstrated that OTDR and spread spectrum multiplexing techniques hold considerable promise for monitoring various structural parameters. In fact it may be the ability of fiber sensors to be multiplexed that will give it a considerable advantage over conventional sensors.

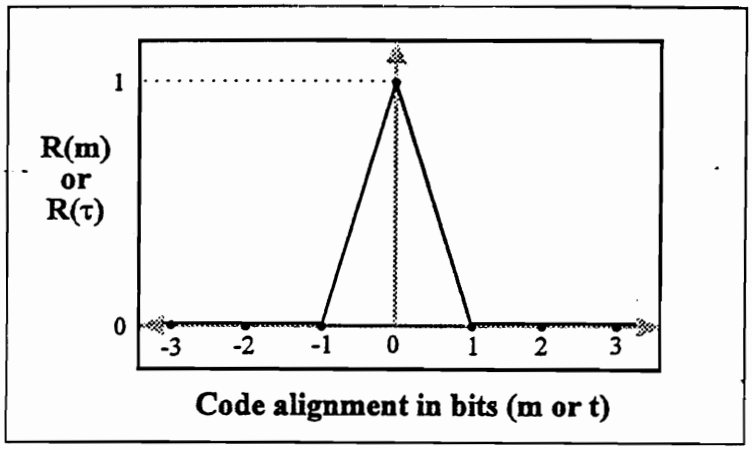

Figure 60. Plot of a typical continuous correlation function.[106]

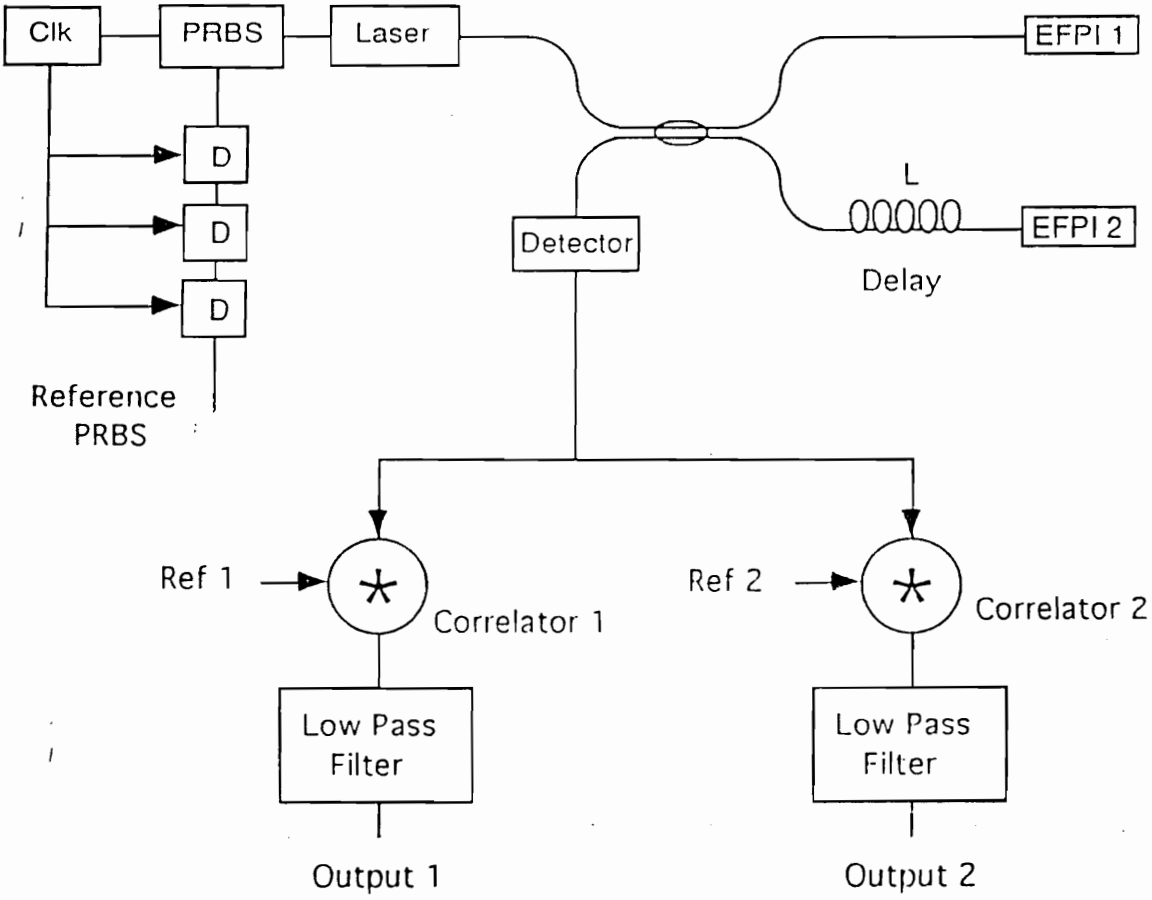

Figure 61. Basic CDM setup for multiplexing two EFPI sensors.

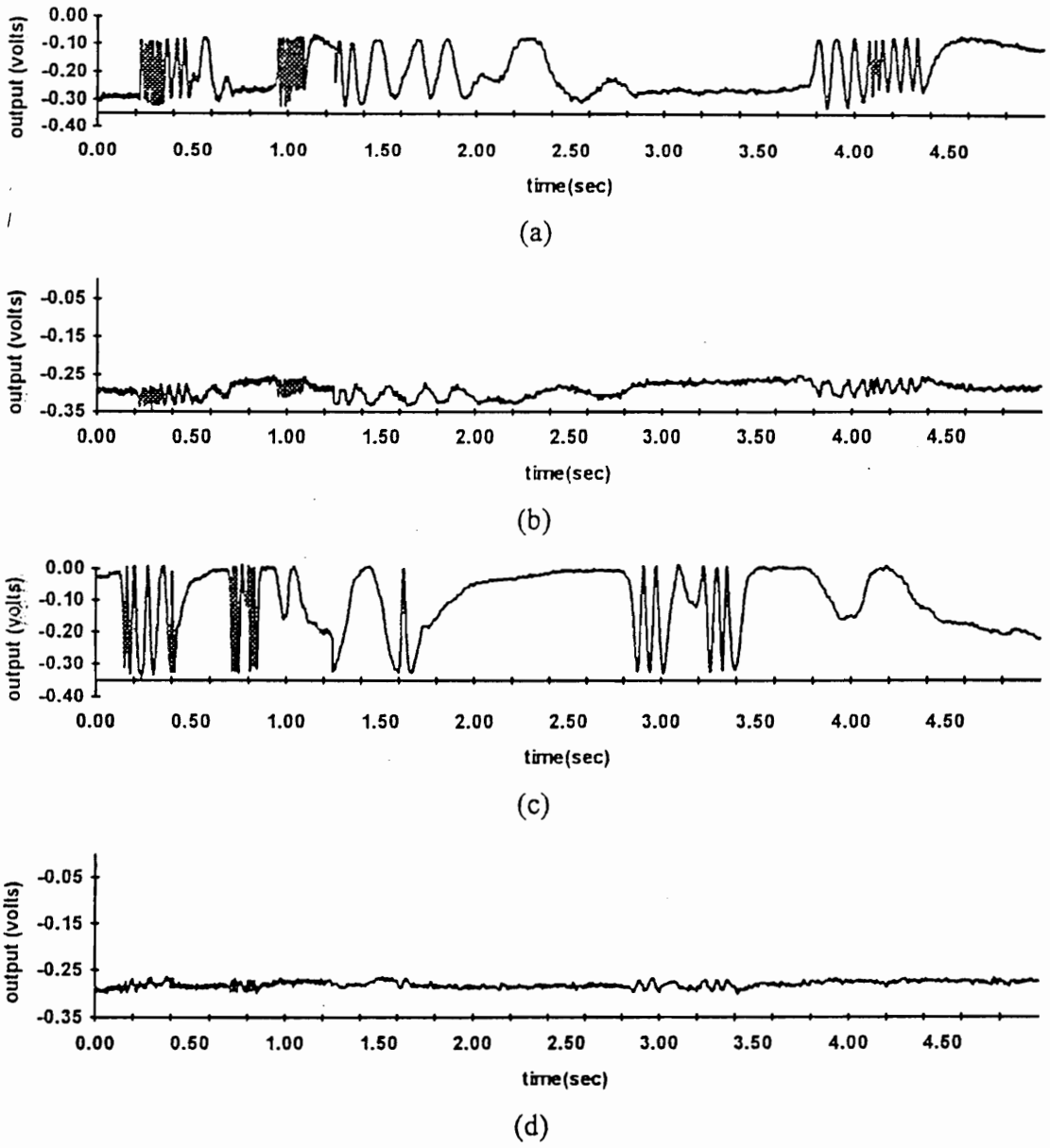

Figure 62. Crosstalk data for 15-bit sequence generated at 45.3 kbits/sec. Test 1: (a) Sensor 2 (disturbed) while (b) Sensor 1 (isolated), and Test 2: (c) Sensor 1 (disturbed) while (d) Sensor 2 (isolated).

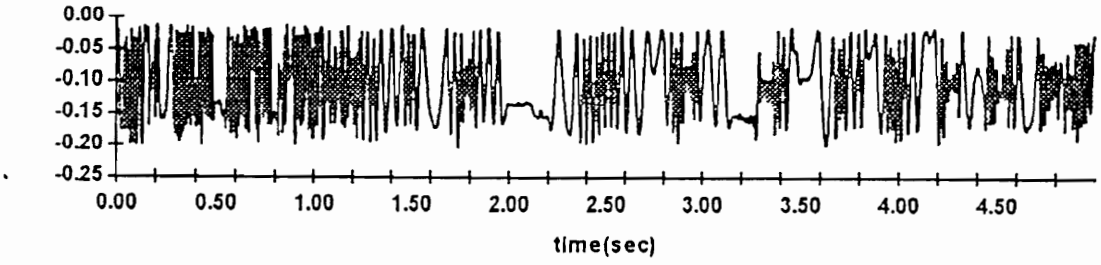

(a)

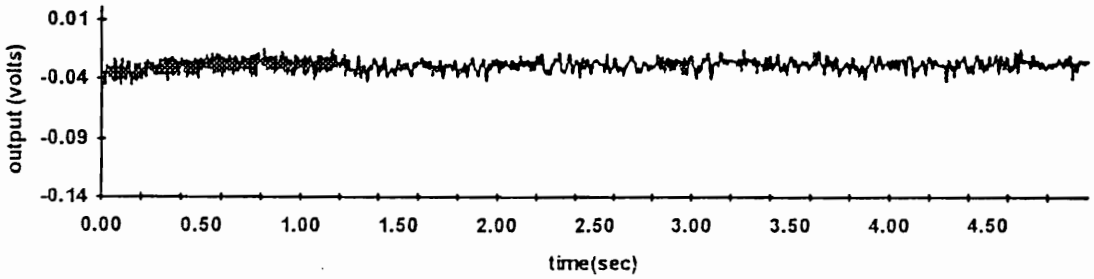

(b)

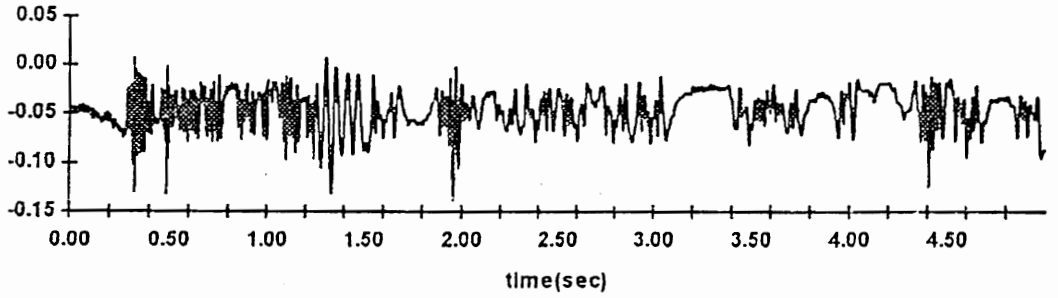

(c)

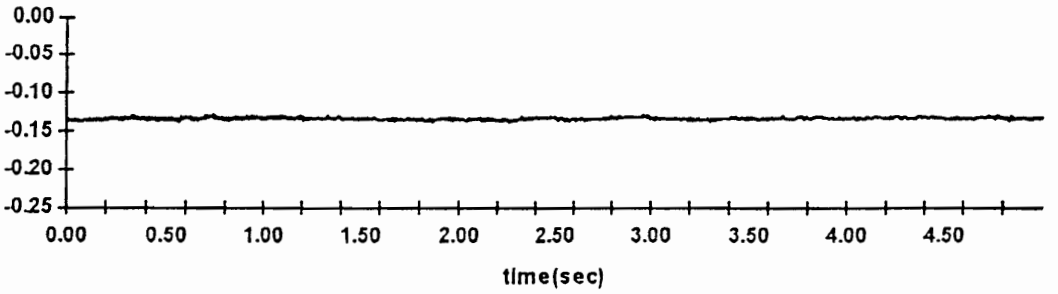

(d)

Figure 63. Crosstalk data for 15-bit sequence generated at 136 kbits/sec. Test 3: (a) Sensor 2 (disturbed) while (b) Sensor 1 (isolated), and Test 4: (c) Sensor 1 (disturbed) while (d) Sensor 2 (isolated).

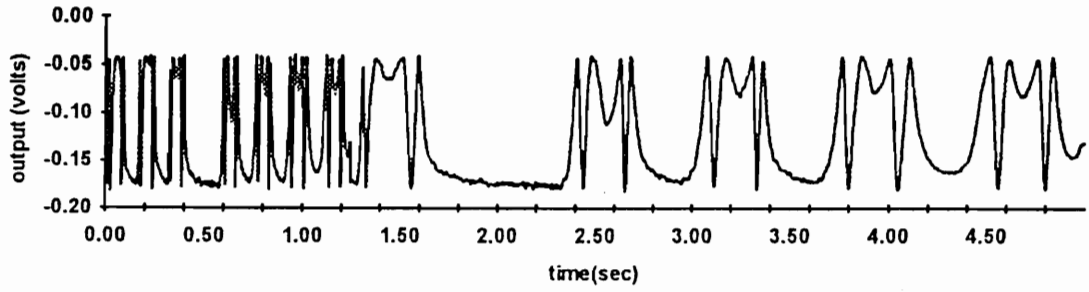

(a)

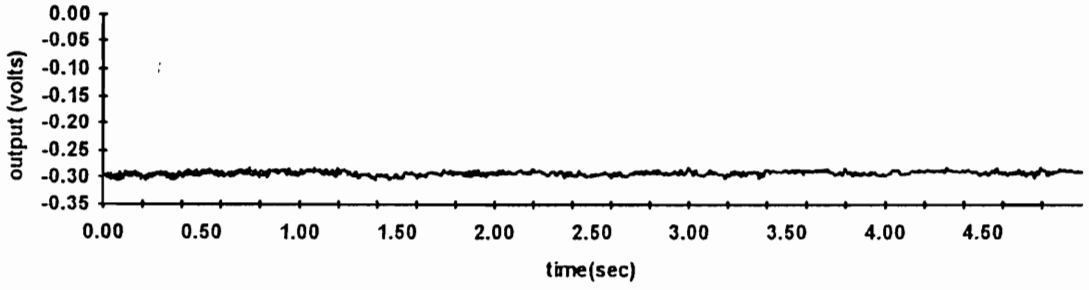

(b)

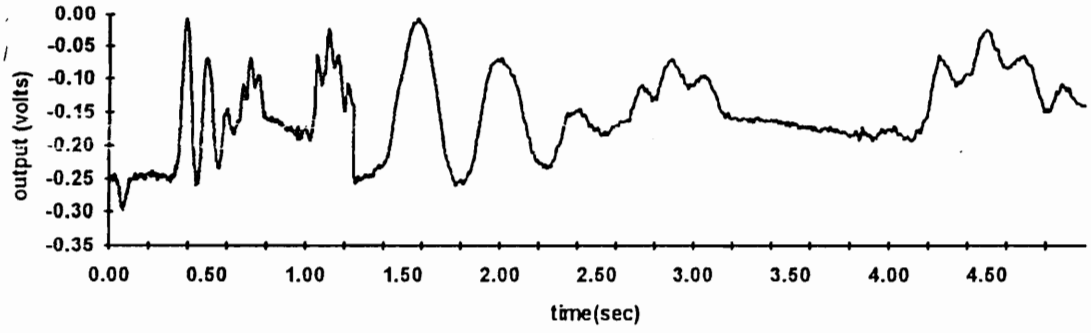

(c)

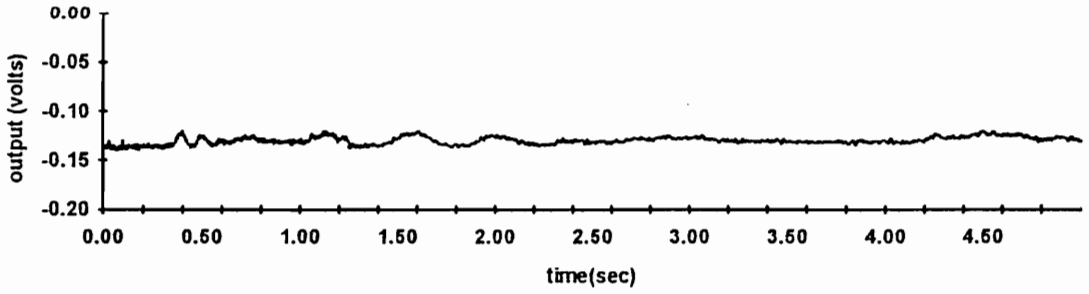

(d)

Figure 64. Crosstalk data for 127-bit sequence generated at 45.9 kbits/sec. Test 5: (a) Sensor 2 (disturbed) while (b) Sensor 1 (isolated), and Test 6: (c) Sensor 1 (disturbed) while (d) Sensor 2 (isolated).

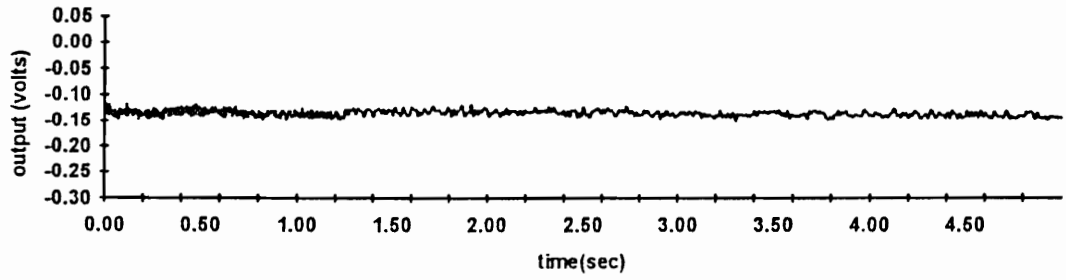

(a)

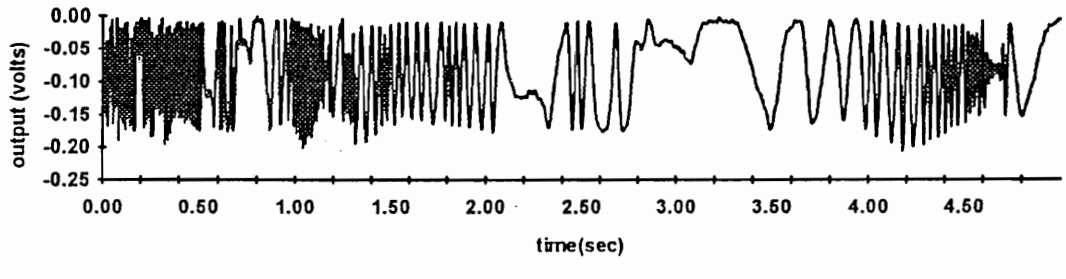

(b)

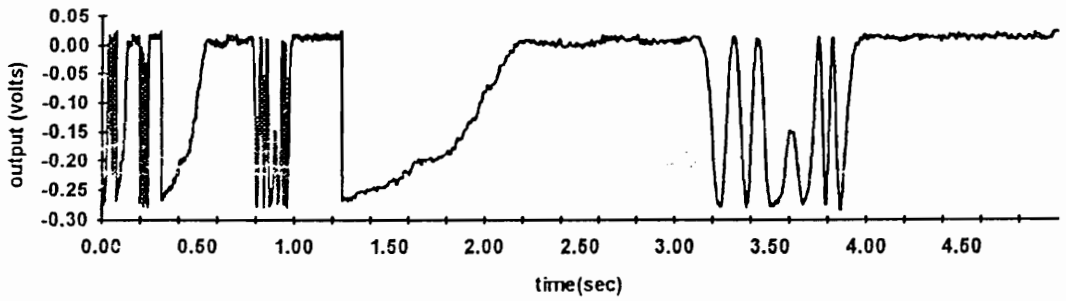

(c)

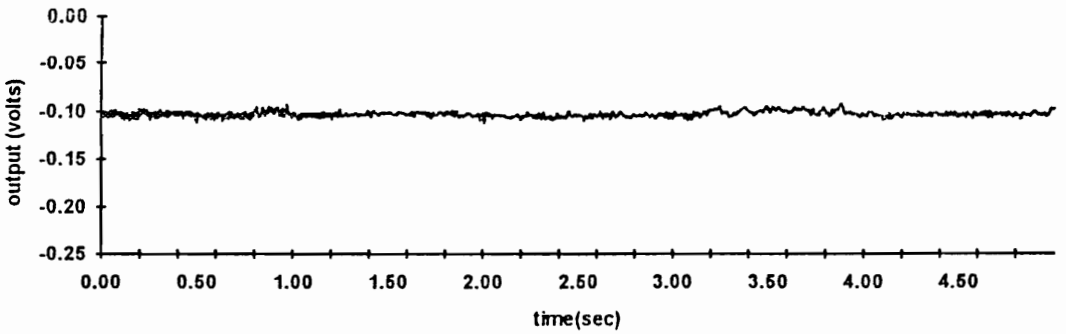

(d)

Figure 65. Crosstalk data for 127-bit sequence generated at 135.6 kbits/sec. Test 7: (a) Sensor 2 (disturbed) while (b) Sensor 1 (isolated), and Test 8: (c) Sensor 1 (disturbed) while (d) Sensor 2 (isolated).

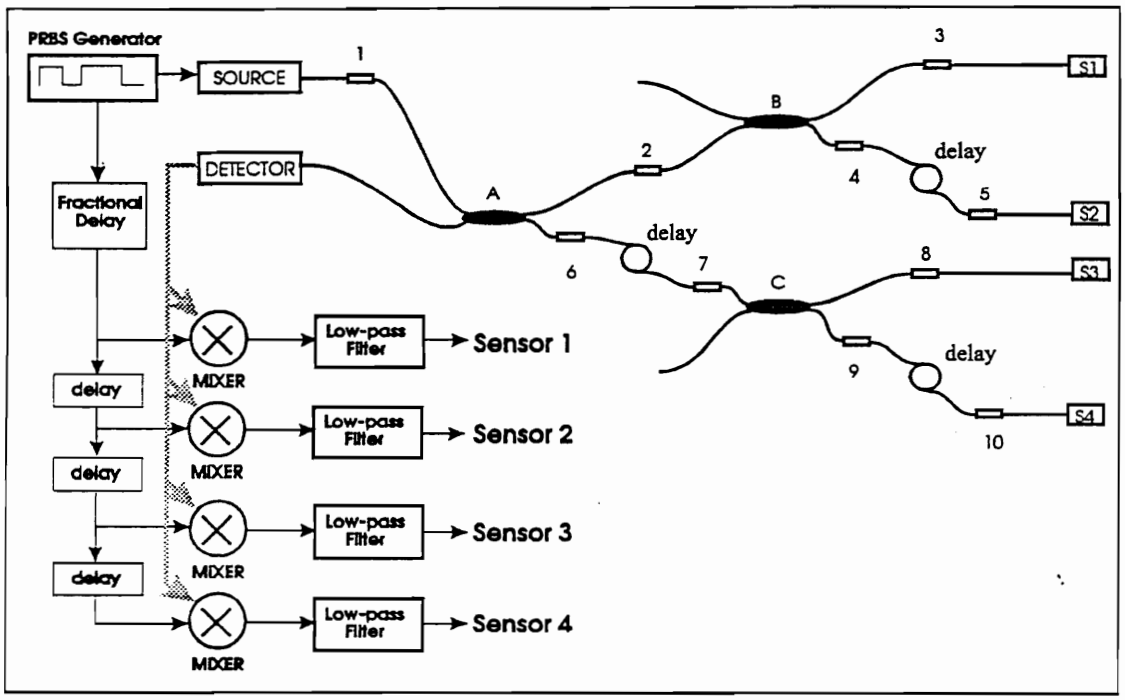

Figure 66. EFPI code division multiplexing system for 4 sensors.[106]

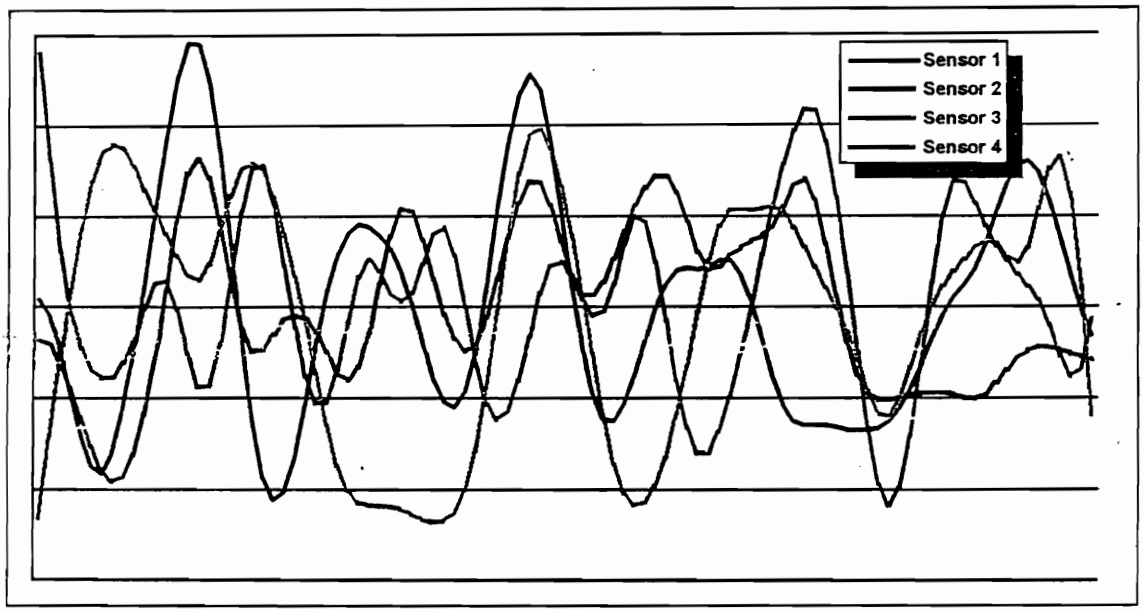

Figure 67. Sensor outputs with all four sensors being arbitrarily strained.[106]

Chapter Five

Practical Considerations

An optical fiber sensor embedded in or attached to a civil structure should be able to reliably and accurately sense condition changes over the entire lifetime of the structure. The civil infrastructure environment, especially when concrete is used, is an exceptionally harsh environment. Specialty coatings are required to protect the optical fiber sensors from corrosion caused by the high alkaline content of the concrete. During construction, extra precautions need to be taken to ensure that the sensor itself and the lead-in/out fibers are sufficiently protected from workers, machines, weather and falling material. After construction, special care must be taken not to sever the fibers at the points where they enter or exit the structural material. Fiber fracture at these points may be the single most important problem that needs to be overcome before fiber sensors can be used for the nondestructive evaluation of structures. This chapter presents a possible alternative to this problem of addressing the embedded fiber sensors. It proposes and demonstrates a novel method of communicating remotely, using flat coil antennas, with an optical fiber sensor system that is completely embedded in the material. Finally, this chapter demonstrates that the operating range of the EFPI sensor strongly depends on the fiber endface cleave angle of the input/output fiber and the target fiber inside the hollow core fiber. While this problem is not always a concern, and is easily avoided, it does have to be taken into account when fabricating EFPI sensors.

5.1 Sensor Addressing[111]

As was described in chapter 2, optical fiber sensor technology offers numerous advantages over conventional sensor technology for monitoring various structural parameters. While optical fiber sensors have advantages over conventional electric sensors, connectorization of optical fiber sensors to the supporting laser, detector and electronics has proven to be

difficult. The conventional approach to connecting the embedded optical fiber sensors and bringing the optical fiber leads out of the material creates obvious points of failure at the points where the fiber enters and exits the material. This greatly complicates the process of joining adjacent structural elements, each containing sensor fibers which must be connected. This section proposes and demonstrates the possibility of having an optical fiber sensor system that can be completely embedded within nonconducting materials. The fiber sensor as well as the supporting opto-electronic components required to launch and receive light into and from the fiber could be embedded in the material, avoiding connector problems. Interaction with the electronics to obtain strain and vibration measurements from the fiber sensor is made via external antenna coils. A more detailed description of the antenna coils is provided by Spillman *et al.*.[112,113]

5.1.1 Background

The conventional approach utilized for connecting the embedded optical fiber sensors is to bring the optical fiber leads out of the composite or concrete material through the edges or planar surfaces of the material. This creates an obvious probable point of failure for the fiber at the point where it exits the material, and greatly complicates the process of joining adjacent structural elements, each containing sensor fibers that must be connected. During the past four years, several research groups have attempted different solutions to the "smart" composite panel interconnect problem.[114,115,116] For research laboratory use, simply applying a small amount of silicone adhesive on the fiber at the point where it exits the material suffices. One of the first practical solutions was to attach small connectors to the ends of the fibers emanating from two adjacent composite panels, and to fit them into recessed pockets within each panel. A disadvantage of this method may be the reduction in structural integrity near the depression in the laminate. Yet another alternative is to terminate the sensor fiber with a good end inside a metal or glass capillary tube near the edge of the material. After trimming the materials, and carefully picking out the small chips of material in the end of the tube, connection could be made to the exposed fiber end. This method may be too cumbersome for practical field installations in the civil infrastructure environment.

5.1.2 Description

In this section the possibility of having an optical fiber system that can be completely embedded within a material is demonstrated. The fiber sensor as well as the supporting opto-electronic components required to launch light into the fiber could be embedded, avoiding conventional connector problems. Interaction with the embedded electronics, to obtain fiber sensor information, is then made with external antenna coils.

The block diagram, shown in Figure 68, labels and locates each of the critical components used. The internal part consists of a laser diode and driver, a modal domain-type sensor, oscillator, modulation and detector circuits, an internal power supply, a ferroelectric and flat coil antenna to receive power and transmit sensor information. The external part consists of the external power supply, the demodulation circuit and a ferroelectric and flat coil antenna to transmit power and receive sensor information. Linear ferrite coils, having a standard core geometry, a rating of 1600 G and operating at 50 kHz were implemented to couple 750 mW of power to the embedded circuitry. A standard laser driver circuit was designed where a 780 nm pigtailed Sharp laser diode was used to couple optical power into a modal domain-type optical fiber sensor. The detector circuit was designed for low power consumption, and to only amplify the AC sensor signal component. Vibration information is carried by the AC component of the sensor output and to achieve a higher signal to noise ratio, it is important to suppress the DC component and only amplify this AC component. Amplitude modulation was used to couple sensor information from the embedded flat coil antenna to the external flat coil antenna.

The demodulation circuit is not a part of the embedded circuitry and its design is not constrained by power requirements. The concept of inductive coupling was implemented and flat coil antennas were used to couple the modulated signal across and envelope detection was used to recover the vibration signal. A more detailed explanation regarding the determination of the exact distance between the coil antennas and the operation of the embedded circuit is given by Spillman *et al.* [113]

5.1.3 Fiber Sensor Design

A modal domain type optical fiber sensor was used to obtain qualitative vibration information from a beam. The structure of a modal domain-type fiber sensor is shown in Figure 69. The input fiber is singlemode at 1300 nm, but few-moded at 780 nm.[117] When operated at 780 nm, distinct lobes can be seen at the fiber output end due to the interference between all the propagating modes. When the fiber is bent or stretched, the output power of each of these lobes changes in a complex way. This power change is monitored and used to detect when an event, such as tapping the beam, occurs.

The operating principle behind the modal domain sensor is the use of intermodal interference in a few-moded fiber as the sensing mechanism. Modes interfere with each other as they propagate through the waveguide giving rise to an interference pattern which can be viewed by examining the projection of light from the endface. This projection will appear as a speckle pattern if viewed on a flat surface. Since the propagation constants of all of these modes are different, changes in the length of the fiber will affect the phase information of each mode differently. If only a few modes are allowed to propagate down the fiber, the interference pattern generated by those few modes is fairly simple. The projection of these few modes on a screen at the far end of the fiber would appear as a few easily distinguishable lobes, instead of a speckle pattern. When the fiber is perturbed, the intensities of these lobes shift. The intensity change of one of these lobes could be monitored to effectively determine when and how much perturbation of the fiber has occurred. In particular, another fiber can be axially offset with respect to the input fiber to receive one of the projected lobes, as is shown in Figure 69. This new fiber can be directed to a photodetector to monitor the intensity of the captured lobe. This setup can effectively measure the changes that occur along the entire length of fiber due to any of the conditions mentioned.

5.1.4 Experimental Results

The entire system that comprised the sensing and communication circuits as well as the power supply designed for the system was assembled. None of the parts were embedded

at this point. The main objective was to ascertain whether the system as a whole was capable of detecting and demodulating vibrations. The sensor was attached to a long beam and this beam was perturbed, by tapping the beam, to induce vibrations. The output of the sensor directly from the photodetector circuit and the output of the envelope detector of the demodulator circuit were simultaneously monitored on two separate channels of a digital oscilloscope. Figure 70 (upper trace) shows the photodetector output signal while Figure 70 (lower trace) shows the corresponding demodulated signal. As can be seen from these Figures, the correlation between the sensor output and the demodulated signal is very high. The only difference is that the signals are 180° out of phase with each other. The results shown in Figure 70 clearly indicate the effectiveness of the designed system in the detection of acoustic vibrations.

This section demonstrated the feasibility of communicating remotely between external sensor system electronics and an electronic optical fiber sensor network. It was shown that coil antennas could be used to couple energy to a power supply used to drive the electronics for the laser diode and driver, oscillator, modulation and detector circuits, and also that flat coil antennas can be used to couple out the modulated detected signal, from a modal domain-type optical fiber sensor. Most importantly, however, it was shown that the original signal can be recovered by demodulating the modulated signal that was coupled out of the material. The concepts developed could potentially allow the coupling of sensor signals between multiple adjacent structural components and the creation of a larger distributed fiber sensor based smart structure. Also, in practice, it may allow the external interrogation of the health of the individual material components, through periodic inspection. In future experiments, circuit designs requiring less power than the present design need to be developed.

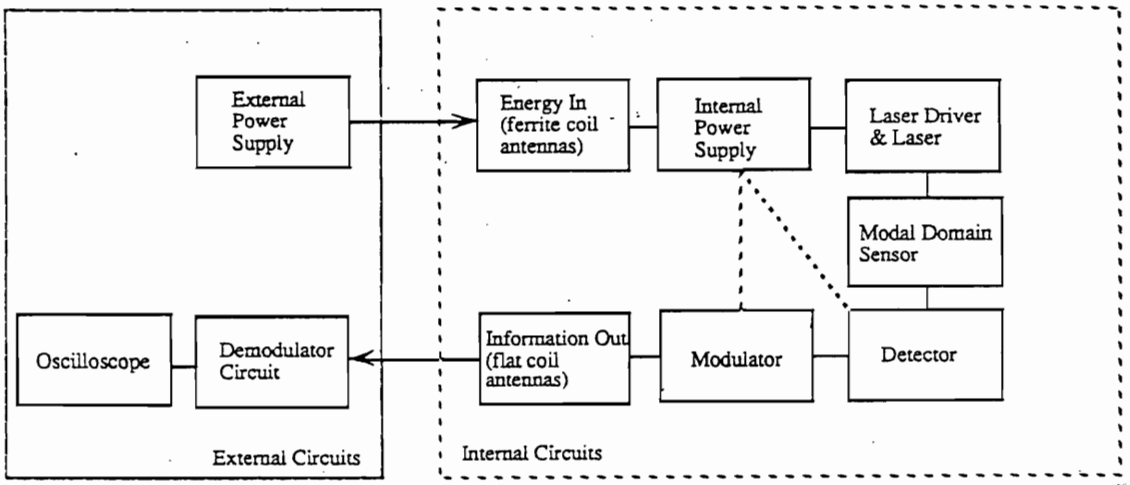

Figure 68. Block diagram of the completely embedded optical fiber sensor system.

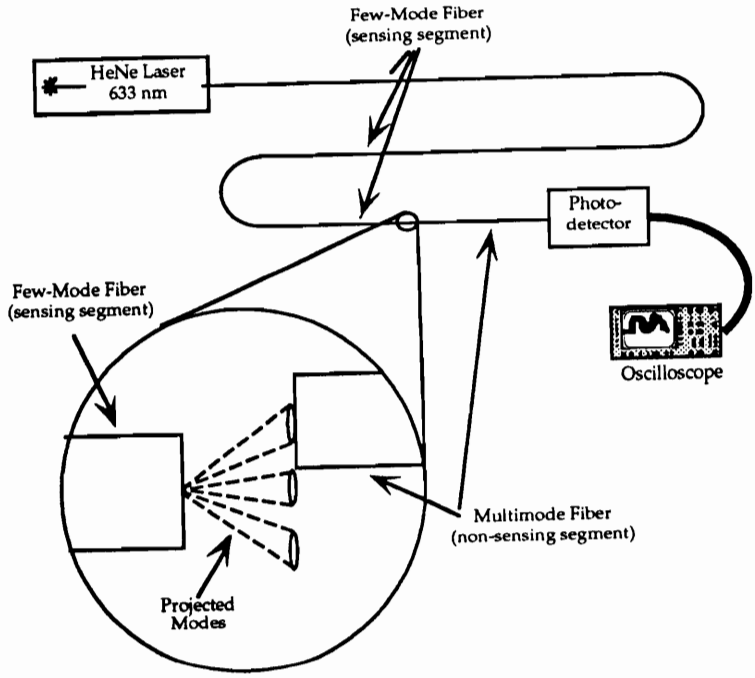

Figure 69. Modal domain type optical fiber setup.

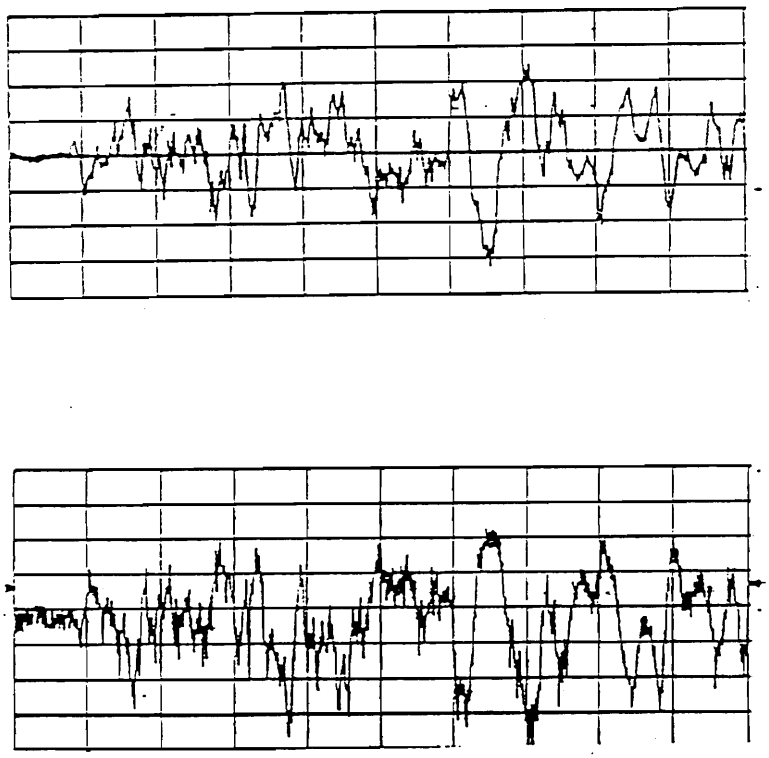

Figure 70. Output signal at the photodetector (upper trace), Output signal corresponding to the demodulated signal.

5.2 EFPI Fiber Endface Angles

Backreflections from the couplers and fiber endfaces are avoided in optical fiber-based communication applications. For the operation of the EFPI sensor, however, the reflections from the glass-air and air-glass interfaces are very important and influence the performance of the sensor. This section discusses and demonstrates the importance of good fiber endface cleaves for the operation of the EFPI sensor.

For communication applications optical fibers are sometimes cleaved at angles greater than 8° to reduce backreflections to -60 dB or less. In the following experiment fibers were cleaved at various angles to investigate the effect of fiber angle on fringe contrast. A York FK12 fiber cleaver was used to cleave angled fibers and a Norland Fiber Interferometer inspection scope was used to check the fiber endface angle. The angles were determined to an accuracy of approximately 0.2 degrees. Fibers can be cleaved at different angles by varying the angle of twist, axial tension, clamp separation, or fiber type and diameter.[118] Assuming that the same fiber is used and the tension is not adjusted, the cleave angle is approximately proportional to the angle of twist to clamp separation ratio. To cleave the fiber, a section of fiber is stripped, clamped on both ends, axially tensioned, twisted by a predetermined amount, and scribed by a vibrating diamond blade. Usually the fiber endfaces are not perfect and can have a saddle shape with an average end angle. This shape is due to the stress pattern that arises from twisting the fiber.

The back-reflected intensity was monitored for different fiber angle cleaves. To ensure that the output intensity from the laser diode remained constant, the laser output power was monitored throughout the experiment. The results from this experiment, shown in Figure 71, indicate, as should be expected, that cleaving fiber at angles reduces back-reflection.

In the next experiment the singlemode 9/125 μm input/output fiber was cleaved so the angle was less than 0.2 degrees, inserted into the 126μm ID hollow core fiber and epoxied to the hollow core fiber. The reflector fiber was cleaved at various angles and also inserted into the hollow core fiber, and to ensure that the fiber could freely slide in and out of the hollow

core fiber no epoxy was applied. Fringe contrast as a function of gap separation was monitored and results are shown in Figure 72. As was expected for angled fibers the signal to noise ratio is greatly reduced as a function of angle. Hence the range of operation for this fiber sensor is greatly reduced. To ensure a full range of operation, it is extremely important to ensure that fiber endface angle of the input/output fiber and the target fiber inside the hollow core fiber are minimized.

This chapter briefly described a few of the practical concerns that need to be taken into account when implementing optical fiber sensors into a civil infrastructure environment. A possible solution to the problem of fiber fracture at the points where it enters and exits the concrete or composite material was suggested. Finally, to ensure a full range of operation of the EFPI sensor, the importance of minimizing the fiber endface angle of the input/output fiber and the target fiber inside the hollow core fiber was shown. Issues that determine the long-term survivability of the fiber sensor such as water, moisture, alkalinity and other environmental parameters that affect the strength of the fiber and its coatings need to be investigated in greater detail before fiber sensors can be fully integrated into a structure.

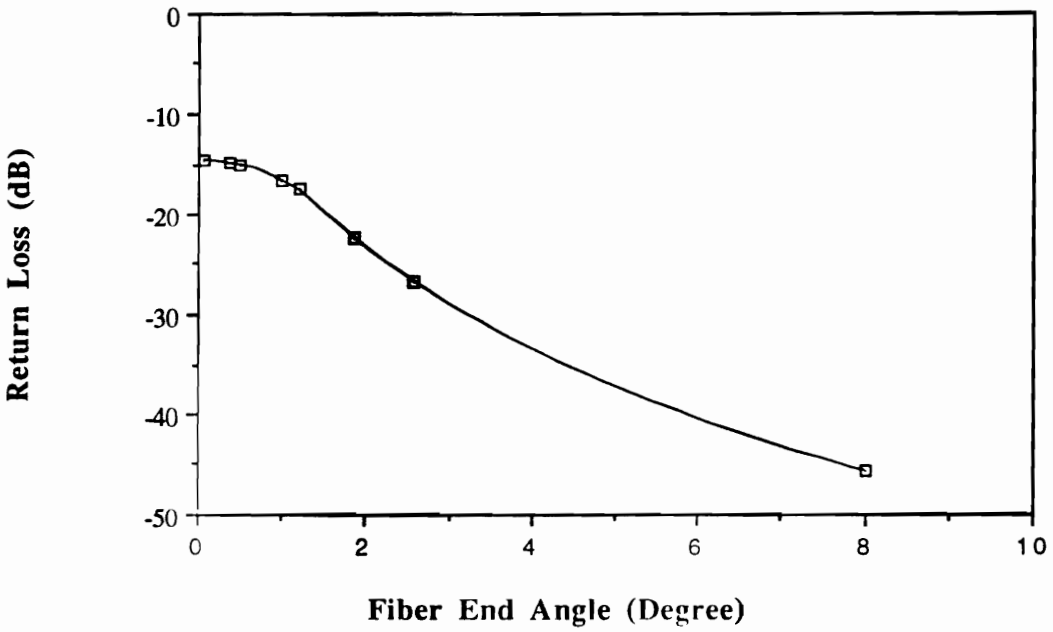

Figure 71. Back-reflected intensity as a function of fiber endface cleave angle.

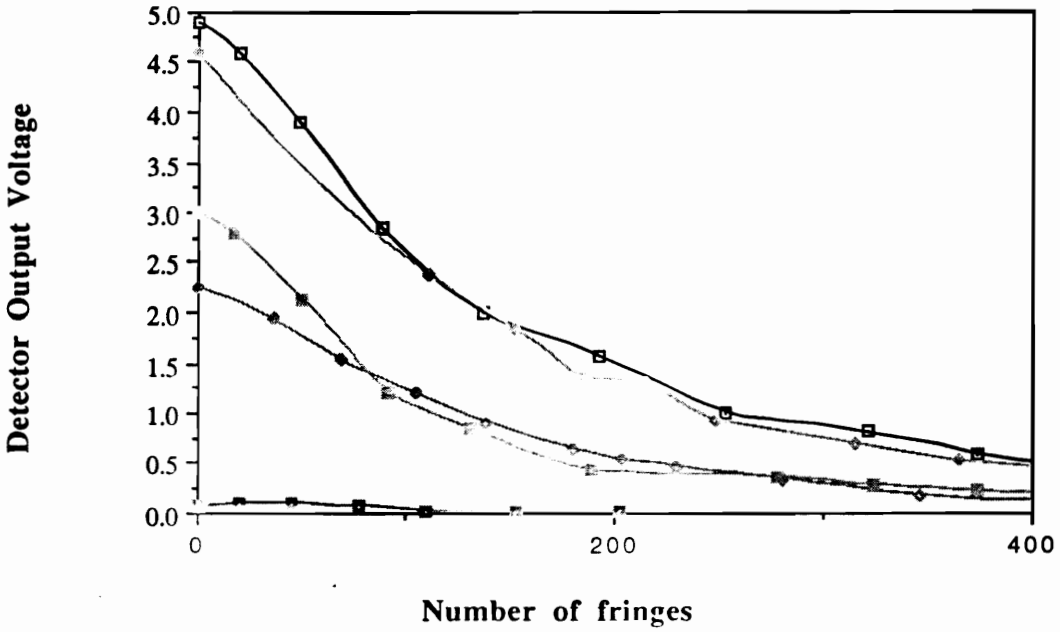

Figure 72. Fringe contrast as a function of gap length for different target fiber endfaces angles.

Chapter Six

Conclusions

A detailed study of optical fiber sensors for the nondestructive evaluation of existing and advanced civil structures was proposed, demonstrated and implemented. A comparative evaluation of fiber optic sensors for monitoring civil structures was systematically developed and based on this evaluation the extrinsic Fabry-Perot interferometric (EFPI) optical fiber sensor was selected. To obtain the signal-to-noise ratio of the sensor as a function of gage length the operation of the EFPI sensor was described using the Kirchhoff diffraction theory approach.

The EFPI sensor and the absolute EFPI (AEFPI) sensor were implemented in the following three different practical civil structure applications:

1. With researchers at the civil engineering department at the University of Southern California, EFPI sensors were used to monitor strain at critical locations near the panel zone of interior and exterior column-to-beam connections. Strain information from the EFPI sensors compared well with the collocated foil strain gages.
2. At the United States Bureau of Mines in Spokane, Washington, EFPI sensors were used to obtain strain data from rebar and cable-type bolts used to reinforce mining roofs. Results correlated very well with theory.
3. Finally, at the Turner Fairbanks Federal Highway Administration in McLean, Virginia, absolute EFPI sensors were used to monitor strain on composite prestressing strands used for reinforcing concrete. Results obtained from the fiber optic strain gage were within 2% of the value measured by the collocated foil strain gage.

For each application, a complete description of the implementation was given and results obtained from these investigations were analyzed in detail and compared with results obtained from collocated foil strain gages to ensure that the results were quantitative, reliable and accurate. Preliminary results demonstrating that spread spectrum and OTDR techniques can be used to multiplex EFPI sensors were also presented.

The majority of fiber optic sensor work performed by researchers thus far in the area of civil structures was focused on obtaining qualitative rather than quantitative information. This dissertation has demonstrated that optical fiber sensors can be used to nondestructively monitor and quantitatively evaluate the condition of civil infrastructure components. This dissertation has also illustrated the importance of having optical fiber sensors that can perform quantitative measurements rather than qualitative measurements. As was pointed out however, much research remains to be done pertaining to the survivability of optical fiber sensors in the civil infrastructure environment.

Finally, practical considerations that need to be taken into account with the implementation of optical fiber sensors in a civil infrastructure environment were discussed. A possible solution to the problem of fiber breakage at the point where the fiber enters and exits the material was presented and demonstrated.

References

[1] Civil Infrastructure Systems Research: Strategic Issues," A Report of the Civil Infrastructure Systems Task Group, National Science Foundation, January 1993.

[2] N.H. Bettigole, "Rebuilding Our Bridges - Why and How," Standardization News, July 1994, pp. 24 - 27.

[3] K.F. Dunker, B.G. Rabbat, "Why America's Bridges Are Crumbling," Scientific American, March 1993, pp. 66 - pp. 74.

[4] J. Dakin, B. Culshaw, *Optical Fiber Sensors: Principles and Components*, Artech House, Boston, MA 1988.

[5] T.G. Giallorenzi, J.A. Bucaro, A. Dandridge, G.H. Sigel, J.H. Cole, S.C. Rashleigh, R.G. Priest, "Optical fiber sensor technology," IEEE J. of Quantum Electronics, vol. 18, pp. 626 - 665, 1982.

[6] E. Udd, *Overview of fiber optic applications to smart structures*, 1988, New York: Plenum.

[7] R.O. Claus, *Fiber Optic Sensor-Based Smart Materials and Structures*, IOP Publishing, Bristol and Philadelphia, April 1992.

[8] U. Meier, "Carbon Fiber-Reinforced Polymers: Modern Materials in Bridge Engineering," Structural Engineering International, 1, 92, pp. 7 - 12.

[9] P. Kim, U. Meier, "CFRP Cables for Large Structures," Proc. of Advanced Composite Materials in Civil Engineering Structures, Las Vegas, Jan. 31 1991, pp. 233 - 244.

[10] A.S. Brown, "Sneaking up on nondefense applications," Aerospace America, March 1994, pp. 32 - 42.

[11] H. Singh, J.S. Sirkis, "Micromechanics of Laminated Composites with Embedded Optical Fibers," proc. of Smart Materials and Structures Workshop, Blacksburg, Va, April 1991..

[12] P. Escobar, V. Gusmeroli, M. Martinelli, "Fiber-optic interferometric sensors for concrete structures," 1st European Conf. on Smart Structures and Materials, Glasgow 1992, pp. 215 - 218.

[13] D.R. Huston, P.L. Fuhr, P.J. Kajenski, T.P. Ambrose, W.B. Spillman, "Installation and preliminary results from fiber optic sensors embedded in a concrete building," 1st European Conf. on Smart Structures and Materials, Glasgow 1992, pp. 409 - 412.

[14] R. Maaskant, T. Alavie, R.M. Measures, M. Ohn, S. Karr, D. Glennie, C. Wade, G.Tadros, S. Rizkalla, "Fiber Optic Bragg grating sensor network installed in a concrete road bridge," SPIE Vol. 2191, pp. 457 - 467.

[15] F. Ansari, "Real-Time Condition Monitoring of Concrete Structures By Embedded Optical Fibers," ASCE Proc. of Nondestructive Testing of Concrete Elements and Structures, San Antonio, TX, April 1992, pp. 49 - 59.

[16] F. Ansari, Q.Y. Chen, "Fiber-Optic refractive-index sensor for use in fresh concrete," Applied Optics, Vol. 30, No. 28, October 1, 1991.

[17] A. Nanni, C.C. Yang, K. Pan, J.S. Wang, R.R. Michael, "Fiber-Optic Sensors for Concrete Strain/Stress Measurement," ACI Materials Journal, May-June 1991, pp. 257 -

[18] J. Calero, S.P. Wu, C. Pope, S. L. Chuang, J.P. Murtha, "Theory and Experiments on Birefringent Optical Fibers Embedded in Concrete Structures," IEEE J. of Lightwave Technology, Vol. 12, No. 6, June 1994, pp. 1081, 1091.

[19] J. Sirkis, "Phase-Strain-Temperature Model for Structurally Embedded Interferometric Optical Fiber Strain Sensors with Applications," SPIE Vol. 1588 Fiber Optic Smart Structures and Skins IV (1991) pp. 26 - pp. 43.

[20] A. Mendez, T.F. Morse, L.J. Reinhart, "Experimental Results on Embedded Optical Fiber Sensors in Concrete," AMD-Vol. 181, Experiments in Smart Materials and Structures, ASME 1993, pp. 53 - 60.

[21] A. Mendez, T.F. Morse, "Overview of Optical Fiber Sensors Embedded in Concrete," SPIE Proceedings, Vol. 1798, No. 22, Fiber Optic Smart Structures and Skins V, MA 1992.

[22] D. Huston, P. Fuhr, P. Kajenski, D. Snyder, "Concrete Beam Testing with Optical Fiber Sensors," ASCE Proc. of Nondestructive Testing of Concrete Elements and Structures, San Antonio, TX, April 1992, pp. 60 - 69.

[23] A.J. Majumdar, "Glass fibre reinforced cement and gypsum products," Proc. Roy. Soc. Lond. A. 319, 1970, pp. 69 - 78.

[24] P.L. Fuhr, D.R. Huston, T.P. Ambrose, D.A. Barker, "Embedded Sensors Results from the Winooski One Hydroelectric Dam," SPIE Vol. 2191, pp. 446 - 456.

[25] R. Wolff, H.J. Miesseler, "Monitoring of prestressed concrete structures with optical fiber sensors," 1st European Conf. on Smart Structures and Materials, Glasgow 1992, pp. 23 - 30.

[26] A.T. Alavie, R. Maaskant, M.M. Ohn, S. Rizkalla, R.M. Measures, "Application and Characterization of Intracore Grating Sensors in a CFRP Prestressed Concrete Girder," SPIE Vol. 2191, pp. 103 - 110.

[27] A. Wang, V. Arya, M. de Vries, K.A. Murphy, R.O. Claus, "Exact analysis of the extrinsic Fabry-Perot interferometric optical fiber sensor using Kirchhoff's diffraction formalism," submitted for publication to Optics Letters.

[28] M. de Vries, K.A. Murphy, V. Arya, S. Poland, R.O. Claus, "Optical Fiber Sensors for Civil Structure Applications: A Comparative Evaluation," First World Conference on Structural Control, 3- 5 August 1994, Los Angeles, California.

[29] A. Wang, S. Gollapudi, K. A. Murphy, R. G. May, R. O. Claus, "Sapphire-fiber-based intrinsic Fabry-Perot interferometric sensors," *Optics Letters*, July 1992, Vol. 17, No. 14.

[30] A. Wang, S. Gollapudi, R. G. May, K. A. Murphy, R. O. Claus, "Advances in sapphire-fiber-based interferometric sensors," *Optics Letters*, Nov. 1992, Vol. 17, No. 21.

[31] A.M. Vengsarkar, J.A. Greene, K.A. Murphy, "Photoinduced refractive-index changes in two-mode, elliptical-core fibers: sensing applications," Optics Letters, 1991, 16, pp. 1541 - 1543.

[32] A.M. Vengsarkar, J.A. Greene, B.R. Fogg, K.A. Murphy, "Spatially-weighted, grating-based, two-mode, elliptical-core optical fiber vibration sensors," Optics Letters, 1991, 16, pp. 1707 - 1709.

[33] K.O. Hill, Y. Fuiji, D.C. Johnson, B.S. Kawaski, "Photosensitivity in optical fiber waveguides: Applications to reflection filter fabrication," Applied Physics Letters, 32, pp. 647.

[34] G. Meltz, W.W. Morey, W.H. Glenn, "Formation of Bragg gratings in optical fibers by transverse holographic method," Optics Letters, Vol. 14, pp. 823.

[35] K. A. Murphy, M. F. Gunther, A. M. Vengsarkar, R. O. Claus "Quadrature phase-shifted, extrinsic Fabry-Perot optical fiber sensors,", *Optics Letters*, Nov. 1991, Vol. 16, No. 21.

[36] K. A. Murphy, M. S. Miller, A. M. Vengsarkar, R. O. Claus, "Elliptical-core, two-mode, optical fiber sensor implementation methods," *IEEE Journal of Lightwave Technology*, 1990, Vol. 8, No. 11.

[37] J. A. Greene, K. A. Murphy, B. R. Fogg, R. O. Claus, A. M. Vengsarkar, "Optical fiber, vibration mode filters incorporating photoinduced refractive index gratings," *Smart Materials and Structures*, 1992, Vol. 1.

[38] K. A. Murphy, V. Arya, A. Wang, R. O. Claus, "Microbend losses in singlemode optical fibers: theoretical and experimental investigation," submitted to the *IEEE Journal of Lightwave Technology*.

[39] K. A. Murphy, V. Arya, A. Wang, R. O. Claus, "Investigation of microbend losses in singlemode optical fibers," *10th Optical Fiber Sensors Conference UK*, 11-13 October, 1994.

[40] A. Wang, K. A. Murphy, "Optical fiber temperature sensor based on differential spectral reflectivity, " *Smart Materials and Structures*, 1992, Vol. 1.

[41] A. Wang, M. F. Gunther, K. A. Murphy, R. O. Claus, "Fiber-optic liquid-level sensor," *Sensors and Actuators*, 1992, Vol. 35.

[42] K.A. Murphy, M.J. de Vries, "A Comparative Evaluation of the Types and Applications of Various Sensors," The Photonics Design and Applications Handbook 1994 Book 3, Laurin Publishing Co., Inc.

[43] D. Hogg, T. Valis, B. Mason, R. Measures, "Temperature compensated strain measurements using fiber Fabry-Perot (FFP) strain gauges," Fifth Annual Fiber Optic Sensor-Based Smart Materials and Structures Workshop, Blacksburg, VA, pp. 31, April 1992.

[44] T. Yoshino, K. Kurosawa, K. Itoh, T.Ose, "Fiber-optic Fabry-Perot interferometer and its sensor applications," IEEE J. Quantum Electron. 1982, QE-18, pp. 1624-1632.

[45] A.D. Kersey, D.A. Jackson, M. Corke, "A simple fibre Fabry-Perot sensor," Opt. Commun., 1983, 45, pp. 71 - 74.

[46] K.L. Belsey, J.B. Carroll, L.A. Hess, D.R. Huber, D. Schmadel, "Optically Multiplexed Interferometric Fiber Optic Sensor System," SPIE Vol. 566, pp. 257, 1985.

[47] C.E. Lee, W.N. Gibler, R.A. Atknis, H.F. Taylor, "In-line fiber Fabry-Perot interferometer with high reflectance internal mirrors," Journal of Lightwave Technology, vol. LT-4, pp. 382 - 385, 1986.

[48] C.E. Lee and H.F. Taylor, "Interferometric optical fibre sensors using internal mirrors," Electron. Lett. 1988, 24, pp. 193 - 194.

[49] K.A. Murphy, M.F. Gunther, A.M. Vengsarkar, R.O. Claus, "Fabry-Perot fiber optic sensors in full-scale fatigue testing on an F-15 aircraft," Applied Optics, 1991.

[50] R.O. Claus, M.F. Gunther, A. Wang, K.A. Murphy, "Extrinsic Fabry-Perot sensor for strain and crack opening displacements from -200 to 900 °C, "Smart Materials and Structures, vol. 1, pp. 237 - 242, 1992.

[51] T.A. Tran, W.V. Miller III, K.A. Murphy, A.M. Vengsarkar, R.O. Claus, "Stabalized Extrinsic Fiber-Optic Fizeau Sensor for Surface Acoustic Wave Detection," J. Lightwave Technology, Vol. 10, No. 10, October 1992, pp. 1499 - 1506.

[52] K.A. Murphy, *Novel Phase-Modulated Optical Fiber Sensors*, Ph.D. Dissertation, Virginia Polytechnic Institute & State University, Blacksburg, VA, August 1992.

[53] D. Marcuse, *Applied Optics*, **23**, pp. 1082 - 1091, 1984.

[54] M. Born, E. Wolf, *Principles of Optics*, Pergamon Press, New York, 1985.

[55] P.P. Banerjee, T.C. Poon, *Principles of Applied Optics*, Aksen Associates Inc. Publishers, 1991.

[56] V.Bhatia, K.A. Murphy, R.O. Claus, T.A. Tran, J.A. Greene, "Absolute strain and temperature measurements using high finesse EFPI cavities," FEORC Fiber Optics Review Conference, Blacksburg, VA, April 1994.

[57] Fiber & Sensor Technologies Inc., Christiansburg, VA, AEFPI sensor technical data sheets.

[58] E.M. Higazy, A.S. Elnashai, M.S. Agbabian, "Experimental Seismic Response Characteristics of Marginal High Strength Concrete Beam-Column Connections," pp. 101 -

[59] M.S. Agbabian, E.M. Higazy, M. Abdel-Ghaffar, "Experimental Observation on the Seismic Shear Performance of RC Beam-to-Column Connections Subjected to Varying Axial Column Force," Earthquake Engineering and Structural Dynamics, 1994, Vol. 23, pp. 859 - 876.

[60] S.F. Masri, M.S. Agbabian, A.M. Abdel-Ghaffar, M. Higazy, R.O. Claus, M.J. de Vries, "Experimental Study of Embedded Fiber-Optic Strain Gauges in Concrete Structures," J. Engineering Mechanics, Vol. 120, No. 8, August, 1994, pp. 1696 - 1717.

[61] E.M. Higazy, "Seismic Shear Performance of Beam-Column Subassemblages in Multistory R/C Structures," Ph.D. Dissertation, Civil Engineering Department, University of Soutern California, Los Angeles, California, April 1993.

[62] J.M. Goris, "Underground Mining," Yearbook of Science and Technology, McGraw-Hill, 1994, pp. 424 -425.

[63] K. Green, G. Langlot, T. Stratton, "Sensing and Monitoring Strain on Steel Cables," Final Rep. to US Bureau of Mines, 1994, Spokane, WA.

[64] J.M. Goris, "Application of cable bolts in underground coal mines," Innovative Mine Design for the 21st Century, Bawden & Archibald, 1993 Balkema, Rotterdam, pp. 1001 - 1008.

[65] J.M. Goris, *Laboratory Evaluation of Cable Bolt Supports (Part 2)*, RI 9342, US Dept. of the Interior, Bureau of Mines.

[66] J.M. Goris, *Laboratory Evaluation of Cable Bolt Supports (Part 1)*, RI 9308, US Dept. of the Interior, Bureau of Mines.

[67] J.M. Goris, T.M. Brady, L.A. Martin, *Field Evaluation of Cable Bolt Supports, Homestake Mine, Lead*, SD, RI 9474, US Dept. of the Interior, Bureau of Mines.

[68] R.G. May, R.O. Claus, K.A. Murphy, "Preliminary evaluation for developing smart ropes using embedded sensors," 1st European Conference on Smart Structures and Material, 1993, pp. 155 - 158.

[69] E.G. Nawy, *Prestressed Concrete*, Prentice Hall, New Jersey, 1989.

[70] 10. M. de Vries, V. Bhatia "Applications of Absolute EFPI Fiber Optic Sensing Systems for Measurement of Strain in Prestrained Strands for Prestressed Concrete,", submitted for publication.

[71] A.D. Kersey, A. Dandridge, "Distributed and Multiplexed Fiber Optic Sensor Systems," J. IERE, Vol. 58, 1988.

[72] K.L. Belsley, J.B. Carroll, L.A. Hess, D.R. Hubber, D. Schmadel, "Optically multiplexed interferometric fiber optic sensor system," Proc. SPIE Int. Soc. Opt. Eng., 1985, vol. 566, pp. 257 - 264.

[73] A.R. Nelson et al., "Passive Multiplexing System for Fiber Optic Sensors," Applied Optics, 19, 2917 (1980).

[74] J.R. Dunphy, G. Meltz, R.M. Elkow, "Distributed strain sensing with a twin-core fiber optic sensors," ISA Trans. 26: 7 - 10.

[75] M.C. Farries et al., "Distributed Temperature Sensor Using Nd^3-Doped Optical Fiber," Electron Letters, 22, 418 (1986).

[76] Mickelson et al., "Backscatter Readout from Serial Microbending Sensors," IEEE J. Lightwave Technology, LT-2, 700 (1984).

[77] A.H. Hartog, "A Distributed Temperature Sensor Based on Liquid Core Optical Fibers," IEEE J. Lightwave Technology, LT-1, 498 (1983).

[78] A.J. Rogers, "Distributed Sensors: A Review," Paper 03, Proc. SPIE 798, Fiber Optic Sensors II, The Hague, 1987.

[79] J.L. Brooks, B. Moslehi, B.Y. Kim, H.J. Shaw, "Time-Domain Addressing of Remote Fiber-Optic Interferometric Sensor Arrays," J. Lightwave Technology, Vol. 5, No. 7, July 1985, pp. 1014, 1022.

[80] A.D. Kersey, A. Dandridge, "Multiplexed Mach-Zehnder Ladder Array with Ten Sensor Elements," Elect. Lett, Vol. 25, No. 19, pp. 1297 - 1299.

[81] A.D. Kersey, A. Dandridge, K.L. Dorsey, "Transmissive Serial Interferometric Fiber Sensor Array," J. Lightwave Technology, Vol. 7, No. 5, May 1989, pp. 846 - 854.

[82] A.D. Kersey, A. Dandridge, A.B. Tveten, "Time-division multiplexing of interferometric fiber sensors using passive phase-generated carrier interrogation," Optics Letter, Vol. 12, No. 10, October 1987, pp. 775 - 777.

[83] H. Ishido, et al., "Review and status of WDM technology and its applications," J. Lightwave Technology, vol. 2, pp. 448, 1984.

[84] A.D. Kersey, "Demonstration of a Hybrid Time/wavelength Division Multiplexed Interferometric Fibre Sensor Array," Electron. Lett., Vol. 27, pp. 554, 1991.

[85] A.D. Kersey, "Multiplexing Options for Quasi-Distributed Sensing in Smart Structures Using Fiber Interferometry," Proc. of the Conf. on Optical Fiber Sensor-Based Smart Materials and Structures, Blacksburg, VA, 1991, pp. 6 - 12.

[86] A. Dandridge, A.B. Tveten, A.D. Kersey, A.M. Yurek, "Multiplexing of Interferometric Sensors Using Phase Carrier Techniques," J. Lightwave Technology, Vol. 5, No. 7, 1987, pp. 947 - 952.

[87] A. Dandridge, A.B. Tveten, T. Giallorenzi, "Homodyne Demodulation Scheme for Fiber Optic Sensors Using Phase Generated Carrier," J. Quantum Electronics, Vol. QE-18, No. 10, October 1982, pp. 1647 - 1652.

[88] E. Udd, *Fiber Optic Sensors: An Introduction for Engineers and Scientists*, John Wiley & Sons, 1991.

[89] J.L. Brooks, R.H. Wentworth, R.C. Yougquist, M. Tur, B.Y. Kim, H.J. Shaw, "Coherence Multiplexing of Fiber-Optic Interferometric Sensors," J. Lightwave Technology, Vol. 3, pp. 1062 - 1071.

[90] A.J. Rogers, "Polarization Optical Time Domain Reflectometery, Electron Letters, 16, 489 (1980).

[91] A.J. Rogers, "POTDR: A Technique for the Measurement of Field Distributions," Applied Optics, 20, 1060 (1981).

[92] J.N. Ross, "Birefringence Measurement in Optical Fibers by Polarization: Optical Time Domain Reflectometery," Applied Optics, 21, 3489 (1982).

[93] D. Uttam and B. Culshaw, "Precision Time Domain Reflectometry in Optical Fiber Systems Using a Frequency Modulated Continuous Wave Ranging Technique," IEEE J. Lightwave Technology, LT-3, 971 (1985).

[94] J.K.A. Everard, "Novel Signal Techniques for Enhanced OTDR Sensors", Paper 05, Proc. SPIE 798, Fiber Optic Sensors II, The Hague, 1987.

[95] B. Zimmerman, "High Resolution Optical Time Domain Reflectometry and its Applications, "Masters Thesis, January 1988, Virginia Polytechnic Institute & State University.

[96] B.D. Zimmerman, R.O. Claus, D.A. Kapp, K.A. Murphy, "Fiber optic sensors using high-resolution optical-time-domain instrumentation systems," IEEE J. of Lightwave Technology, Vol. 8, 1990, pp. 1273 - 1277.

[97] B. Zimmerman, R.O. Claus, "Recent Progress in Optical Time Domain Techniques," Proc. of the Conf. on Optical Fiber Sensor-Based Smart Materials and Structures, April 3 - 4, 1991, pp. 13.

[98] J.J. Mlodzianowski, D. Uttamchandani, B. Culshaw, "Simple Fibre-Optic Multiplexing System using Pseudorandom Sequence," Elect. Lett., Vol. 24, No. 23, pp. 1436 - 1438.

[99] P. Vilbrandt, "Wireless Data Communications," Sensors, May 1993, pp. 19 - 21.

[100] D.D. Sampson, R.A. Griffin, D.A. Jackson, "Photonic CDMA by Coherent Matched Filtering Using Time-Addressed Coding in Optical Ladder Networks," J. of Lightwave Technology, Vol. 12, No. 11, November 1994 pp. 2001 - 2010.

[101] Y.D. Rao, D. Uttamchandani, B. Culshaw, P. Steer, J. Briancon, "Spread spectrum technique for passive multiplexing of reflective frequency-out fibre optic sensors exhibiting identical characteristics," Opt. Comm., Vol. 96, pp. 214, 1993.

[102] H.S. Al-Raweshidy, D. Uttamchandani, "Spread spectrum technique for passive multiplexing of interferometric optical fiber sensors," SPIE Vol. 1314, Fiber Optics, 1990, pp. 342 - 347.

[103] M.E. Marhic, "Coherent Optical CDMA Networks," J. Lightwave Technology, Vol. 11, No. 5/6, May/June 1993, pp. 854 - 864.

[104] X.S. Yao, J. Feinberg, R. Logan, L. Maleki, "Limitations on Peak Pulse Power, Pulse Width, and Coding Mask Misalignment in a Fiber-Optic Code-Division Multiple-Access System," J. Lightwave Technology, Vol. 11, No. 5/6, May/June 1993, pp. 836 - 846.

[105] R.C. Dixon, *Spread Spectrum Systems*, 2nd ed., John Wiley & Sons, New York, 1984.

[106] S.H. Poland, J.P. Bengtsson, M. Bhatnagar, K.C. Ravikumar, M.J. de Vries, R.O. Claus, "Multi-Measurand Multiplexed Extrinsic Fabry-Perot Interferometric Sensors," Proc. SPIE Int. Soc. Opt. Eng., Orlando, Feb. 1994, vol. 2191, pp. 58 - 66.

[107] J.D. Holmes, Coherent Spread Spectrum Systems, John Wiley & Sons, New York, 1982.

[108] K.C. Ravikumar, *Spread Spectrum Techniques for Distributed Multimeasurand Optical Fiber Sensors*, Master of Science Thesis, Virginia Polytechnic Institute & State University, Blacksburg, Virginia, October 1993.

[109] M. Bhatnagar, *Multiplexing of Interferometric Fiber Optic Sensors for Smart Structure Applications Using Spread Spectrum Techniques*, Master of Science Thesis, Virginia Polytechnic Institute & State University, Blacksburg, Virginia, April 1994.

[110] A.D. Kersey, A. Dandridge, M.A. Davis, "Low-crosstalk code-division multiplexed interferometric array," Elect. Lett., vol. 28, No. 4, pp. 351 - 353

[111] M.J. de Vries, A. Malik, X. Fang, N. Vellayadhun, T. Qazi, R.O. Claus, S. Durkee, W. Spillman, "Completely embedded optical fiber sensors," Proc. SPIE Vol. 2191Smart Structures and Materials Conf., pp. 373 - 379.

[112] W.B. Spillman, S. Durkee, W.W. Kuhns, "Adaptive processing for non-contact inductive smart structure sensor interrogation system using hierarchical neural networks," Proc. of the SPIE Smart Structures and Materials Conf., Vol. 2192, pp. 209 - 220.

[113] W.B. Spillman, S. Durkee, "Non-contact power/interrogation system for smart structures," Proc. of the SPIE Smart Structures and Materials Conf., Vol. 2191, pp. 362 - 372.

[114] R.E. Morgan, S.L. Ehlers, and K.J. Jones, "Composite-embedded fiber optic data links and related material/connector issues, "Proceedings of SPIE Vol. 1588, Fiber Optic Smart Structures and Skins IV (1991), pp. 189 - 197.

[115] S.L. Ehlers, K.J. Jones, R.E. Morgan and J. Hixson, "Composite Embedded Fiber Optic Data Links in Avionics Packaging," Proceedings of the Conference on Optical Fiber Sensor-Based Smart Materials and Structures, April 3 - 4, 1992, Blacksburg, VA, Technomic Publishing Co..

[116] Z.J. Lu and F.A. Blaha, "Application issues of fiber optic sensors in aircraft structures," Proceedings of SPIE Vol. 1588, Fiber Optic Smart Structures and Skins IV (1991), pp. 276.

[117] B.D. Duncan, Modal Interference Techniques for Strain Detection in Few-Mode Optical Fibers, Masters Thesis, April 1988.

[118] York Technology LTD., FK12 Sales Guide, 1994, pp. 8.

Vita

Marten Johannes Cornelius de Vries was born on May 20, 1965 in Novara, Italy, and is a citizen of the Netherlands. He completed his Bachelor of Science degree in 1989 and received the Master of Science degree in 1992, both from the Bradley department of Electrical Engineering at Virginia Polytechnic Institute & State University.

Mr. de Vries has worked in the research area of optical fiber sensors and communications at the Fiber & Electro-Optics Research Center as an undergraduate research assistant, two years, a graduate research assistant, one year, a graduate project assistant, two years, and a research associate for two and a half years. His research interests include developing optical fiber sensors, devices, instrumentation and communication systems for civil infrastructure monitoring and Intelligent Transportation Systems.

Mr. de Vries is a member of the SPIE - International Society for Optical Engineering, the Institute of Electrical and Electronic Engineers (IEEE), Eta Kappa Nu (HKN), the Omicron Delta Kappa (ODK) national leadership society and was the past-president and founder of the student chapter of the Optical Society of America (OSA) at Virginia Tech, of which he is still a member. In 1993, the Optical Society of America Education Council awarded Marten an Optics Education Grant for his efforts in coordinating teaching programs in optics at local high schools and elementary schools.

Mr. de Vries enjoys many different sports such as tennis, squash, speedskating, scuba diving, and snowboarding.

OPTICAL FIBER SENSORS FOR ADVANCED CIVIL STRUCTURES

by

Marten Johannes Cornelius de Vries
Dr. Richard O. Claus, Chairman
Electrical Engineering

(ABSTRACT)

The objective of this dissertation is to develop, analyze, and implement optical fiber-based sensors for the nondestructive quantitative evaluation of advanced civil structures. Based on a comparative evaluation of optical fiber sensors that may be used to obtain quantitative information related to physical perturbations in the civil structure, the extrinsic Fabry-Perot interferometric (EFPI) optical fiber sensor is selected as the most attractive sensor. The operation of the EFPI sensor is explained using the Kirchhoff diffraction approach. As is shown in this dissertation, this approach better predicts the signal-to-noise ratio as a function of gap length than methods employed previously.

The performance of the optical fiber sensor is demonstrated in three different implementations. In the first implementation, performed with researchers in the Civil Engineering Department at the University of Southern California in Los Angeles, optical fiber sensors were used to obtain quantitative strain information from reinforced concrete interior and exterior column-to-beam connections. The second implementation, performed in cooperation with researchers at the United States Bureau of Mines in Spokane, Washington, used optical fiber sensors to monitor the performance of roof bolts used in mines. The last implementation, performed in cooperation with researchers at the Turner-Fairbanks Federal Highway Administration Research Center in McLean, Virginia, used optical fiber sensors, attached to composite prestressing strands used for reinforcing concrete, to obtain absolute strain information.

Multiplexing techniques including time, frequency and wavelength division multiplexing are briefly discussed, whereas the principles of operation of spread spectrum and optical time domain reflectometery (OTDR) are discussed in greater detail. Results demonstrating that spread spectrum and OTDR techniques can be used to multiplex optical fiber sensors are presented. Finally, practical considerations that have to be taken into account when implementing optical fiber sensors into a civil structure environment are discussed, and possible solutions to some of these problems are proposed.